Master thesis

Investigation of melting rate and corrosion behaviour of de-icing agents for winter service

David Stinglmayr, BSc

under supervision of:

Univ.Prof. Dipl.-Chem. Dr.rer.nat. Hinrich Grothe

Institute of Materials Chemistry

TU Wien

Abstract

The Austrian Federal Railways (Österreichische Bundesbahnen ÖBB) have the legal obligation to provide winter maintenance services for about 5000 km of rail network and about 1100 railway stations in all of Austria. This costs the ÖBB group about 40 Mio Euros per year. To reduce de-icing salt induced corrosion and therefore save considerable budget every year, they commissioned a project to the TU Wien, in which a comprehensive list should be compiled with data on every available de-icing salt. This information should include melting rate, corrosion behaviour, storage and dispersion capabilities, impact on the environment and costs. Based on this evaluation, it should be easy to pick the best de-icing agent for every situation, providing adequate winter maintenance at the lowest possible costs, and with the least harm done to corrodible structures and the environment.

For this undertaking, two experiments were designed and built, one for measuring the melting rate precisely and efficiently, and a second one for evaluating the corrosion behaviour of de-icing agents on metal samples.

For the melting rate an entirely new method was developed, measuring the time it takes for an ice sample to melt under the influence of a de-icing salt at a constant temperature. For the corrosion behaviour metal plates were weathered with de-icing salt solutions and the amount of corrosion products was determined.

Additionally, chemical analysis was performed on the corroded metal samples to gain information about the corrosion process in saltwater environment and subsequently establish a method to measure the progress of corrosion on an exposed structure. With profilometry, X-ray photoelectron spectroscopy and X- ray powder diffraction the surface of the samples and the bulk of the corrosion products were analysed to determine chemical composition, roughness, and corrosion rate.

Kurzfassung

Die Österreichischen Bundesbahnen (ÖBB) haben die gesetzliche Verpflichtung Winterräumungsarbeiten für über 5000 km Schienennetzwerk und ungefähr 1100 Bahnhöfe und Haltestellen durchzuführen. Die Kosten für den ÖBB Konzern belaufen sich dabei auf etwa 40 Mio. Euro pro Jahr. Benutzt werden dafür Tausalze auf Basis von Natriumchlorid (NaCl), was beträchtliche Korrosionsschäden zur Folge hat. Um die Kosten für diese Schäden zu verringern, wurde die TU Wien beauftragt eine Anzahl gebräuchlicher Tausalze auf Taurate, Korrosionsverhalten und Lager- und Verteilungsfähigkeit zu untersuchen und eine Kostenrechnung aufzustellen. Diese Liste an Daten soll als Grundlage dienen, das am besten geeignete Taumittel für die ÖBB zu finden.

Für dieses Projekt wurden zwei Messsysteme erstellt, eines wurde benutzt um Taurate und Tauleistung genau und zeiteffizient zu bestimmen, mit dem anderen wurde das Korrosionsverhalten von Tausalzen auf Metalloberflächen untersucht. Für das Tauratenexperiment wurde eine komplett neue Messmethode entwickelt, mit der es möglich ist, präzise die Zeit zu messen, welche eine definierte Masse an Tausalz braucht, um eine definierte Masse an Eis zu schmelzen. Um das Korrosionsverhalten bestimmen zu können, wurde eine Korrosionskammer gebaut, die Metallplatten abwechselnd dem Tausalz und Luftsauerstoff aussetzt. Nach einer bestimmten Zeit wurde die Masse an Korrosionsprodukten bestimmt und so die Korrosionsrate ermittelt.

Zusätzlich wurde an den korrodierten Metallplatten chemische Analysen durchgeführt. Ziel davon war es Informationen über den Korrosionsprozess von Metallen in Anwesenheit von Salzwasser zu gewinnen und eine Möglichkeit zu entwickeln, den Korrosionsfortschritt an exponierten Stellen zu bestimmen. Benutzt wurden Profilometrie, Röntgenphotoelektronenspektroskopie (XPS) und Röntgendiffraktometrie (XRD) um chemische Zusammensetzung, Rauheit und Korrosionsrate der Metalloberfläche und der Korrosionsprodukte zu untersuchen.

Acknowledgements

First and foremost, I would like to thank Prof. Hinrich Grothe for letting me be part of this project and his working group. Supervising me and providing help both during the work and while writing this thesis.

I am grateful to Teresa Seifried and Ayse N. Koyun, who supported me with their knowledge and advice throughout the whole time of this project.

I am also thankful to our project partners Prof. Bernhard Hofko and Dr. Markus Hoffmann for to the cooperation in this project.

Special thanks go to Michael Gruber, who was my supervisor during my work at the civil-engineer laboratory and was essential to the development of the new measuring methods.

I would also like to acknowledge the team of technicians in the AG Hofko, who helped me operate the corrosion systems.

Further I would like to thank the teams of the Analytical Instrumentation Center and the X- Ray Center of the TU Wien for helping us with the chemical analysis of our samples.

Lastly, I would like to thank the Österreichische Bundesbahnen (ÖBB) the Austrian Research Promotion Agency (FFG) and the Bundesministerium für Verkehr, Innovation und Technologie for sponsoring this project.

1. Introduction

The definition of de-icing is the mechanical, physical, or chemical removal of ice, snow or frost from a given surface, or, in some cases, to dampen the negative effects of the ice. Types of de-icing agents reach from salts, organic reagents, and mineral aggregations to heating systems and mechanical labour. This thesis engages specifically in de-icing salts and their benefits and disadvantages, especially in their corrosion behaviour. The main area where de-icing is commonly practiced is transport. May it be cars, trains, or aircraft, if the temperature falls below the thermodynamical freezing point of water (0°C), each transport system has their individual problems, with historically very different de-icing methods and –agents.

- Railway system

On a railway track the problem with the potentially most catastrophic outcomes, during the months of winter, is the freezing of a switch. The switch is one of the most vital parts of a railway, making it possible to change direction, passing or ranking trains in stations. The consequences of improper switch placement are dire, and since beginning of railway transportation, measures have been taken to ensure the proper function of the switch, particularly under cold conditions. Historically, the switches were tended to by, so called, railway crews, who de- iced the rails and switches manually with brooms and other mechanical aids, or sometimes with kerosine torches, to heat up the frozen rail passage. De-icing salts are completely unsuitable for this application because of the corrosive behaviour of salt. Rails are made of grade 900 rail steel (Christodoulou et al., 2016) or an equivalent type of steel. This grade of steel combines high strength, excellent cycle fatigue behaviour and high radial stress endurance, but has very poor chemical resistance to corrosion (Rojan et al., 2019). It contains no ally material like chromium or nickel, which are mainly responsible for corrosion resistance.

Nowadays, most switch systems are heated to a temperature above 0°C. A very simple, but inefficient method to keep the railway free from ice (Hong & Woo, 2013). Heating railways takes huge amounts of energy and comes with a high monetary cost, so researchers around the world are tasked with developing more efficient ways of de-icing railways (Chiaradonna et al., 2020) (Oh et al., 2019).

- Aircraft

Aircraft de-icing takes place both on ground and in the air to ensure a safe and unproblematic flight. Ground de-icing is usually done by applying liquid agents on the surface of the plane, mostly consistent of ethylene glycol or propylene glycol. Other additives include chemical compounds which improve certain properties like corrosion behaviour, surface tension, pH or viscosity. For de-icing in air there are different methods depending on the type of aircraft and the route it is travelling. Again, fluid de-icing can be used, but some plains use mechanical or thermal de-icing methods. Most noticeable problem with these systems is the toxicity of the chemicals in use. Ethylene glycol and propylene glycol show a low toxicity and harmfulness towards the environment and most of these additives earlier described only intensify these properties (Cornell et al., 2000). Ground de-icing has to be performed in a hangar, where all chemicals can be caught and properly disposed. But even with these drawbacks and safety requirements, these de-icing agents are still better to use than salts. Again, the corrosion behaviour does not allow the use of much less expensive, much less dangerous de-icing salts. Even the tiniest bit of corrosion in jet engines or propeller rotors can have devastating effects and thus it cannot be justified to use chemicals which accelerate the oxidation of metals used in aircraft.

- Roads and pavement

Roads and pavement have historically been prepared with de-icing salt. Here no great harm is done by the corrosive behaviour of sodium chloride, the by far most used salt. It is very inexpensive, readily available in great amounts and it was believed, that it does not harm the environment. However, since the beginning of winter services, scientific reports have described problems with great amounts of salt in the environment, but have mostly been ignored (Crowther & Hynes, 1977). In more recent years more and more concerns have been appeared about the salinity of water bodies (Novotny et al., 2008), damaging the natural habitat of certain plants and animal species (Karraker et al., 2008) and groundwater quality (Hellstén et al., 2005). These concerns have resulted in restrictions of usage of de-icing agents in relation to environmental requirements (Magistrat der Stadt Wien, 2003).

1.1 The project

The project from which this master thesis is a part of is a multidisciplinary project and the client was the ÖBB, which is the Austrian Federal Railways. The ÖBB is responsible for winter maintenance along their rails and on their stations. Winter maintenance is usually done with de-icing salt, it is easy to distribute, it works fast, and it dissipates without residue. The most inexpensive and therefore the most used de-icing salt is sodium chloride (NaCl). It seems like the optimal solution for winter maintenance but has one major disadvantage namely the corrosion behaviour. Metallic surfaces present on the platform (benches, waiting areas and rails) are attacked and corrode much faster in presence of chloride ions, creating damages in the million euro range every year.

ÖBB tasked the project group, consisting of civil engineers and chemists from the TU Wien to find a de-icing salt or mixture, which fit their needs the best. For this we had to establish four main criteria in which all de-icing salts would be tested and graded. These criteria are melting rate, corrosion behaviour, storage and distribution capability and economic considerations.

Storage, distribution, and economy were the responsibility of our project partners at the facility of civil engineers, while corrosion and melting rate fell into our field of chemical research activity. First, we had to find a way to measure and compare melting rates and corrosion behaviour in a scientific and statistically valid way. A secondary task, set by the FFG (Österreichische Forschungsfördergesellschaft), was to analyse the corrosion behaviour of metals in chloride rich environment.

The first task we performed was to establish which salts could be used as replacement for NaCl, therefore we searched the literature for salts, which could be used as de-icing agents and tested them for their usability. Second, we tried to develop organic supplements, which could be mixed with the NaCl to supress its corrosion behaviour. Literature shows that some chemicals can have a corrosion inhibiting effect on metal surfaces, so we tried to find the best one. Some of the substances suggested by literature were discarded immediately, because the local government in Vienna has implemented some strict rules regarding environment friendliness and over-fertilization of the ground, and some organic materials did not comply with that.

The two properties important for establishing the capability of a good de-icing salt are the melting rate and the corrosion rate. Therefore, the first part of this thesis is dedicated to these two physicalities. A specific explanation of the two merits will be provided in the following sections.

The second part of this thesis is a scientific approach of the corrosion process of metal surfaces in the winter service environment, specifically qualification and quantification of corroded materials. Different chemical and physical analysis methods were tested, to measure the amount of oxidized material and the state and progression of the corrosion process. These analysis methods will be further explained in chapter 2.

1.2 Melting rate

The melting rate and the melting capacity are two values which are used to quantify the efficiency of de-icing agents (Robert et al., 1992). The melting rate is a series of values, which show how much salt is needed to melt a defined amount of ice at any given time and temperature. When salt is brought onto an ice surface the ice begins to melt rapidly. This is because the thermodynamical freezing point is a colligative property which means it is influenced by the number of particles solved in the medium. The more salt particles come in contact with the ice the lower the freezing point gets, which therefore means that the ice is melting at a lower temperature. This phenomenon is called freezing point depression (Wedler & Freund, 2012). The molten water then starts to dilute the salt, which weakens the melting power. This results in a slower increase of the melting rate over time, converging asymptotic to a particular value. This value, where the melting rate is not increasing anymore is called the melting capacity.

The melting capacity is the value, where the system is in equilibrium, which means no more ice is melting. In that manner, the melting capacity is the maximum of ice a certain amount of salt can melt. For better explanation an example (Figure 1) is provided. Here a typical melting rate curve is shown. The y-axis shows the melting rate, which is, as mentioned above, the mass of molten water related to the mass of salt in the system. The x- coordinate shows the time. The curve depicts how much ice can be melted by 1 g of de-icing agent at a certain temperature and a certain amount of time. This value can be upscaled to the amount of ice at the railway station and we can calculate the amount of salt needed to provide adequate winter service at the railway station.

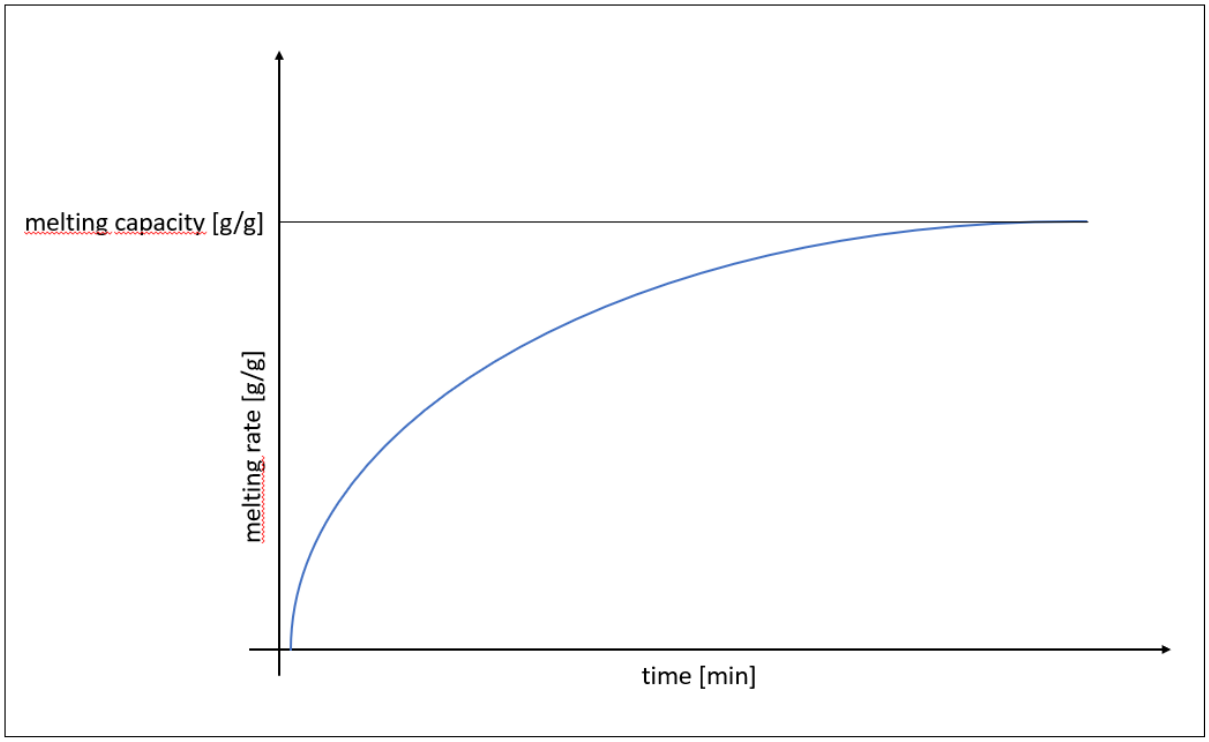

Figure 1: An example of a typical melting curve (blue) with the melting capacity shown (black).

Two methods to determine the melting rate values were used: a) The already established ice melting test (Robert et al., 1992) and b) a new method developed specifically for this project. For the ice melting test a), a defined amount of water is frozen in a flat form. Then a defined amount of de-icing agent is poured onto the surface. The de-icing agent is left on the ice for a certain amount of time, then the agent alongside the molten water is discharged. Then the mass of the remaining ice is determined. Thus, the amount of molten ice can be calculated by subtraction of the ice before and after the experiment. This is done at different times, so a melting rate curve can be obtained. Advantages of this method are the controllability of the time increments between measurements and the obvious similarity of this experiment to the environment at the railway station. Disadvantages are the low efficiency of the measurements, the fact that the temperature in the sample plates is difficult to control and that the measurement process is prone to errors.

The second melting rate test b) was developed by us to overcome the disadvantages of the ice-melting test a), which has many similarities with the de-icing process at the train station, but the results fail to produce the theoretical melting capacity found in literature. This is probably caused by the fact, that some of the molten ice in the discharge process is held back by the rest of the frozen ice plate. Investigation of the plates after the experiment showed some sort of ice slurry, which covered the remaining plate. For an accurate, scientific comparison of the de-

icing agents, this was hardly acceptable. So, we came up with an idea, based on the experimental setting of the twin plate ice- nucleation assay (TINA) experiments (Kunert et al., 2018). Instead of big ice plates, used in the ice- melting test a), we use small ice quantities, in a vial plate submerged in a cryostat and determine the point in time when all ice is completely molten. This procedure overcomes the ice slurry problem and is also way less time consuming, because more samples can be processed at the same time. As shown in chapter 3.1 our method also exhibits more accurate results compared to literature values. This method was then used to measure and compare selected de-icing agents.

1.3 Corrosion

Corrosion is defined as the process of metals to chemically react with oxygen to their respective metal oxides. All base metal elements are thermodynamically more stable as an oxide than as refined metal, so it is only a matter of time until a metal surface corrodes. Oxides usually have vastly different material properties than the refined metal, rendering them useless for the application metals are used. This results in corroded machines or buildings breaking down or falling apart. In short, corrosion is completely undesirable or even dangerous, depending on the application. Therefore, scientists are researching and developing methods to prevent or slow down the corrosion process.

A report from the association for materials protection (AMPP) shows that the estimated global cost of corrosion damage in the year 2013 was US$ 2,5 trillion, which represented about 3,4% of the global GDP (Koch et al., 2016), so it seems only natural to try and minimize the impact of corrosion on our economy.

Corrosion is an electrochemical process, metal atoms get oxidised and therefore electrons need to be transported. Corrosion reactions can be separated in two half- cell reactions, with the anodic reaction usually being the oxidation of the metal atoms, e.g:

$$Fe(s) \rightarrow Fe^{2+}(aq) + 2e^{-}$$

$$Al(s) \rightarrow Al^{3+}(aq) + 3e^{-}$$

The cathodic reaction uses the electrons to reduce oxygen or hydrogen atoms.

$$2H^+(aq) + 2e^- \rightarrow H_2(g)$$

$$O_2(aq) + 4H^+(aq) + 4e^- \rightarrow 2H_2O$$

$$O_2(aq) + 2H_2O + 4e^- \rightarrow 4OH^-(aq)$$

Which of these cathodic reactions take place is not easily determinable, unless the process is set up under laboratory conditions and closely monitored (McCafferty, 2009).

Corrosion of iron has been intensively studied in the past, so we can describe the process more precisely. Literature shows that in systems with neutral pH the iron atoms undergo two intermediate stages before forming iron oxide. These stages are γ- FeO(OH), which is called lepidocrocite and α- FeO(OH), which is called Goethite. Subsequently the stable magnetite Fe_2O_3 is formed (Tamura, 2008). This provides a measurement to quantify the progress of the corrosion. If we can determine the stage of the process, we can find out if the process is slow or fast. This indicates if the used de-icing agent has a positive or negative effect on the corrosion rate.

While chloride ions do not directly take part in the redox- mechanism of the corrosion process, they still have a corrosive effect, especially on iron. Without chloride ions present the formed iron oxides cover the underlaying iron and protect it from oxygen. Chloride ions can react and break down this protective layer, making it possible to further corrode the material. In literature there are three main models are shown on how the chloride ion reacts with the oxide layer:

I. Adsorption displacement: An O^{2-}- ion is displaced by a Cl^--ion

II. Chemico- mechanical: the adsorption of Cl^-- ions results in repulsive forces between the adsorbents, which in turn results in cracks on the surface

III: Migration- penetration: Ion migration via cation vacancies and O^{2-}- ions

To summarize: Chloride ions make sure the protective layer never fully covers the metal, facilitating oxygen with more and more places it can react with the metal.

(Montemor et al., 2003), (Jovancicevic et al., 1986)

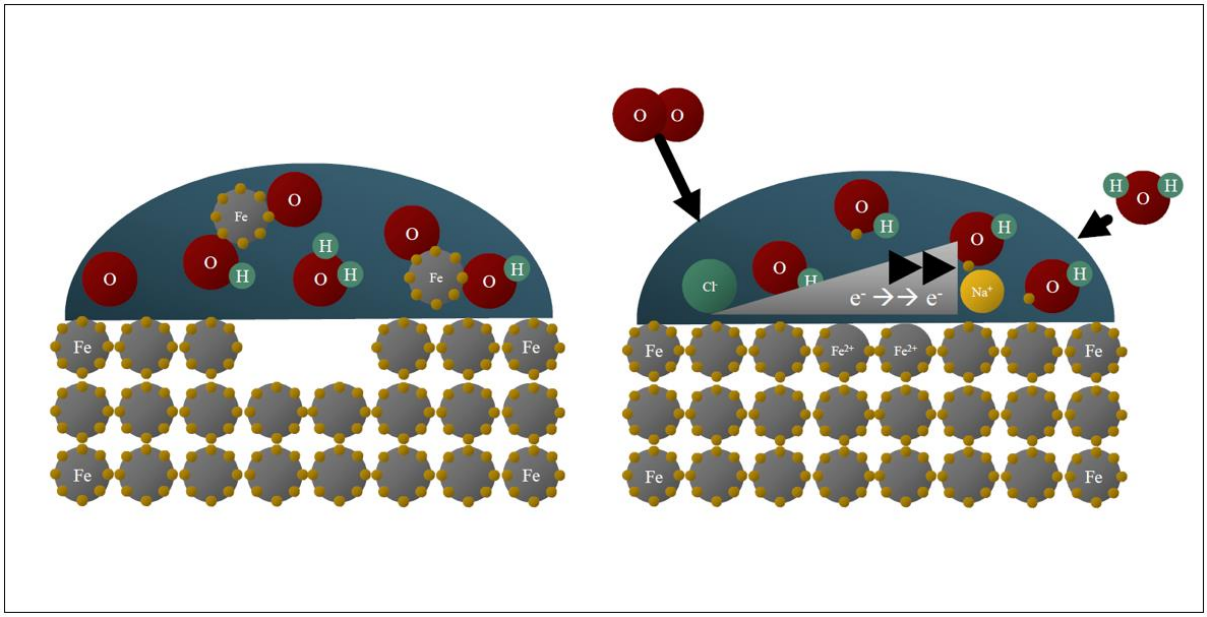

Figure 2: Impact of de-icing salt on the corrosion process of steel. Corrosion is accelerated by easier access of water and oxygen gas (Hoffmann et al., 2021).

Form this information we can conclude that a corrosion process needs three requirements to take place. i) It needs a metal surface, ii) oxygen, and iii) some sort of electrolyte, in most cases water, in close proximity. So, if we want to inhibit this process, we have to make sure that at least one of those requirements is not present. Another way to slow down the corrosion process is to make sure no chloride is contained in our de-icing agent.

We tried two different ways to solve the corrosion problem. a.) We can facilitate a de-icing agent without chloride. For example, sodium acetate is also used as de-icer, however 1 kg of sodium acetate costs about 5 times more than sodium chloride and has only about half the melting rate at 30 minutes. So, to de-ice a railway platform, compared to sodium chloride, double the amount of sodium acetate would be needed, while being much more expensive.
b.) A more cost-efficient way would be to use NaCl but counter its aggressive corrosion behaviour by adding an anti-corrosion agent, e.g., a saccharide. Sugars have been reported to have a strong corrosion inhibiting effect (L. R. Chauhan & Gunasekaran, 2007) and they do not violate constraints given by our clients regarding overfertilization of the soil or changing the pH of the ground water. The way corrosion inhibition works in this regard is twofold. Firstly, some organic molecules tend to adsorb onto a metal surface, even better then water molecules do, so they form a organic protection layer on the metal surface (Muralidharan et al., 1995). Secondly, sugars are substances that can be oxidised themselves, which means that if an oxygen molecule interacts with the sample surface it reacts with the organic material and does not corrode the metal.

On the basis of this research, we developed a testing program with sodium chloride mixed with glucose, arabinose, mannose and maltose.

2. Theoretical background

2.1 Atomic force microscopy (AFM)

AFM is an imaging method used by scientists since 1985 to examine surfaces of crystalline materials but also amorphous biological matter. The technique uses a sharp metal tip (diameter: 10 – 20 nm) to scan the sample surface. From the position of the tip, a topographical map of the sample surface can be created. The huge advantage of this method is that true atomic resolution can be achieved (Binnig et al., 1987). The tip is located on a so-called cantilever, a flexible, at structural element which bends under the influence of the forces brought upon the tip. The behaviour is that of a spring meaning that if the tip latches on the surface it bends downwards and if the tip is lowered down it bends the other side. The position of this cantilever is usually observed by a reflected laser beam directed at the at upper side of the structure. The exact location and bending state of the cantilever can be calculated from the position of the laser dot on a quad diode. So not only vertical but also horizontal information can be gained, which is important for further surface analysis. Figure 3 shows the structure of a typical AFM- Setup.

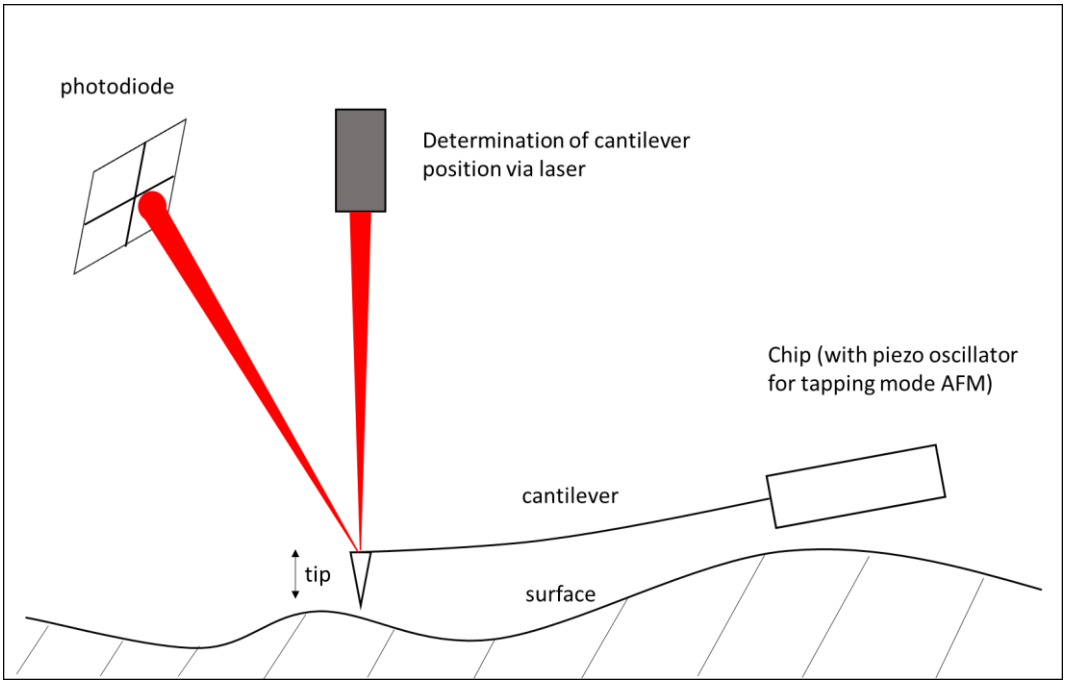

Figure 3: Depiction of a typical AFM- Setup. The tip is located on a bendable cantilever, which can be used to track the position of the tip with a laser

AFM measurements are carried out in one of two modes, which are named after the motions of the tip: a) constant force or b) constant height mode. In a) constant force mode the tip is readjusted in height to compensate for the topographical features of the sample. This height adjustment is recorded and used to create the AFM- image. In b) constant height mode the vertical position of the sample and the tip is kept at a certain distance and only the detection of the cantilever is recorded.

Additionally, a function called AC- or tapping mode can be used. Here a piezo oscillator swings the cantilever and the tip. The tip only encounters the sample surface at the end of an oscillation and is therefore easier preserved. Typical frequencies for the tip are around 1000 to 1200 kHz. Lateral shear forces can be nearly eliminated, scratching of soft samples is reduced and the removal of any loose particles on the sample surface can be avoided by this technique. This is linked to a greater complexity in controlling and analysis of data, but modern microscopes are generally able to use this mode, to preserve the tips, which are hard to manufacture and expensive. The result of an AFM- measurement usually is a topographical picture of the sampled surface, containing information about the properties of the material. Impurities can be found on those pictures, lattice defects, but also more macroscopic information can be found. Small cracks, too little to find with a microscope, properties of the interface of semiconductors, just to name a few. Another crucial application of AFM is the determination of surface roughness, especially in corrosion science. We used this facet of the method, to examine if there is a correlation between the surface roughness of metal samples after a controlled corrosion process and the amount of corrosion products, which were formed at that process. The idea is to use a non- destructive method to determine the corrosion state the sample is in. To quantify roughness as a property numerous parameters are commonly used, depending on the requirements of the examined component.

Table 1: Roughness parameters

Name	Symbol	Definition	Formula
Arithmetic average height	R_a	Average absolute deviation of the roughness irregularities from the mean line	$R_a = \frac{1}{l}\int_0^l \lvert y(x)\rvert dx$
Root mean square roughness	R_q	Standard deviation of the distribution of surface heights	$R_q = \sqrt{\frac{1}{l}\int_0^l \{y(x)\}^2 dx}$
Ten- point height	R_z	The difference in height between the average of the five highest peaks (p) and the five lowest valleys (v)	$R_z = \frac{1}{n}\left(\sum_{i=1}^{n} p_i - \sum_{i=1}^{n} v_i\right)$
Maximum height of peaks	R_p	The maximum height of the profile above the mean line	
Maximum depth of valleys	R_v	The maximum depth of the profile below the mean line	
Mean height of peaks	R_{pm}	The mean of the maximum height of peaks R_p obtained for each sampling length	$R_{pm} = \frac{1}{n}\left(\sum_{i=1}^{n} R_{pi}\right)$
Mean depth of valleys	R_{vm}	The mean of the maximum depth of valleys R_v obtained for each sampling length	$R_{pv} = \frac{1}{n}\left(\sum_{i=1}^{n} R_{vi}\right)$

(Gadelmawla et al., 2002)

Figure 4 shows a stylised form of a surface and explains the parameters in table 1.

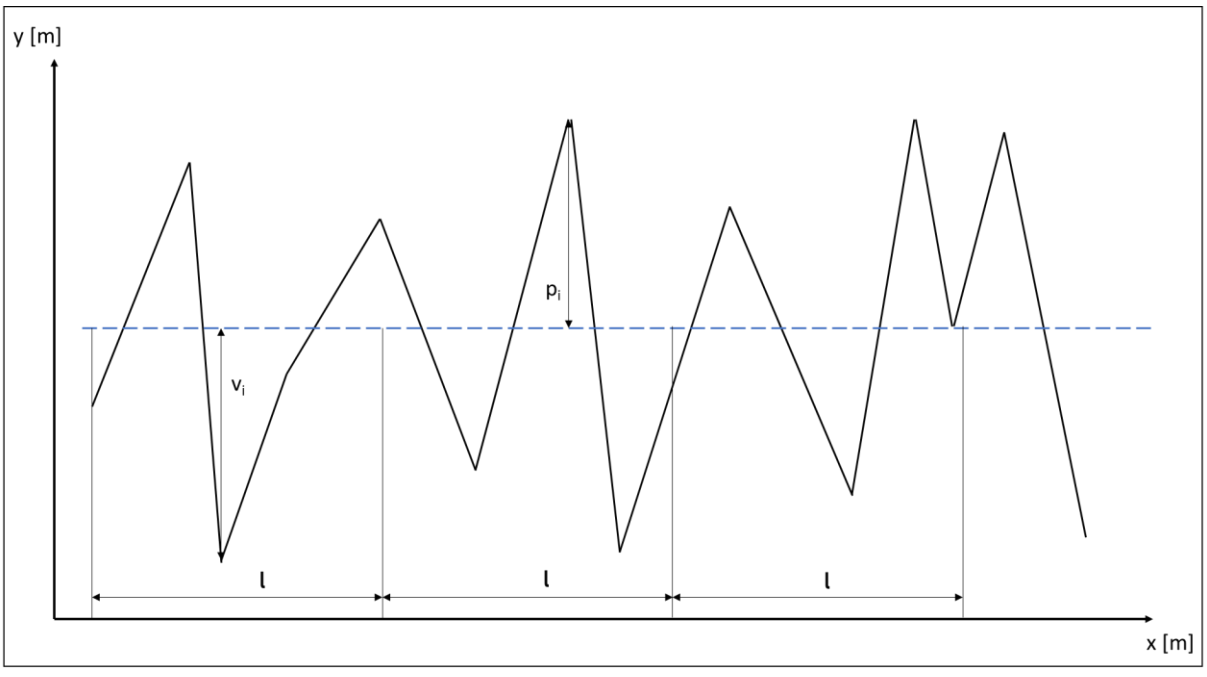

Figure 4: Sketched example of a sample surface with the roughness data plotted. (Gadelmawla et al., 2002)

Table 1 shows a variety of commonly used parameters to characterize the texture of a sample surface. For our experiments we used the Arithmetic Average Height, which is most universally used and a good estimate for the overall roughness.

Topographical picture of the sample surface is not the only result of an AFM measurement, the method offers a lot more. AFM is one of the very rare methods to really touch the sample, so using it to measure height is not even close to all the information that can be gathered. Humans can feel the difference when we touch grass or concrete. We can sense if something is wet or dry, hard or soft. Sensory receptors can be found all over the human body, not only in the outer skin layer but also in bones, internal organs, and the cardiovascular system. These receptor cells react on different stimuli, such as pressure, temperature, or an electrical potential between two surfaces, and relay signals to our brain for further processing, which creates such sensations as pain and proprioception, and our whole sense of touch apparatus. It seems very ambitious to rebuild the receptor system of the human body but some of these properties can be measured and even quantified by the AFM, to gain further information about the nature of the sample.

We can use the rigidity of a material as example. The stiffness we feel on a metal surface comes from the high resistance opposed to our finger pushing in. In other words, we have a very high increase in repulsive force per distance of deformation. Rubbery surfaces do not have these forces, at least not to that extent, on the contrary, some materials show strong attractive forces, which let the AFM- tip "snap" onto the surface. And so, the AFM is perfectly capable of measuring these attractive and repulsive forces on the sample surface, which makes it possible to get data which is otherwise impossible to obtain. The basis of this analysis is the force - way diagram, which can be measured with the AFM. An example of such a graph can be seen in figure 5. From the form of these diagrams, material data can be drawn. (Friedbacher, G., Bubert, 2011) (Muševič, 2000)

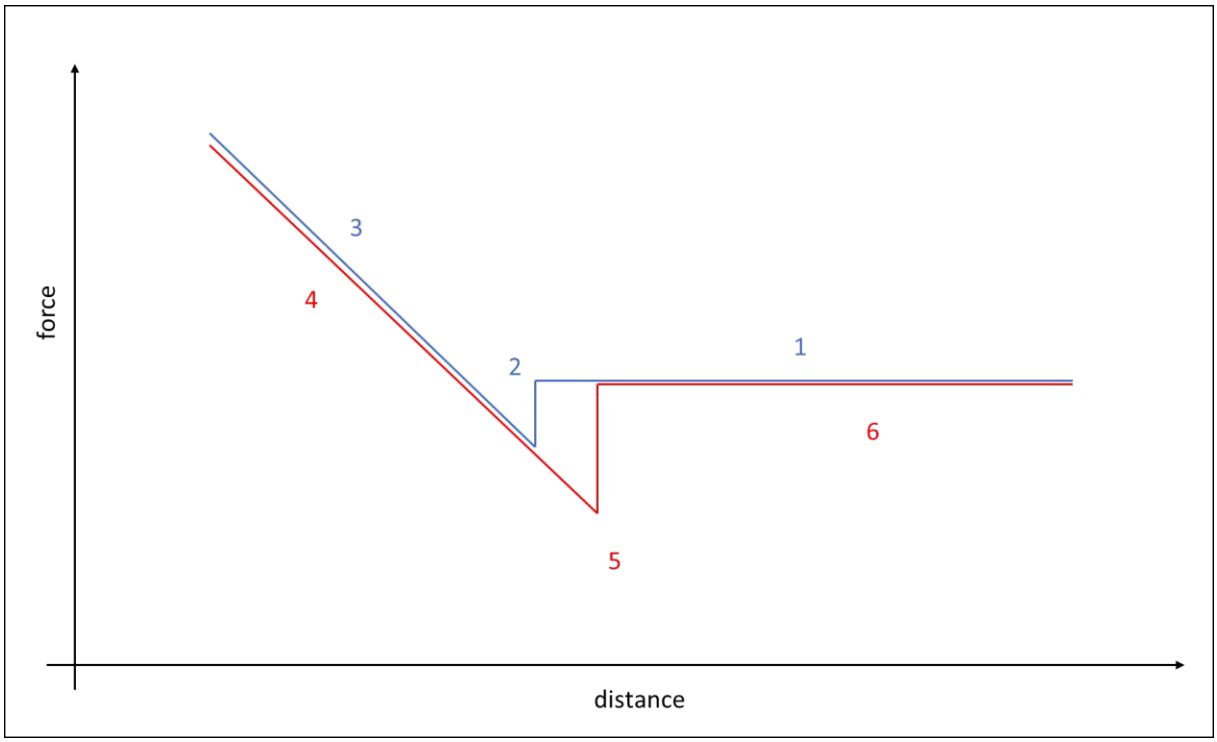

Figure 5: Example of a Force - Way diagram. There are two graphs, one shows the approach of the AFM- tip (blue) the other one shows the withdrawal (red). At marker 1 the tip approaches but is not in close proximity of the surface. The lower we go in distance the closer the tip gets to the surface. Then at one point (Marker 2) the attractive forces let the tip snap onto the surface. If we lower the distance even further the repulsing forces become stronger and stronger (Marker 3). From this position we try and withdraw the tip from the sample. We increase the distance and therefore lower the repulsive forces (Marker 4). Then the attractive forces hold the tip on the surface for a little bit before snapping away (Marker 5). Then the tip withdraws without interference again.

2.1.1 LASER profilometry

Additionally to the AFM, a laser profilometer was used to determine the roughness of the sample surface. The surface area is scanned with a LASER beam instead with an AFM- tip. The distance from the laser beam to the surface can be calculated from the angle the laser is scattered back. Scanning the sample and determine the height of many dots gives a similar result as with the AFM- system. Figure 6 shows the principle of a Laser profilometer (Giesko et al., 2007).

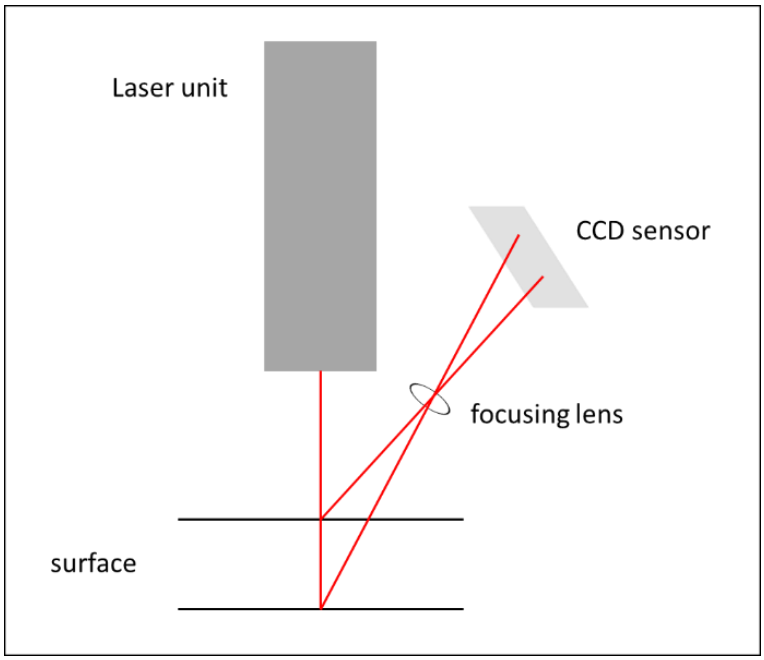

Figure 6: Depiction of the Laser profilometer. The Laser beam (red) is shown at two different surface heights, which change the position at which the beam reaches the CCD sensor.

The main difference between atomic force microscopy and Laser profilometry is the sensitivity. As mentioned above the AFM can reach atomic resolution, while the profilometer comes nowhere close to that. The best lateral solution achieved with this method is 50 µm. But this also means that the AFM is limited to very small scanning areas and small height differences. At higher surface roughness the piezo crystal in the motion apparatus of the AFM system cannot reach the highest peaks or lowest valleys, resulting in false results or broken tips. Here is where the profilometer has its strengths, a greater area of extremely rough sample can be measured without any problems. In this work we mainly used the Laser profilometer for our surface analysis, with some more sensitive measurements on the AFM.

2.2 X- Ray Photoelectron Spectroscopy (XPS)

XPS is a commonly used, very effective way to analyse sample surfaces. It provides information about surface chemistry and is often used in material characterisation. XPS can provide quantitative information of the surface. The average depth of analysis is about 5 nm, depending on the material.

The main disadvantage of XPS is, that it is not an imaging technique. While it is possible to analyse chemical composition, information is only gained as average over a sample. This is why XPS and AFM are often used complementary, with AFM providing data about the topographical model and XPS providing information on the chemical composition.

The idea of XPS is to irradiate the surface area with soft X -ray photons. These photons transfer their energy completely onto an electron close to the nucleus. If the energy from the photon exceeds the binding energy of the electron, it leaves the electron shell and transfers into the vacuum level. This process is called the "Photoelectric Effect". From the kinetic energy of this now free electron the binding energy can be calculated, being a characteristic metric for any given element.

$$E_{kin} = h\nu - E_B - \Phi_S$$

with E_{kin} being the kinetic energy of the free electron, h is Planck's constant, ν represents the frequency of the radiation, E_B represents the binding energy of the electron and Φ_S stands for the work function, which is a small, mostly constant energy, which has to be expended for the electron to leave the outmost shell of the atom (Friedbacher, G., Bubert, 2011).

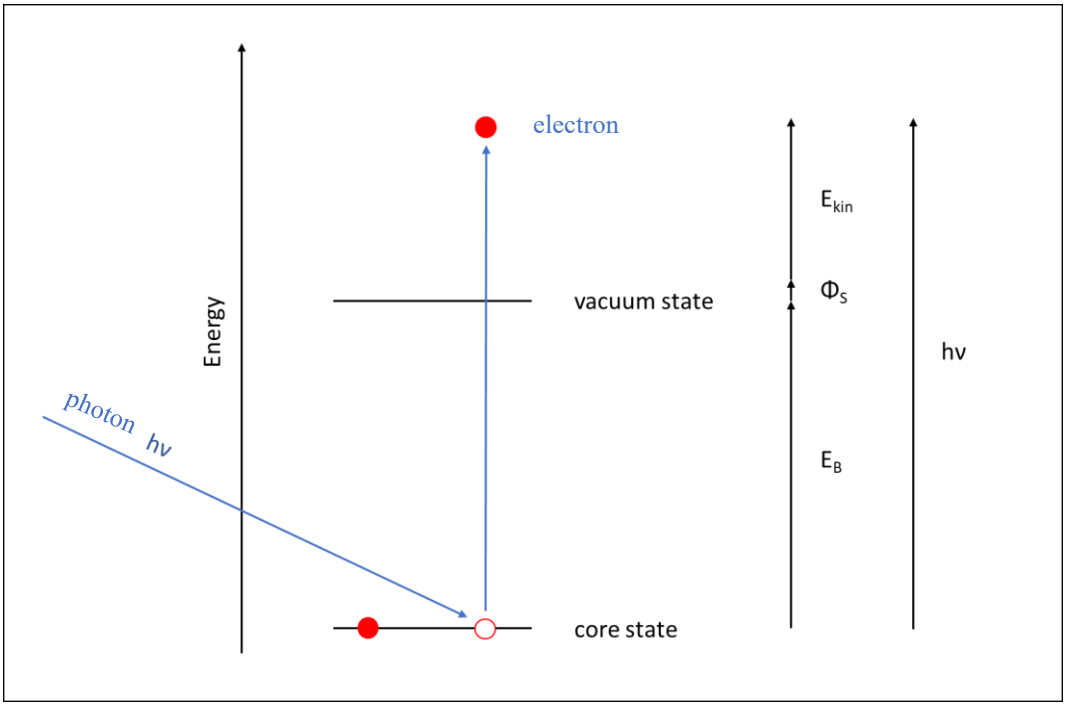

Figure 7: Principle of XPS. An electron is lifted by X- ray irradiation and afterwards the kinetic energy is measured. Knowing the radiation energy and the kinetic energy, the binding energy can be evaluated. The work function is usually assumed constant and can therefore be neglected. (Aziz & Ismail, 2017)

In fact, XPS is so incredible surface specific that it is related to the mean free path of a free electron in a crystal lattice. The mean free path of an electron depends on the kinetic energy of that electron. In a typical XPS- measurement the energy ranges from 250 eV to 1000 eV, which corresponds to a free path of around 8 monolayers of atoms. This means the electrons measured only can come from the outer 50 nm of the sample (Friedbacher, G., Bubert, 2011).

This form of measurement offers the possibility to analyse atoms on the surface individually. As stated before, the binding energy pattern we get from the XPS is characteristic for every element. We can determine the chemical composition of the sample material, and therefore identify surface reactions, as for example, corrosion.

Additionally, XPS spectra provide information about oxidation state and chemical environment of the surface atoms. Absorbed or adsorbed molecules on the surface or different chemical bonds formed by a surface atom can shift the binding energy of core level electrons. This gives detailed data of chemical transition states or transport processes on the sample surface and can be used in this thesis to further investigate the corrosion process (Friedbacher, G., Bubert, 2011) (Aziz & Ismail, 2017).

To be able to provide this kind of detailed information the XPS- system needs a very high energy resolution. In modern systems this is provided by a concentric hemispherical analyser (CHA). Other energy analyser systems do not provide a high enough resolution to justify their use on a larger scale (Kelly, 1999). Figure 8 shows the structure of a CHA.

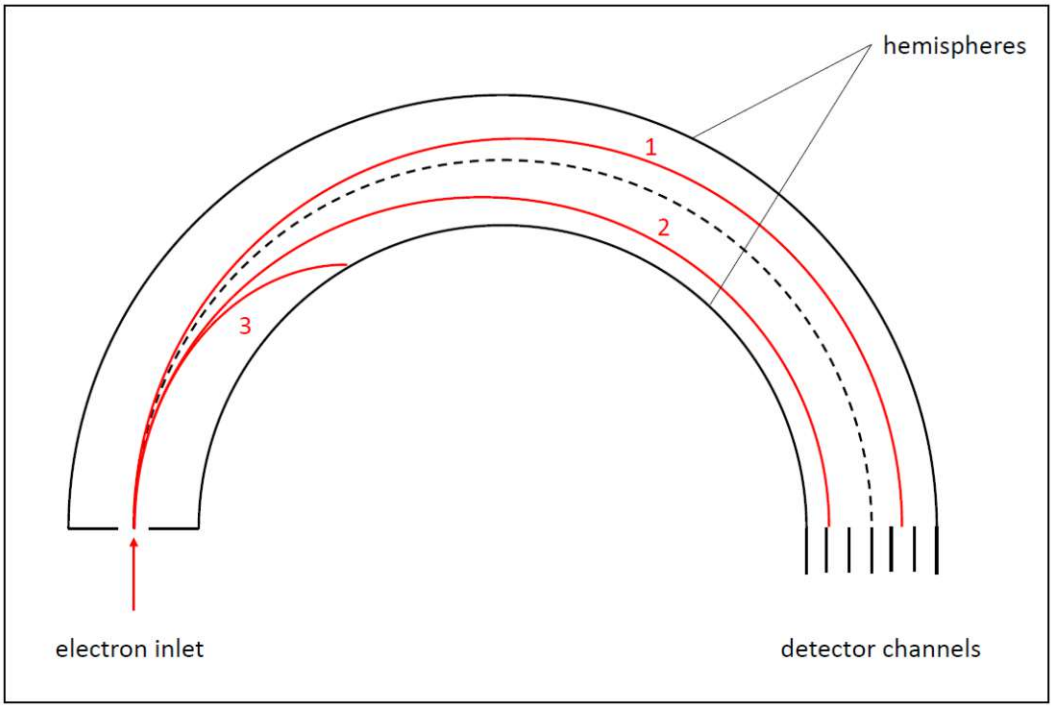

Figure 8: Schematic structure of a CHA, electrons with pass energy follow the dotted line, slight deviation from the pass energy results in paths 1 and 2, electrons with bigger differences in energy hit the wall and are lost (depicted in path 3)

The CHA consists of two concentric hemispheres which have different electrical potential. These potentials form an electric field between the two hemispheres, which in turn can divert electrons from their straight path. Electrons enter on the one side of the hemisphere and are

forced on a curve through the analyser. The electric field is adjusted in a way that only electrons with a specific kinetic energy can reach the other side. The energy needed to pass through the analyser in the middle of the two hemispheres is called passing energy. The passing energy for XPS- measurements is usually in a range from 20 eV – 100 eV. The analyser can divide the electrons by their energy due to the deviation from the passing energy results in slightly altered trajectories in the hemisphere, and in turn results to the fact that electrons getting recognized by a different detector channel. Therefore, the XPS is also able to provide quantitative data about our sample surfaces.

2.3 X- Ray Diffraction (XRD)

XRD is one of the most used analytical techniques to characterise solid, crystalline structures. The sample is irradiated with monochromatic X- ray radiation. The photons interact with the electron shell of the atoms and are diffracted. The diffraction pattern only depends on the wavelength of the radiation and the position of the atoms. If used on a single- crystal this method gives a reflex- pattern from which information of the lattice parameters and crystal structure can be drawn.

This reflex pattern can be described with the Laue- condition, which states that the incoming wave vector k_{in} subtracted from the outgoing wave vector k_{out} must be equal to a reciprocal lattice vector G.

$$\Delta \boldsymbol{k} = \boldsymbol{k}_{out} - \boldsymbol{k}_{in} = \boldsymbol{G}$$

$$\boldsymbol{G} = \frac{2\pi}{\boldsymbol{a}_{hkl}} * n$$

with k being the wave vectors, G represents the reciprocal lattice vector, which can be calculated by dividing 2π by a_{hkl} which is a normal lattice vector, and n represents the periodicity (Waseda et al., 2011).

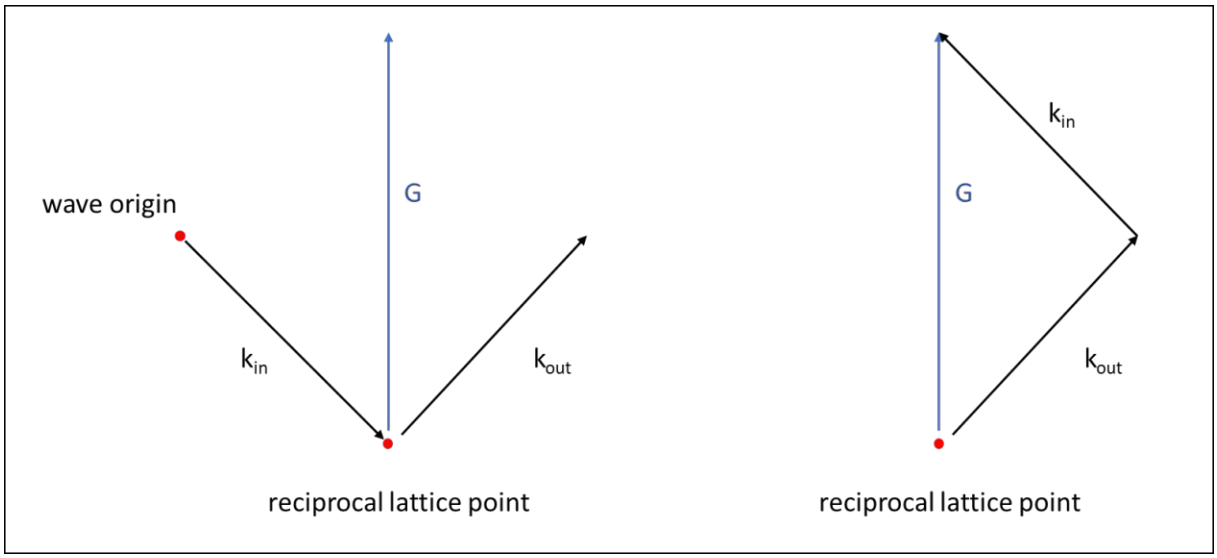

Figure 9:Laue's condition. On the left side the diffraction process is depicted, while on the right side we see the subtraction of the wave vectors.

In analytical chemistry, very rarely single crystal samples are analysed, so the way more important method is the powder diffraction. Here the sample is ground into a finely granulated powder and then analysed. The result of this method is different to the one from the single crystal XRD. Instead of a reflex pattern we get Debye- Scherrer rings. Figure 10 shows an example of the different results of single crystal and powder diffraction.

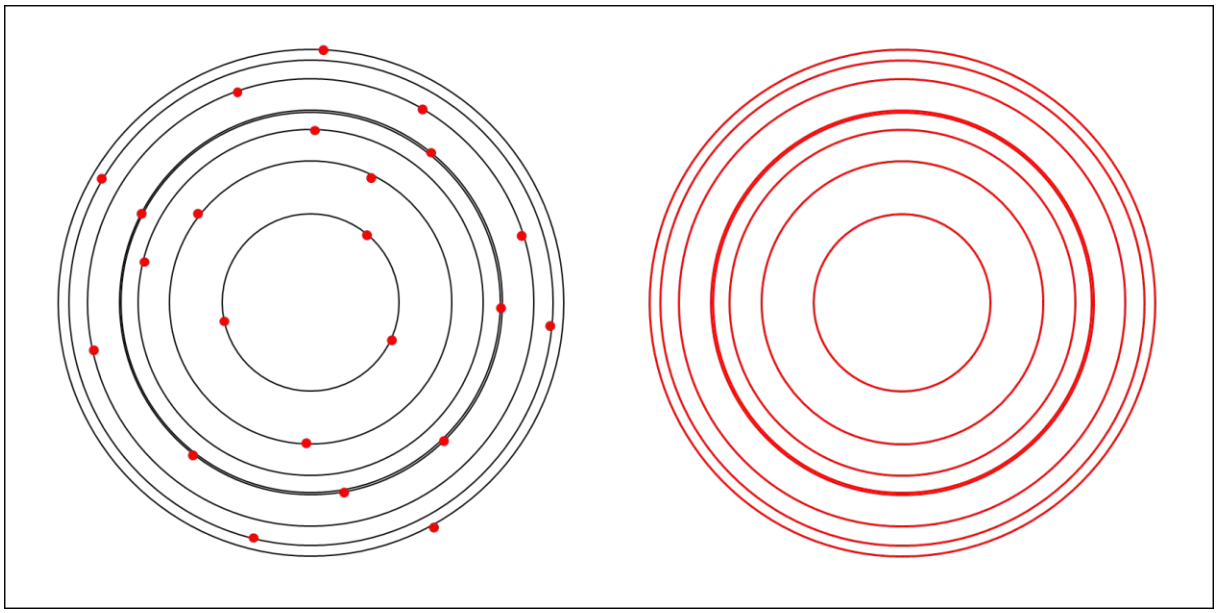

Figure 10: An example of two diffraction results, on the left side a single crystal diffractogram, with point shaped reflexes, while on the right side the same substance but powdered with annular signals.

Modern XRD- systems even go a step further and do not need to record the entire Debye-Scherrer rings anymore. Today's systems use the Bragg- Brentano- geometry which allows the equipment to record a cut through the rings. This is possible by the special geometry where the

X- ray source and the detector are moved around in coordinated angles, whale the sample lies still. This allows for the system to forgo the big detectors, which are needed to capture the hole result. Bragg- Brentano- diffractometers deliver a reflex intensity over the detector angle as a result (A. Chauhan, 2014). For a better understanding figure 11 shows one of our measurements as an example. Each of these peaks represents one Debye- Scherrer Ring, the counts on the y- Axis stand for the intensity and the 2θ position represents the distance between the rings.

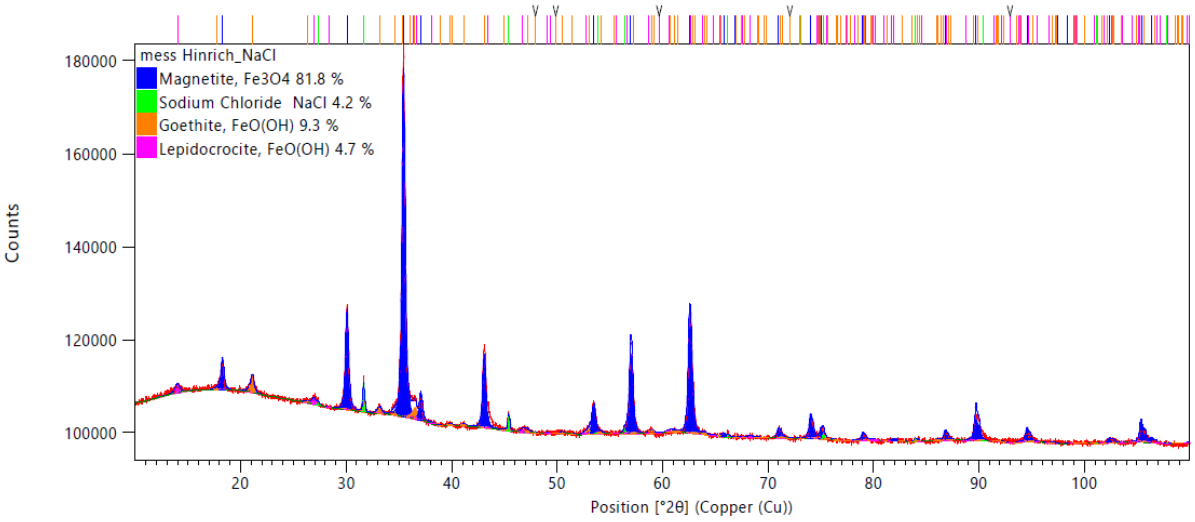

Figure 11: An example of a XRD spectrum measured with Bragg- Brentano geometry.

Nowadays these systems are by far the most used ones, because of their great angle resolution and their routine use in analytical chemistry. Powder XRD is able to provide qualitative and quantitative data about the bulk composition of a crystalline sample. Huge databases of XRD data exist, with which the analysed sample can be compared, and the phase composition can be identified, as shown in figure 11.

3. Experimental Part

3.1 Melting Rate

3.1.1 Climate Chamber

Melting rates of de-icing agents were determined by two different approaches, the first one being the climate chamber. Plates of ice were created by filling approximately 250 g of water into a metal plate with a diameter of 205 cm and a height of about 2 cm and freezing it overnight in the climate chamber at the desired temperature. The climate chamber used was a BINDER MKF 720 and the chosen temperatures were -2.5°C, -5.0°C, -7.5°C and -10.0°C. The BINDER

MKF 720 can best be described as glovebox, in which the temperature can be set and be hold constant, so the climate chamber did not have to be opened for the whole experiment, which allowed for the temperature not to be influenced by outside conditions. In this manner 6 ice-plates were created and on the next day, 10 g of de-icing salt, prepared in a little container, was evenly distributed on the surface of each ice- plate. By weighing the plates before and afterwards, the exact amount of ice and salt were determined. After that step the salt was left to melt the ice for certain amounts of time (5 min, 10 min, 30 min, 60 min, 120 min and 240 min) after which one plate at a time was emptied into a waste beaker and weighed again. The difference between the mass at the time and at the beginning is the amount of ice that has been melted by the de-icing salt. From these measurements the melting rate has been calculated by dividing the amount of molten ice by the amount of added salt. This gives a graph from which one can determine the amount of de-icing agent needed to melt a given amount of ice in a given time.

For statistical reasons each of these measurements had to be repeated three times, which ramps up to massive amount of time. It took 3 days to measure one melting curve, so with this very inefficient method it would have taken months to get the desired melting rate results. Another problem with this method was, that the temperature accuracy in the climate chamber was not distributed evenly, the difference was as much as 3° from one side of the chamber to the other, which produced untraceable results. The countermeasure to this problem was to set up compensating factors to balance the difference in temperature. This was done by doing the same experiments as described earlier in this section, but instead of emptying the plates at different times all mass losses were measured at the same time. The different melting rates were then processed to calculate correction factors which compensated for the different temperatures at different places in the climate chamber. The measurement of the correction factors was repeated three times for statistical certainty. The big advantage of this method is that the experiments did not have to be rerun, the results which had been already generated, could just be adjusted afterwards by multiplying them with the calculated factors. With this precaution the results were a lot more sensible. Figure 12 shows an example of such a melting rate curve and the effect of the compensation.

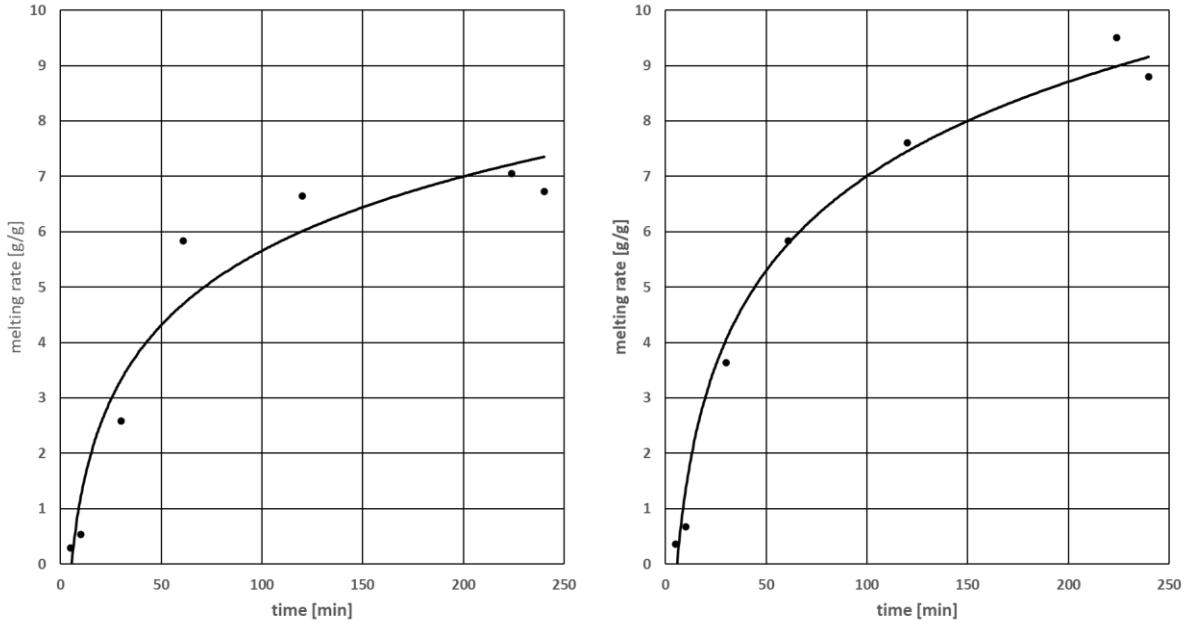

Figure 12: Melting rate of NaCl at -5,0°C, original data (left) and adjusted for temperature drift (right). Correlation factor jumped from 0.93 on the left to 0.98 on the right. The fitting was done with a logarithmic approximation

3.1.2 Cryostat

As mentioned in section 3.1.1 the melting rate experiments in the climate chamber have some severe disadvantages. Time inefficiency, temperature changes, and additionally, the fact that the measurement is falsified by water, which should be emptied, but is hold back under and inside the ice plate. Therefore, it is not included in the amount of water, which is counted as molten, and thus is distorting the melting rate to an unrealistic lower value. This can be observed by the theoretical melting capacity of NaCl. This value should be 11,8 g/g (Nilssen et al., 2016) but is approximately 10 g/g here (see figure 12). For our measurements we used 10 g of de-icing salt and 250 g of ice sample. From these values it can be calculated that approximately 20 g of water was hold back by the ice plate. Given that the extent of this effect is probably different each measurement, this method of melting rate determination was declared invalid and another one had to be found.

To tackle this problem specifically we developed a more accurate method which had: a) a lower amount of ice to avoid water remaining in the ice and b) a higher number of samples to improve the statistics. The process of this method is as follows: Firstly, small amounts of water are pipetted into a vial plate. Such PCR vial plates are made of polypropylene, and are normally used to store micro tubes, but for our needs, we used it as a sample holder. A maximum of 35 such samples per plate were prepared. More than 35 samples cannot simultaneously be observed by the camera. As can be seen in figure 13, more sample cavities cannot be depicted accurately

because of the angle of the lense. These samples are covered with parafilm and, overnight, frozen at a temperature of -20°C. On the next day another vial plate with the same size is filled with small amounts of the solid de-icing salt. Once the water samples are frozen, they are transferred into a cryostat (HUBER ministat 240) in which the desired temperature is already adjusted. After 30 min the temperature in the vial plate matches the temperature of the cryostat and the salt can be given upon the ice crystals, all at the same time. Then the ice is left to melt completely. This process is observed by a camera (CANON EOS 2000d) which takes a picture every minute. From these pictures the exact melting time can be measured.

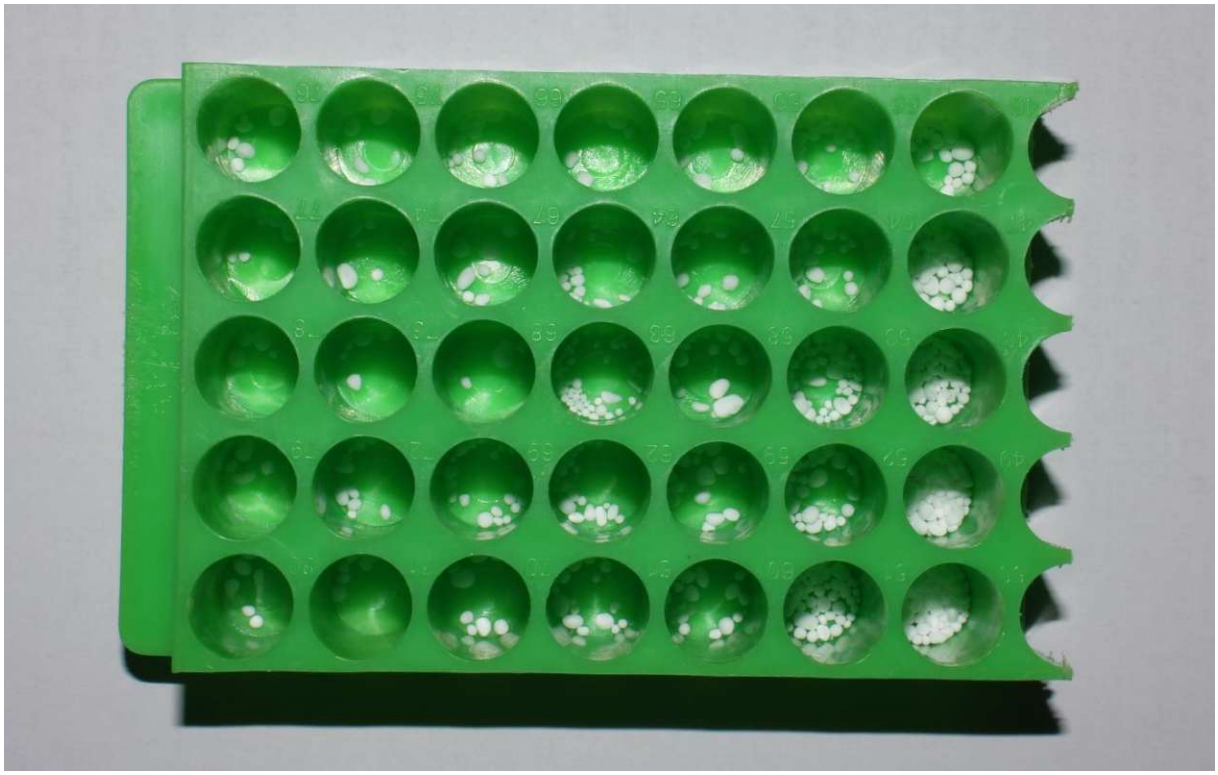

Figure 13: A picture of the vialplate used in this experiment. Each vial holds a defined amount of de-icings alt which will be used to determine the melting rate of this salt. This image shows that if the camera is positioned directly above the idle of the plate the cavities on the edges are not completely visible. This restricts the size of the plate.

The amount of ice is always the same, but the amount of salt varies in each vial, so that after the melting process each vial has a different salt- concentration. With these concentrations the melting rate in each vial can be calculated and combined with the time it took to melt the whole ice cube. That way up to 35 data points on a melting rate curve can be obtained in one experiment, which makes it far more time efficient than the climate chamber experiment. The results are precise and repeatable. However, there was one major drawback which had to be solved. The first experiments showed way too high melting rates and melting capacities. Figure 14 exhibits one of the first experiments in the new cryostat setup. It is shown that the measured melting capacity in this experiment is 15,2 g/g, a significant increase from the theoretical value

of 11,7 g/g. We assumed that this was related to the contrast between salt and ice in the small cavity.

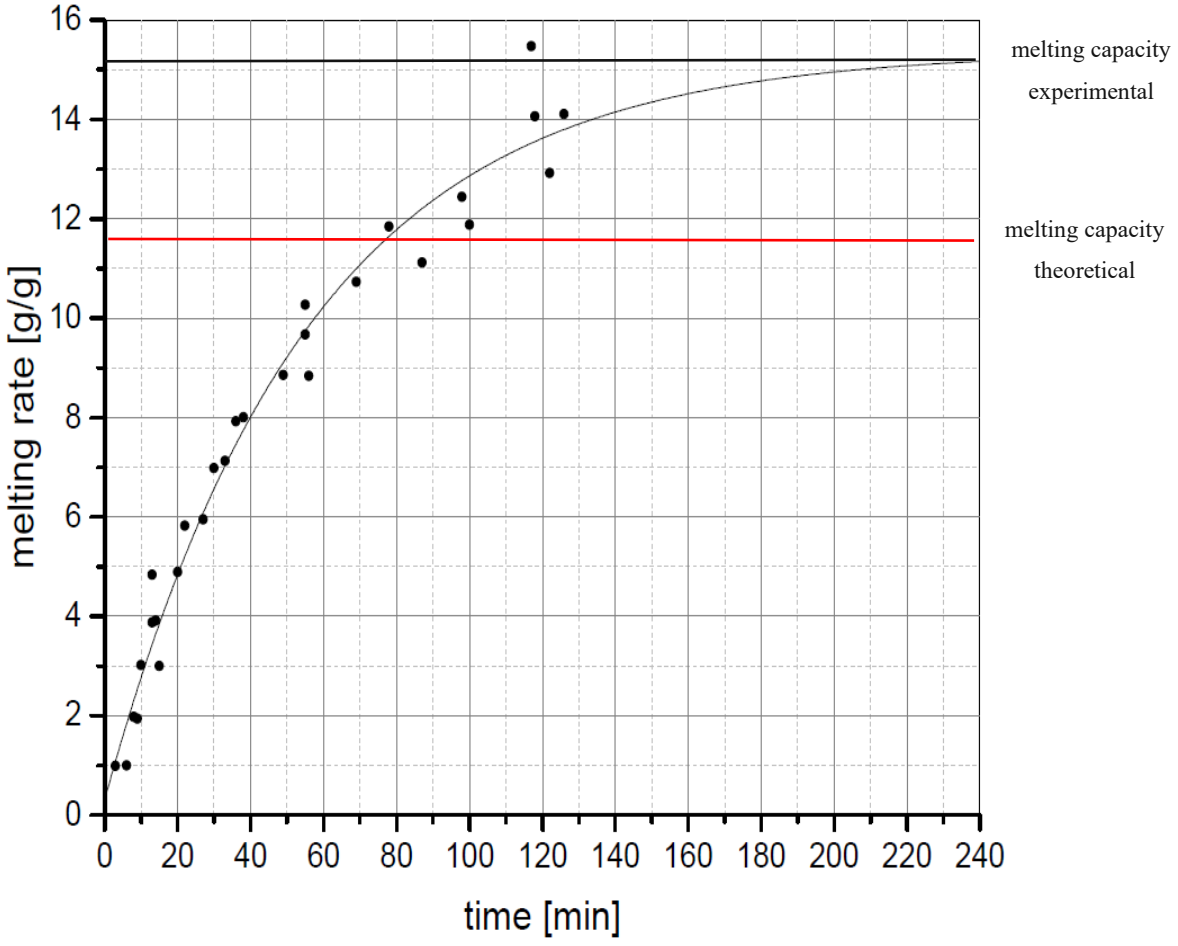

Figure 14: A graph of the melting rate of NaCl, at -5,0°C, in the beginning of development. Additionally shown are the measured melting capacity value (melting capacity experimental) and the melting capacity value from literature (melting capacity theoretical)

Some testing proofed if the size of the ice cubes changed the results, but only the melting rates altered slightly, and the capacity stayed the same. The next step was to switch the process around, which means to give the ice cubes onto the provided melting agent. This gave some nearly linear graphs as shown in figure 15. We assume that the offset relates to the different immersion levels the samples pass through in the time of melting. Some ice cubes provide high surface to the salt, simply because of the way they are located in their vial. Others are immersed just with a tip. Greater surface early means quicker melting, which provides more molten water, which consequently provides even more surface and better thermal conduction. This would mean that the melting time would depend on the orientation of the ice- samples, and the deviation would be multiplicatory, because early melting would mean faster melting time and the lack of early melting would prohibit further temperature exchange and therefore slow the

process even more down. This would also explain the worse statistical correlation of this experiment. So, we switched back to the process where we provided the ice- cubes before and put the melting salt on top of the samples.

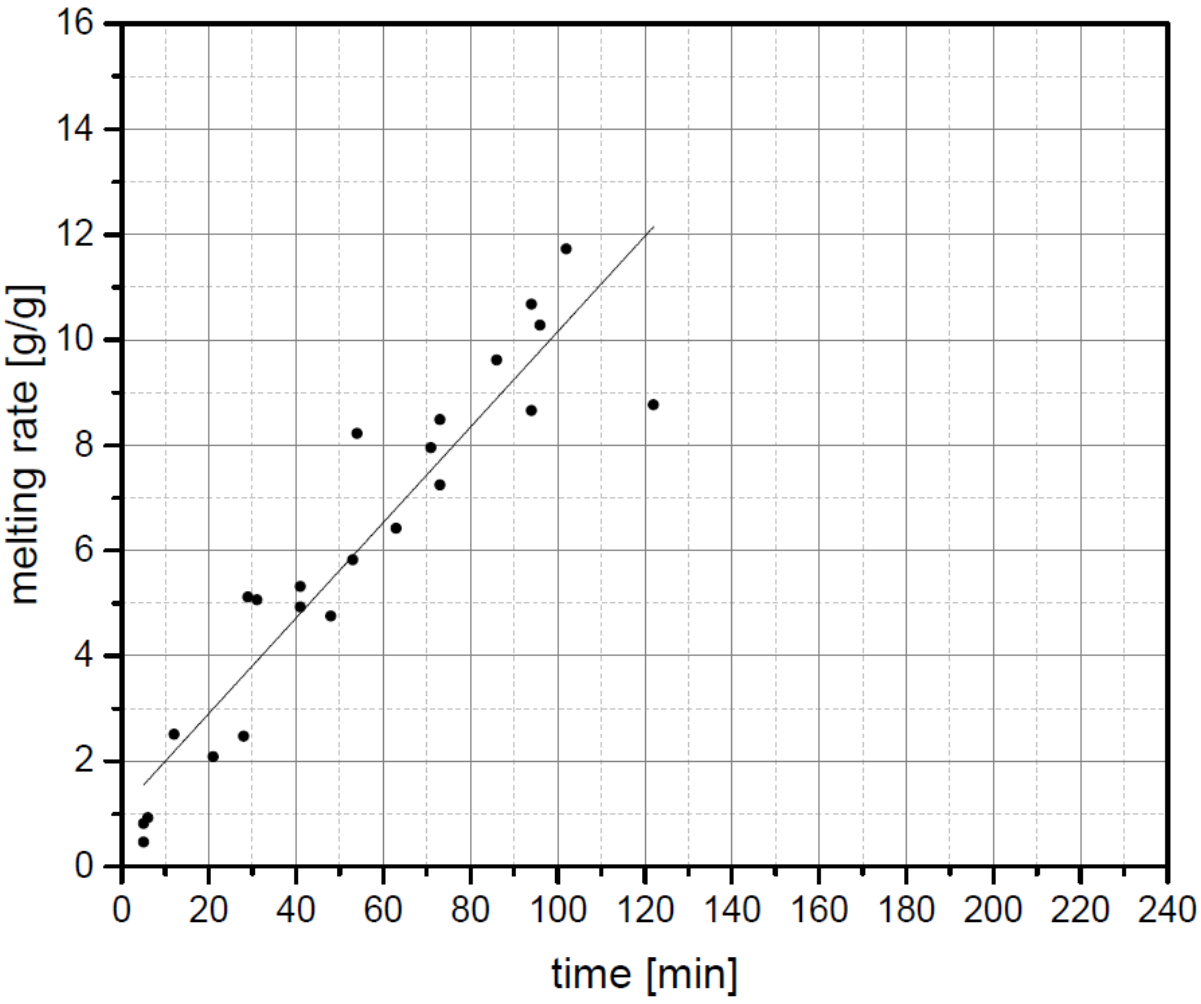

Figure 15: A graph of the melting rate of NaCl, at -5,0°C, where ice was given onto the salt instead of reversed.

Finally, a more severe problem was discovered. Since a camera is installed above the bath of the cryostat, the insulating coverage of the cryostat is not placed onto the cooling bath. The cover would block the camera from taking pictures of the samples. This exposes the samples to the environment in the laboratory air. Normal lab conditions comprise a temperature of 20°C and a pressure of about 1000 mbar. The vial plates used for this experiment consist of polypropylene, which does not have a good heat conductivity, so the samples were somewhat insulated. The cooling of the cryostat bath always stood in contrast to the heating of the lab environment, and lead to a different temperature in the sample vial than the cryostat, or the environment for that matter. Before, the results were always compared to the theoretical values for the bath temperature, that is why they were too high. The temperature in the plates was a

little higher than the coolant substance in the cryostat bath. With that came the problem of an accurate temperature measurement inside the vial. The cavities of the sample holder were too small to fit in a thermocouple. So, to be able to measure the temperature in such a cavity, another, larger vial, consistent of the same material, was placed into the bath. This vial was filled with a high concentrated sodium chloride- water solution, so that it would remain liquid at the low experiment temperatures. In this vial a thermocouple (ATEX p600-EX) was installed to control the vial temperature. Then the temperature of the cryostat bath was adjusted to get the vial temperature to the desired values. There was always a difference of +1°C, so for a sample temperature of -5,0°C, the cryostat had to be adjusted to -6,0°C. With these corrections the new cryostat setup was far more stable and accurate than the climate chamber experiment. We were now able to meet the theoretical melting capacity within a range of 0,5 g/g. We used this setup as our main experiment. As section 4.1 shows this method was used to measure and compare melting rates and melting capacities of all melting agents and combinations of those. Figure 16 shows the melting rate curve of the final cryostat setup compared to the climate chamber. We can see that the melting capacity of the cryostat experiment is clearly closer to the theoretical value of 11,8 g/g than the climate chamber experiment.

After the experiment was finally finished some additional tests were carried out to optimize the process. We wanted to know how long the samples took to adjust to the temperature of the cryostat from the freezer. This was done by filling an Eppendorf vial with the same amount of salt water the samples would have. Then a thermometer was placed into the vial and the time it took to adjust to the cryostat temperature was taken. The vial was the same material as the vial plate we used for the experiments which should have a similar heat conductivity and capacity. After just 15 minutes the saltwater sample had increased its temperature from -20°C (from the freezer) to -6°C, which was the measurement temperature. This experiment showed that it would suffice to leave the samples for 20 minutes it the cryostat before starting the measurement.

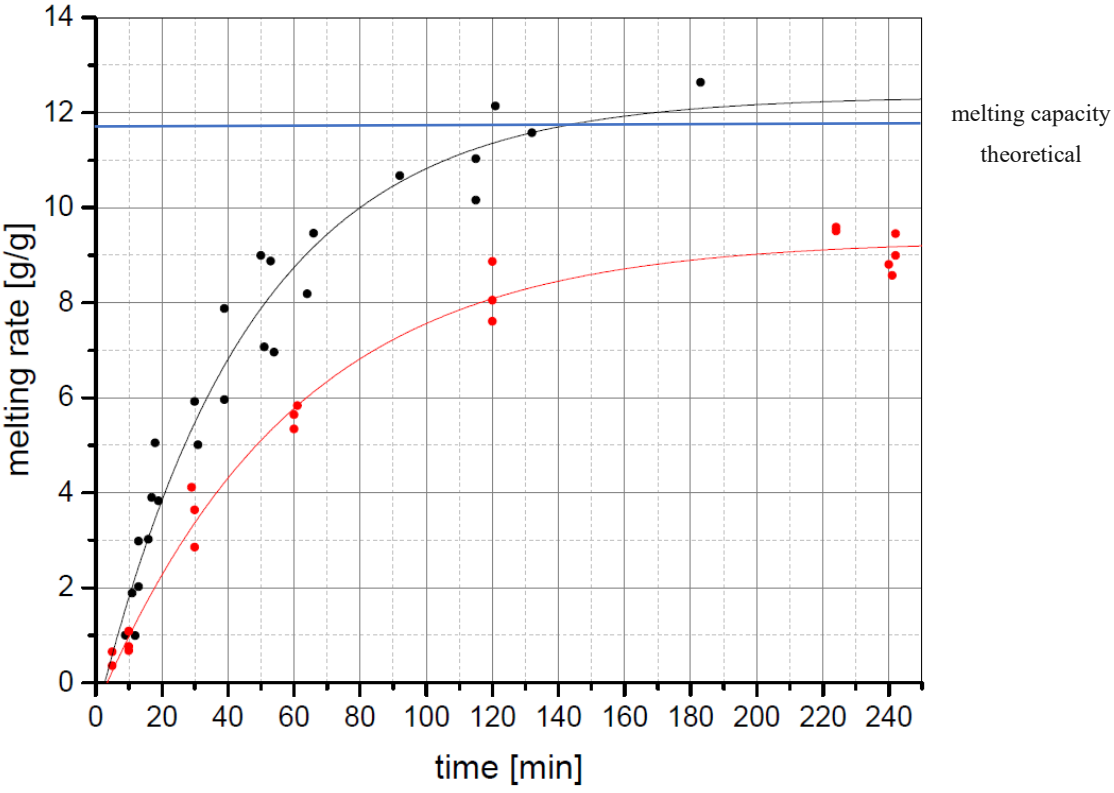

Figure 16: Comparison of the two melting rate experiments at -5,0°C: cryostat (black) shows a melting capacity of 12,3 g/g and climate chamber (red) with a melting capacity of 9,2 g/g. These graphs are fitted with a sigmoid function to represent the asymptotic trend. Also shown is the melting capacity of NaCl at -5°C, taken from literature (blue line).

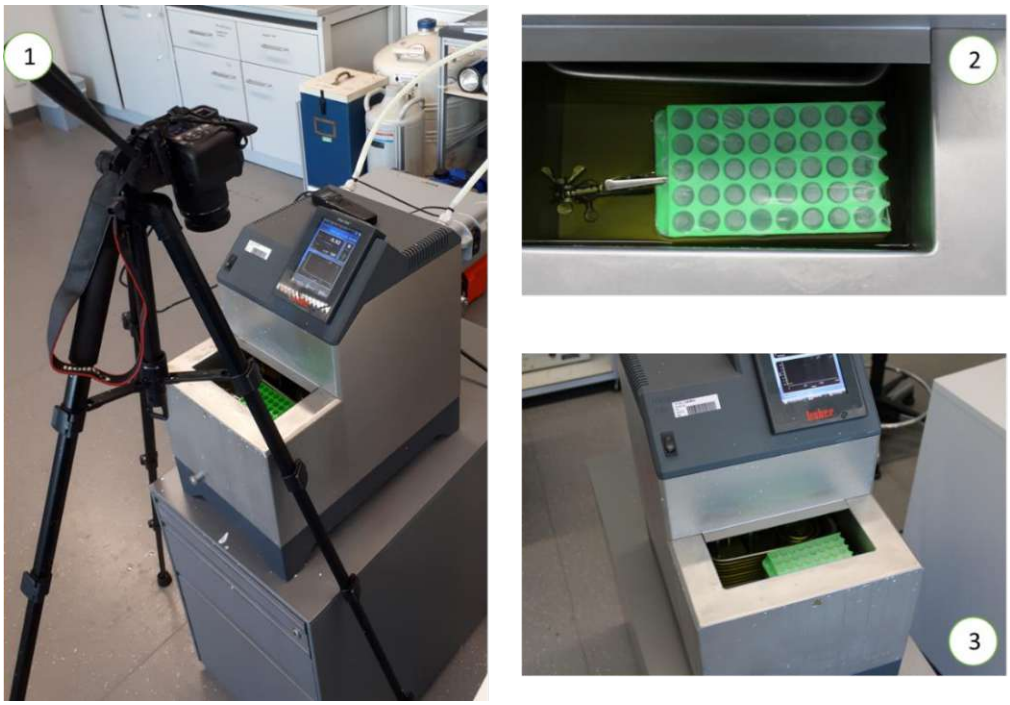

Figure 17: Some pictures of the final melting rate setup. Image 1 shows the experiment itself, the ice cubes in the green vialplate are slowly melting and the camera is recording the process. Images 2 and 3 show the samples cooling down to the desired temperature.

As mentioned in the introduction the goal of this project is to measure and compare the melting rate of different de-icing salts. We used this setup to do that and the salts we used are listed in the table below. The symbols we used are just abbreviations, not always the correct chemical formula, we used them to label samples and results. These symbols come up again in later parts of this thesis again but are always explained.

Table 2: List of used de-icing salts

Name	Formula	Symbol
Sodium chloride	NaCl	NaCl
Sodium acetate	$CH_3COONa.3H_2O$	NaAc
Sno- N- Ice		SNI
Potassium carbonate	K_2CO_3	K_2CO_3
Magnesium chloride	$MgCl_2.6H_2O$	$MgCl_2$
Calcium chloride	$CaCl_2.2H_2O$	$CaCl_2$
Sodium formate	CHO_2Na	NaFo
Potassium acetate	CH3COOK	KAc
Potassium formate	CHO_2K	KFo
NaCl + 8% Glucose		NaCl + Glu
NaCl + 8% Arabinose		NaCl + Ara
NaCl + 8% Mannose		NaCl + Man
NaCl + 8% Maltose		NaCl + Mal

From these substances we measured the melting rate and determined the best suited to be used for winter maintenance on a railroad platform. As table 2 shows not only pure de-icing agents were used, in some cases we tested salts with water of crystallisation included. This was done deliberately, because pure salts are usually much more expensive that the ones with water of crystallisation. Sno-N-Ice is a commercially available de-icing product, combining the high melting rate of sodium chloride with good anti- corrosion behaviour due to some patented organic components. It was requested by our clients ÖBB, that we include this commercial product in our experiments.

3.2 Corrosion

Experiments on metal corrosion in this thesis had two main goals, a) the corrosion process itself and b) the qualitative and quantitative analysis of corrosion products and the corroded metal surface.

Typical materials used on ÖBB platforms are unalloyed steel (EN 10025 S235JR), copper and galvanised steel. We used plates of 15 cm length, 10 cm width and with a thickness of about 2 mm. As first attempt the process of corrosion was basedon the salt spray test (DIN EN ISO

9227). This highly standardized test was used as starting point but was modified to fit the further requirements of our experimental needs. The difference between DIN EN ISO 9227 and our experiments was that in the standard procedure different metal materials are placed in the same NaCl spray. We wanted to vary the salt sprays and leave the metal samples the same. This required some differences in spraying nozzles and storage of the samples during the experiment. The first structure we came up with was an open box made of acrylic glass. Figure 18 shows a simple drawing of this setting.

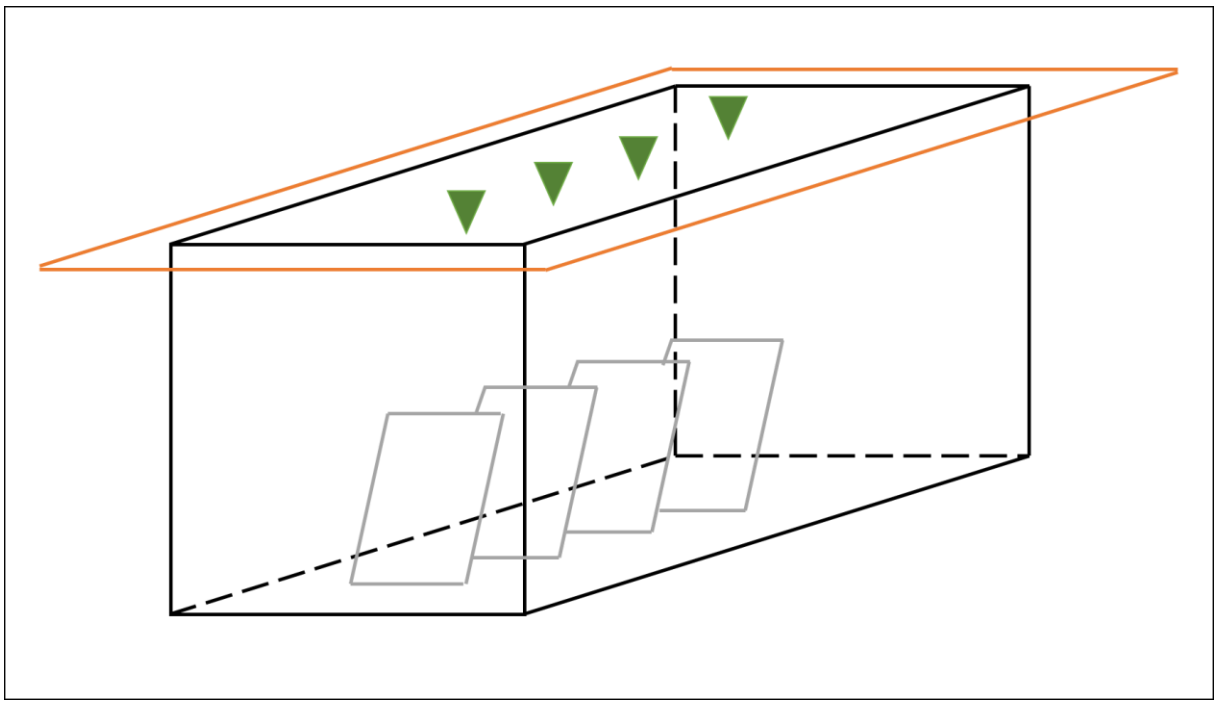

Figure 18: Sketch of the first corrosion chamber: An open acrylic glass box with a sheet of Styrofoam on top (yellow). In this Styrofoam sheet are 4 holes filled with garden sprinkler nozzles (green), which spray the salt solutions onto the metal samples (grey). At the bottom of the box is a hole which leads into a hosepipe so the used solution can discharge.

The dispersion system for this method are garden sprinkler nozzles made from polyethylene. These nozzles are not as small as the ones used in the standardised test and should therefore be a lot more resisting against clogging and breaking down. The nozzles were linked to a submersible garden pump (KÄRCHER sp1 dirt), which stands in a container, filled with the salt solution. At first the discharged fluid was directed back to the container with the pump and used again to spray onto the samples. This idea was quickly rejected because the standard (DIN9227) states that metal ions in the salt solution can interfere with the corrosion process. This means that the corrosion products which were washed down from the sample plates would in turn be sprayed on the samples again, which could have a different effect on every single plate, which in turn leads to entirely avoidable statistical errors. So, we decided to spray with fresh salt solution only. This decision came with its own problems, the most pressing being that

the garden nozzles had a way too high throughput to be sustainable for an experiment which was set to be about 3 weeks in time.

The first attempt at a change was to use other nozzles. Basically, there are two types of spray nozzles, two- substance nozzles and impingement nozzles. Two- substance nozzles use compressed air to break up the liquid stream into very small droplets. This is what is used in the standardized test described earlier. These nozzles are very precise and efficient but have the disadvantage of being very expensive. Impingement nozzles use the geometry inside the nozzle to disperse the liquid and are more versatile because they do not need an air connection and are way cheaper. Two different types of impingement nozzles and a pump which could comply with our requirements of pressure and throughput were purchased. Testing these nozzles in relation to spray pattern and flow volume was carried out and supplied sufficient results, but after a few days every single nozzle started to clog up and lowered the flow volume until it stopped completely. After some further testing and examining the insides of the nozzles it became clear, that they had started corroding. The constant contact with salt solution corrodes all kind of iron alloys, even stainless steel. So, the next step was to try out similar nozzles with ceramic inner parts. Again, this worked well for some time but then started to clog up completely. It turns out, even if the inner parts of the nozzle are made from ceramics, the casing and inlet are made of steel, which corroded in the process. These experiments consumed 4 weeks and 15 nozzles. Finally, we abandoned this system and got back to the plastic nozzles. To balance the high flow through we built an automatic switch, which made sure that the system sprayed in regular, periodic intervals of 3 min and then paused 117 min for drying the samples. This was the only setting which allowed spraying with an appropriate amount of salt solution. We would have liked it to spray every hour for a shorter period, but the storage space on the automatic power plug was too low, so we had to use the mentioned spray pattern. This setup still needed about 30 L of salt solution per day, which still is huge amount, but just barely manageable for us.

We corroded the metal samples with different de-icing agents in our corrosion chamber, only to find after a while that the produced results were not stable enough to support a solid statistical analysis. The problem was that the corrosion was way too slow and did not produce significant change in mass before and after the process.

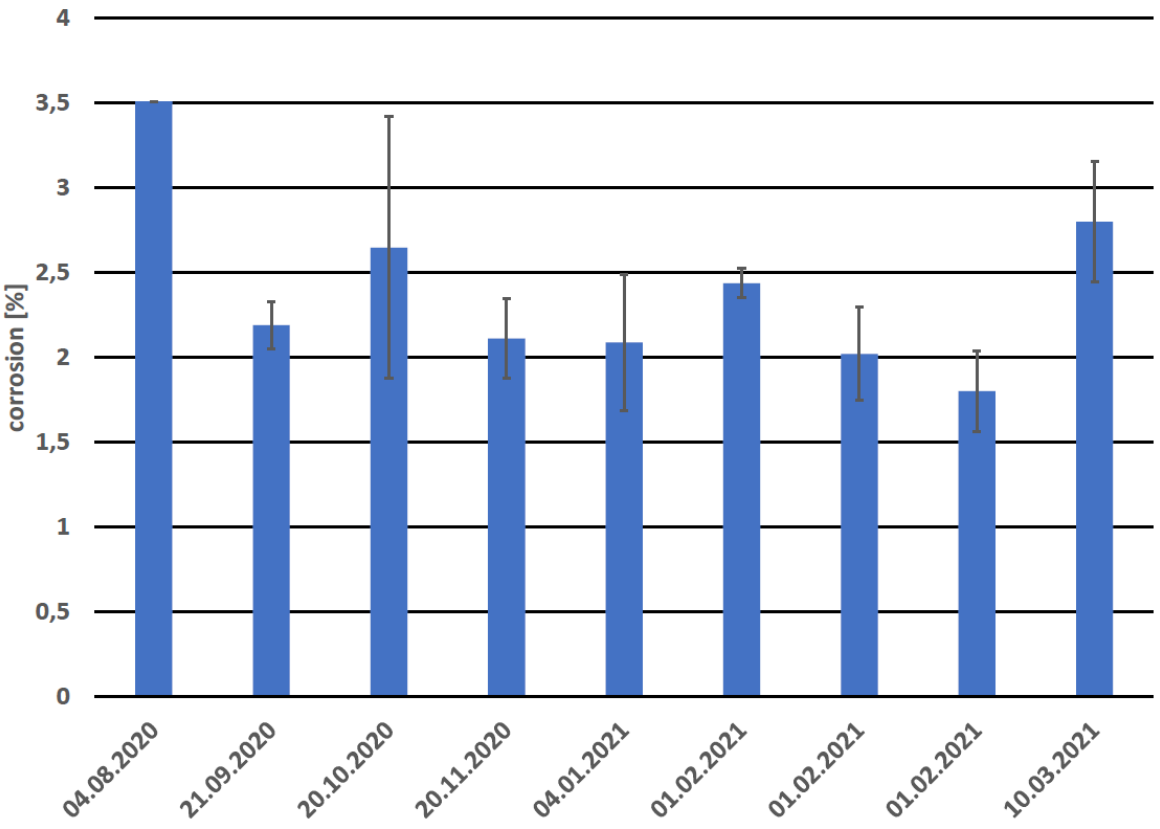

Figure 19: Comparison of the experiments in the spray chamber. Here are the results of the de-icing agent NaCl on the iron plates. These are the only samples that produced usable results, copper and galvanized iron showed even less corrosion. The figure shows very different results of some experiments even though the conditions were the same. It also shows a fairly high standard deviation compared to the absolute values. The graph shows a deviation of about 1% with a mean result of 2,2%.

We decided to design a different type of corrosion chamber. Firstly, we improved the spraying pattern. In the standardized test the samples are befogged the whole time, whereas with our experiments only every two hours the solution was sprayed onto the plates. We managed to get different automatic power plugs which could switch on more often, and settled on a pattern of spraying for 1 min every 45 min. However, the corrosion only rose marginally, making the spray pattern basically irrelevant. Our conclusion was that the different results were due to the different environmental influences like temperature and air pressure, during the spray experiments. This was an inherent problem, because the laboratory room in which our chambers were situated, was way too large to completely control temperature and air pressure.

In search for alternatives, we tried submersing the plates in the salt solution. That approach would be way easier to control, and it would not consume such horrendous amounts of salt. Only one metal plate would be placed in a small container filled with 1 L of a 5% de-icing agent solution. After 3 weeks the plates were processed like the spray samples and weighed. These experiments showed even less corrosion than the spray chamber samples. Another redesign was

needed. The final setup allowed us to submerse the plates for a defined period of time and then lift them up to make contact with air, then the samples were submersed again. This would go on for the 3 weeks the other experiments lasted as well. The pattern we chose was 10 min in the solution, then 50 min out in the environment, as suggested by test results shown in figure 20. One big advantage of this system was that the size of the setup is small and robust, so it could be placed in the climate chamber and investigate the corrosion behaviour at different temperatures. Finally experiments with this periodical immersion at a temperature of 35°C showed enough corrosion to be reproducible and we were able to measure the metal- salt combinations

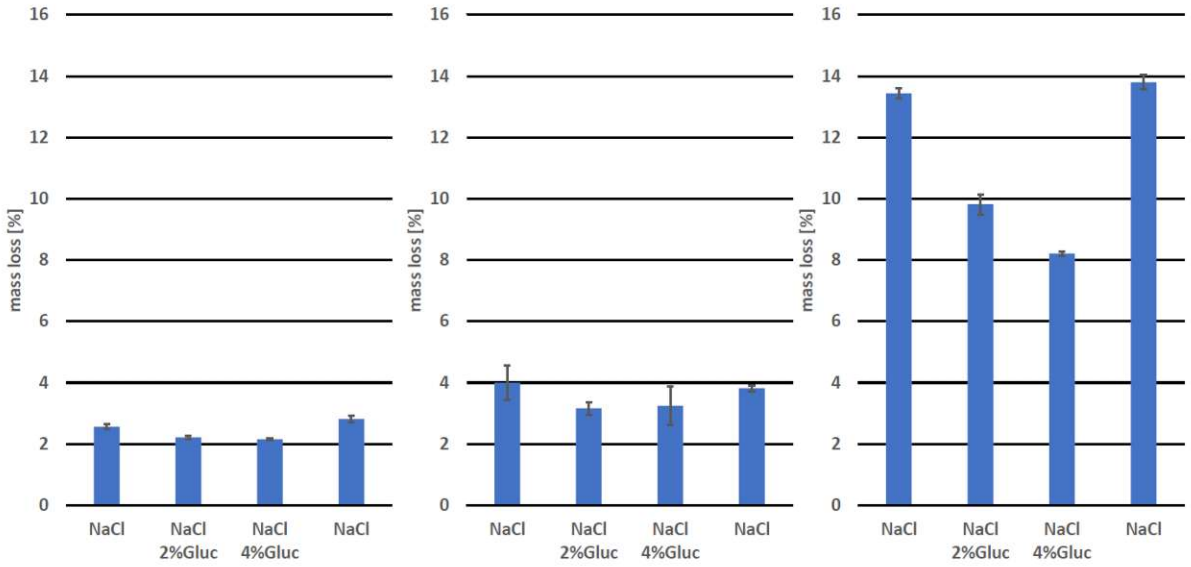

Figure 20: Here shown is the comparison between lifting patterns and different temperatures from the immersion experiments. We ran 3 experiments, the first one at room temperature with a immersion cycle of 1 min in the solution and 30 min out. The results can be seen in the left. The second experiment was also at room temperature but with a cycle of 10 min in and 50 min out, results in the middle. The last experiment was in the climate chamber at 35°C with a cycle of 10 min to 50 min, and the results are shown on the right. Each of these experiments contained four stands, with two containers filled with NaCl solution and container each with a NaCl/Glucose mixture of different concentrations.

For efficiency purposes we used 12 stands which could hold up to 3 sample plates each and would lower them into a container filled with the different salt solutions. These stands were put in a small temperature-controlled transport container. To prevent the steel container from corroding from splashes of salt water, the whole inside was covered with plastic foil and tape. Finally we had an operating corrosion process system (Figures 21 und 22).

Figure 21: A picture taken of the final corrosion system. The grey containers are filled with different de-icing salt solutions. Every hour the sample plates are immersed into the solution for 10 minutes. Then they are lifted to give the oxygen time to corrode the metal.

Figure 22: A picture of the final setup. Three of the corrosion systems are stationed in a temperature- controlled transport container.

To round up the experiment we had to get rid of the corrosion products on the metal surface of the plates. The standard (DIN9227) suggests dibasic Ammonium citrate as rust solvent and so we submersed the corroded plates in a 20% solution of the solvent for one hour. Subsequently the rest of the corrosion products were mechanically removed. This method proved to be very time consuming and did not remove all the rust. So, we decided to apply an ultrasonic cleaning bath to get rid of the corroded metal more efficiently. After some testing with different liquids as cleaners we deemed the dibasic ammonium citrate as the best solvent.

To summarise: The final experiment we used for our measurements was a 7 step process. a) plates of different metals were cleaned with water and acetone and then completely dried, usually overnight, at a temperature of 50°C. b) The dried plates were weighed, and pictures were taken for documentation. c) The samples were placed in an immersion stand inside a temperature-controlled container at 35°C. This stand lifted the plates automatically in and out of a container with salt solution for 21 days. The pattern we used for immersion was 10 min in the solution and 50 min out in the environment. The salt solutions were changed every 7 days. d) After the corrosion process was finished the plates were taken out their stands, rinsed with water and dried at 50 °C. This step was put in before the actual cleaning process because we noticed that dry rust was way easier to remove than wet rust. e) After drying, the plates were photographed and then placed in an ultrasonic bath filled with a 20% solution of dibasic ammonium citrate and cleaned until no more corrosion products were noticeable. f) In addition, the plates were weighed after certain time periods and deemed clean when the weight did not go down noticeable. g) After that the plates were dried one last time and weighed for the final mass loss results. After that, pictures were taken of the clean and dried samples. This process produced following results: a line of pictures of all samples, one before the corrosion process, one with the process finished and the plate full of rust and one of the rust- free, cleaned samples. The second result being of course the difference in mass before and after corrosion, from which the different de-icing solution could be compared in their corrosiveness.

Figure 23: This picture shows the development of one Fe- plate during our corrosion process.

With this process we decided to run all experiments, so that we could compare the corrosion behaviour of our de-icing agents on different materials. Table 3 shows the different substances we used, as well as the substances we mixed with NaCl to test the corrosion inhibition.

Table 3: List of used de-icing agents

Name	Formula	Symbol
Sodium chloride	NaCl	NaCl
Sodium acetate	$CH_3COONa.3H_2O$	NaAc
Sno- N- Ice		SNI
Potassium carbonate	K_2CO_3	K_2CO_3
Magnesium chloride	$MgCl_2.6H_2O$	$MgCl_2$
Calcium chloride	$CaCl_2.2H_2O$	$CaCl_2$
Sodium formate	CHO_2Na	NaFo
Potassium acetate	CH_3COOK	KAc
Potassium formate	CHO_2K	KFo
Calcium magnesium acetate	$(CH_3COO)_2(Ca,Mg)$	CMA
NaCl + Glucose	$C_6H_{12}O_6$	NaCl + Glu
NaCl + Arabinose	$C_5H_{10}O_5$	NaCl + Ara
NaCl + Mannose	$C_6H_{12}O_6$	NaCl + Man
NaCl + Maltose	$C_{12}H_{22}O_{11}$	NaCl + Mal
NaCl + glycerine	$C_3H_8O_3$	NaCl + Gly
NaCl + potassium carbonate		NaCl + K_2CO_3
NaCl + potassium acetate		NaCl + KAc
NaCl + potassium formate		NaCl + KFo
NaCl + sodium acetate		NaCl + NaAc
NaCl + sodium formate		NaCl + NaFo

Additionally, we tested the concentration effect of the corrosion inhibitors. The corrosion rate of NaCl mixed with different amounts of Glucose was measured, to determine the amount of sugar or other inhibitor material was needed to gain the optimal effect.

3.3 Profilometry

Atomic Force Microscopy (AFM)

In a first attempt we tried to use AFM measurements to take some of the sample plates, corrode them as described in chapter 3.2, but do not get rid of the corrosion products with the ultrasonic bath. The uncleaned plates would be placed under the AFM and analysed. We hoped to find some correlations in roughness and mass loss, compare the corrosion on iron, copper and galvanised steel and investigate some characteristic corrosion patterns, like for example, pitting corrosion, induced by the chloride ion, on the metal surface.

However, the first problem we encountered was the size of our samples. Thy AFM setup we used was a WITEC alpha300 RSA+ system, where the microscope stage was just too small to mount the 15 cm x 10 cm plates. We had to cut the samples with an angle grinder into smaller pieces, which would fit onto the sample stage. This led to some abrasion of rust, but on the inner space of the new smaller plates our sample was still intact and could be measured.

The measurement with the AFM- tip itself also proved to be difficult, because of the roughness. We decided to measure 30 µm x 30 µm squares on different spots of the sample surface. The difference in height, even in these tiny squares, was too much for the AFM- setup to handle, resulting in a few broken tips and some non- interpretable texture measurements. Basically, it was impossible to obtain results with any statistical merit. We had to look for another method, one that had to be less sensitive and therefore not as susceptible to the roughness of our sample.

Laser Profilometry

Our method of choice was the Laser profilometry. It has a similar operating mode as the AFM, gives virtually the same result, but is way less sensitive. This means that processes on an atomic level are not possible to examine, but for the roughness comparison, it suffices completely. The setup used was the FRT microprof 100, with a provided evaluation software called FRT Mark 3, where we had the advantage of this specific machine often being used to measure asphalt samples. This means it had a custom-built sample table, which is specifically made to hold larger objects. So, here there was no problem in mounting the whole sample without cutting it before. It was also possible to analyse much larger areas of the samples, making this the system of choice for our texture measurements.

As samples we chose the corroded and cleaned plates. Our experience with the plates led us to expect that we would get more consistent results with the samples after cleaning. The scanned part of the sample was a rectangle with a size of 4 cm x 1 cm, in the middle of the sample plate, the lateral resolution was 50 µm. The custom- made sample table allowed for a very precise mounting of the sample, exactly in the middle. This rather unusual scanning shape was chosen to represent the sample better. The nature of our corrosion chamber determines that the de-icing solution flows down the sample plates, leaving grooves in irregular intervals in the sample. The shape of the scanned area should account only for a few grooves but at a higher length. From this way of measuring, we expected a better statistical accuracy.
The results are plotted in chapter 4.

3.4 X- Ray Photoelectron Spectroscopy (XPS)

The XPS measurements were done by the Analytical Instrumentation Centre (AIC) of the TU Wien. There the samples were analysed with a SPECs XP spectrometer. Radiation was generated by an Al Kα – radiation source (µFocus 350, 1486,6 eV) and detected by a WAL-150 hemisphere analyser. Passage energies were 100 eV or 30 eV, increments were 0,5 eV or 50 µeV, depending on the kind of measurement. The first settings were used for survey spectra, the second for detail spectra. The incitation energy was 1486,6 eV with an average radiation angle of 51°, pressure in the chamber was $2x10^{-9}$ mbar. The spectra were calibrated like stated in ISO 15472. Data analysis was done with CASA XPS software.

A range of samples was measured, one from each of our materials, iron, copper, and galvanised steel. From each material we selected three samples, one completely uncorroded, one corroded with NaCl and one corroded with NaCl mixed with 3 % Glucose, to compare the corrosion progress against a zero- point and to find out to which extent Glucose can lower the corrosion rate. The sample plates were cut with an angle grinder to pieces with a size of about 1 cm x 1 cm, to ensure the measuring chamber could be loaded with all samples at the same time. Figure 24 shows the samples inside the chamber with their respective points of analysis.

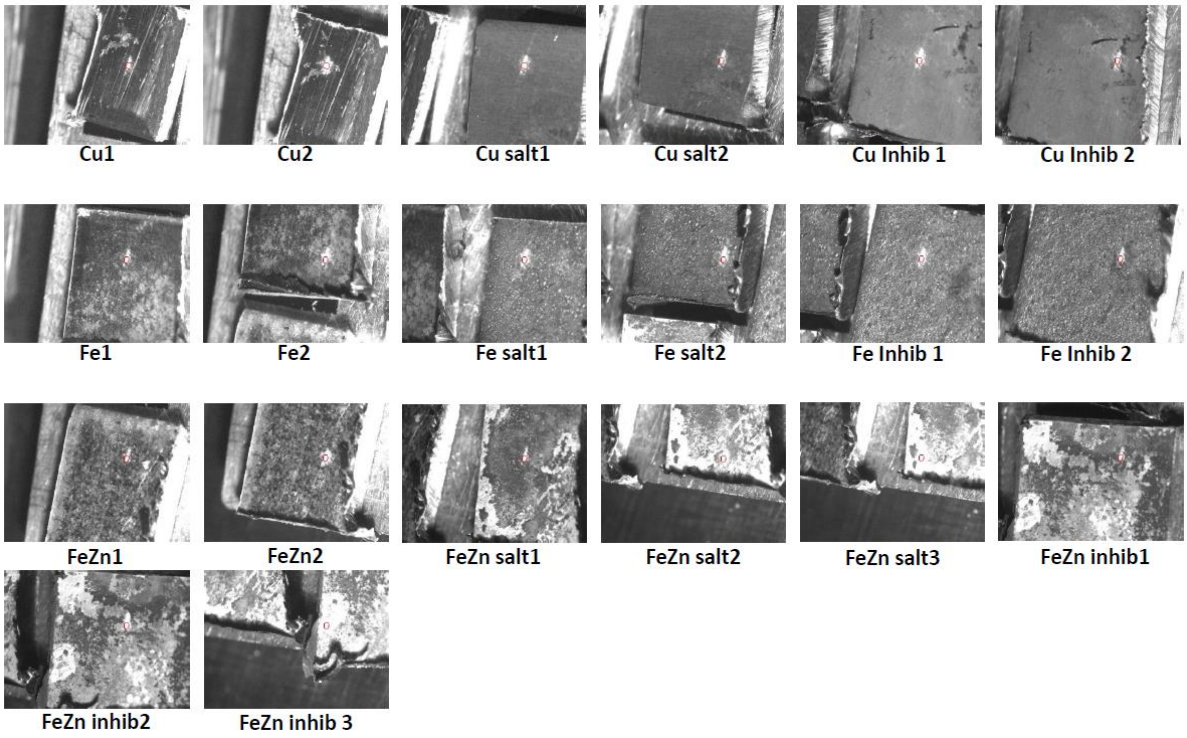

Figure 24: A picture of the XPS samples inside the measuring chamber. Every sample was measured at two or three different points to get information of local differences in chemical composition of the surface.

At the first measurement the analysis stated that the main component in our samples is carbon, which was because of the amount of dust which had settled on the sample surface. Due to the extreme surface sensitivity of the XPS this layer of dust was responsible for most of the signals from this measurement. To gain better data the iron samples were transferred into the sample chamber again, the chamber was evacuated, but then the samples were heated to 415°C for 60 minutes. This should desorb the dust particles and make it possible to take XPS spectra of our samples. At the second trial the experiment worked properly, and the results are discussed in chapter 4.

3.5 X- Ray Diffraction (XRD)

To measure the bulk composition of the corrosion products formed on the sample we used powder x- ray diffraction. To get samples we used plates right after the corrosion process. Before they were cleaned in the ultrasonic bath the rust was mechanically removed and collected. This was only possible with the iron plates, copper did not produce meaningful amounts of corrosion products, while the products of the galvanised steel plates parted by themselves during the corrosion process and then partly dissolved in the salt solution.

The collected iron rust was dried, pulverised and then taken to X- Ray Centre of the TU Wien. There it was analysed by a Bragg- Brentano diffractometer Philips Empyrean with copper radiation and a Gallipix detector. Evaluation and assignment were performed with a PDF4+ data- base.

In all samples residual amounts of the de-icing salt were found. These amounts were abstracted from the measurement because they are obviously no corrosion products. So, the results show a relative chemical compensation corrected for the salt amount in the sample.

4. Results and discussion

4.1. De-icing agents

4.1.1. Melting rate

Melting rate curves of different de-icing salts and NaCl with additives have been measured. Table 4 gives names, formulas, and symbols of used salts. Figure 25 refers to the abbreviations in this table.

Table 4: List of used de-icing salts

Name	Formula	Symbol
Sodium chloride	NaCl	NaCl
Sodium acetate	$CH_3COONa.3H2O$	NaAc
Sno- N- Ice		SNI
Potassium carbonate	K_2CO_3	K_2CO_3
Magnesium chloride	$MgCl_2.6H_2O$	$MgCl_2$
Calcium chloride	$CaCl_2.2H_2O$	$CaCl_2$
Sodium formate	CHO_2Na	NaFo
Potassium acetate	CH3COOK	KAc
Potassium formate	CHO_2K	KFo
NaCl + 8% Glucose		NaCl + Glu
NaCl + 8% Arabinose		NaCl + Ara
NaCl + 8% Mannose		NaCl + Man
NaCl + 8% Maltose		NaCl + Mal

The column diagram in figure 25 shows the melting rates of the de- icers after a duration of 60 minutes. This time value has been proposed by our clients at ÖBB for comparison with their in-house standards. Table 5 shows the melting rates at different durations.

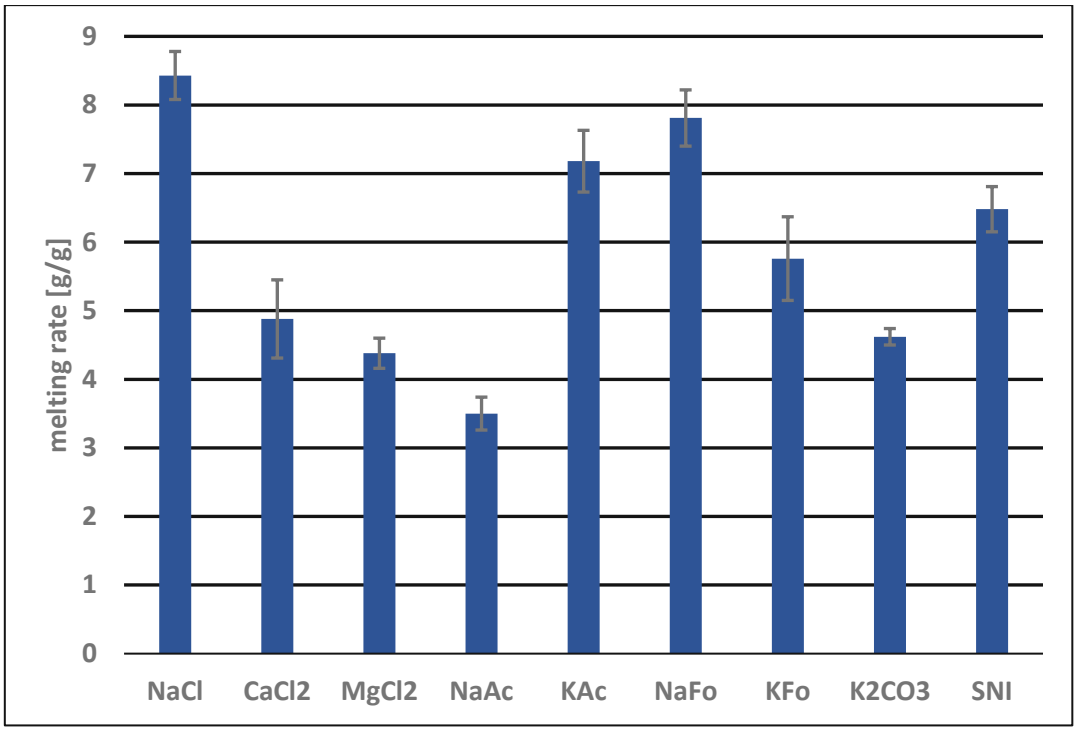

Figure 25: Results of the melting rate experiments at a time of 60 min

Table 5: Melting rate results

De-icing salt	Melting rate [g/g]		
	30 min	**60 min**	**100 min**
NaCl	5,27	8,43	10,76
$CaCl_2$	3,12	4,88	6,10
$MgCl_2$	2,74	4,38	5,59
NaAc	1,99	3,50	4,98
KAc	4,64	7,18	8,87
NaFo	5,00	7,81	9,74
KFo	4,39	5,76	6,25
K_2CO_3	2,96	4,62	5,76
SNI	3,91	6,48	8,60

NaCl has the highest melting rate of all tested de-icing agents, closely followed by sodium formate and potassium acetate. Interestingly, the Sno- N- Ice ® product which is on a NaCl basis with little organic additives has a significantly lower melting rate than pure NaCl. De-icers which performed the worst are $CaCl_2$, $MgCl_2$ and NaAc. The crystallization status of these three components include water of crystallization, therefore the concentration of these salts is lower as in pure de-icing agents, which explains their extremely low melting rates.

Figure 26 shows the comparison of the melting curves of pure NaCl and NaCl + 8% of different sugars, which act as a corrosion inhibitor. None of the sugars has a significant impact on the

melting rate of NaCl, the graph just shows marginal differences in melting rate until the 100 minute- mark. Interestingly, the shape of the curves differs between the sugars. While arabinose and maltose cause a lower melting rate at the start, they catch up at the end and converge towards a common melting capacity, glucose and mannose are at the start completely indistinguishable from the pure NaCl. While glucose always comes close to the melting rate of NaCl, mannose stops increasing sharply at around 60 minutes and trends towards a lower melting capacity than all the other sugar additives. We concluded that at 30 min to 60 min – which have been chosen as benchmark for this project – the melting rates are not that much lower, so that the addition of sugar is justified as a viable option for a de-icing agent. Detailed melting rate curves with statistical evaluation can be found in the appendix of this thesis.

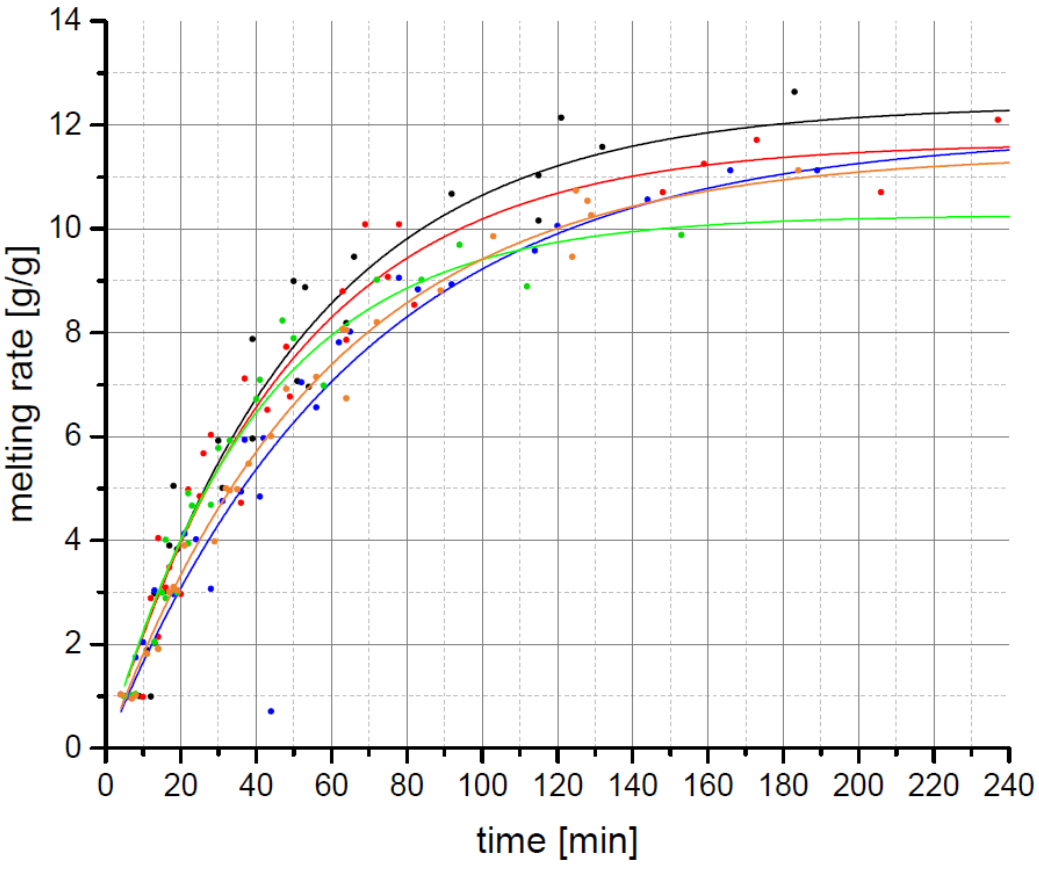

Figure 26:Melting curves of NaCl (black) and NaCl with added 8 % of different sugars. Shown are glucose (red), arabinose (blue), mannose (green) and maltose (orange).

4.1.2 Corrosion behaviour

Figure 27 shows the mass loss due to our corrosion process. Table 6 shows again shown the used salts with the short symbols. The results in figure 27 represent only the iron sample plates.

As described in literature (Křivý et al., 2019), the most corrosive salt is NaCl. Comparing all the tested de- icing substances, it has by far the highest mass loss with 14,18 w%. The Sno- N-Ice ® product shows significantly lower mass loss than pure NaCl (10,63 w%).

The other chloride containing de-icing agents - calcium chloride and magnesium chloride – show surprisingly low corrosion behaviour. Here the water of crystallisation had no impact because we adjusted the amount of salt stoichiometric, so that the concentration of pure salt would be exactly 5 %. Hence, the mass losses, 5,4 % of $CaCl_2$ and 3,72 % of $MgCl_2$, are directly comparable to every other de-icing salt.

The by far best corrosion behaviour was found for potassium carbonate. It is the only substance which has a mass loss lower than the reference value of pure water (H_2O in the diagram), namely 0,88 %. Sodium acetate and potassium acetate have a similarl corrosion behaviour with 4,43 % and 4,53 %.Sodium formate and potassium formate show the worst corrosion behaviour of any of the groups with 6,03 % and 10,02 %.

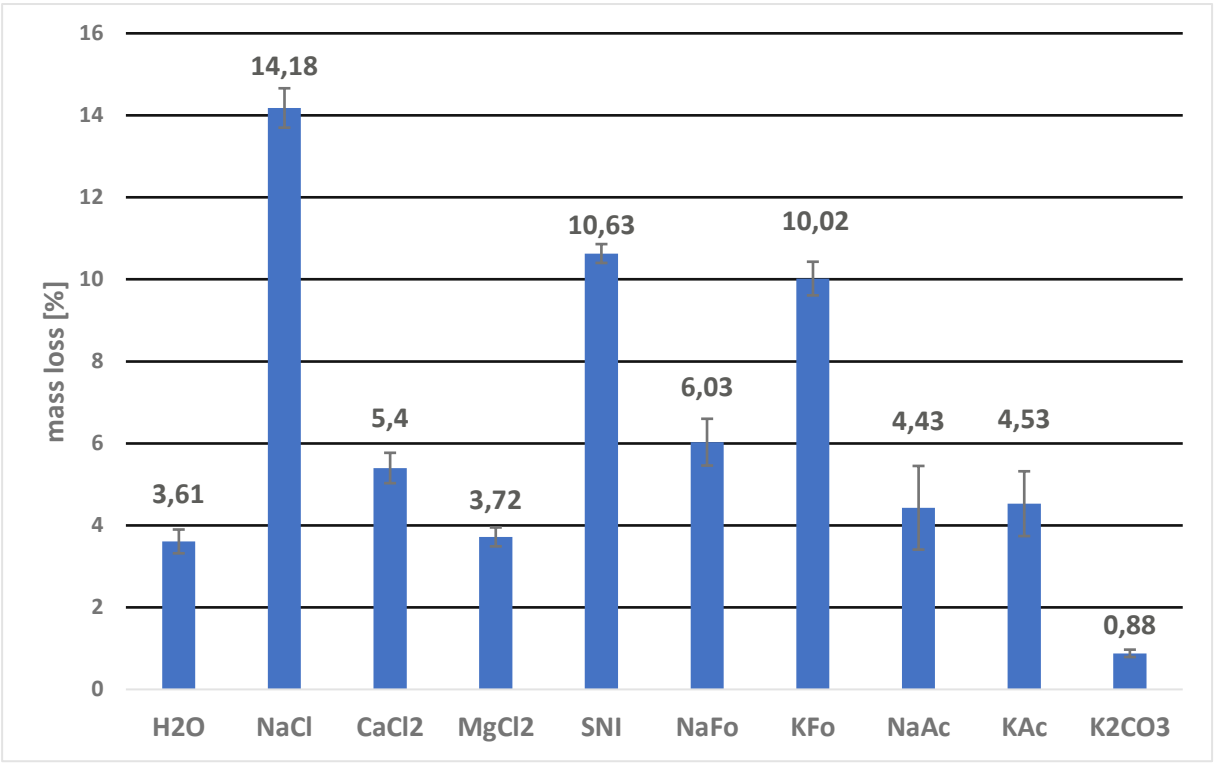

Figure 27: Depiction of the results of the corrosion from different de-icing salts of iron samples

Table 6: List of depicted de-icing agents

Name	Formula	Symbol
Sodium chloride	NaCl	NaCl
Sodium acetate	$CH_3COONa.3H2O$	NaAc
Sno- N- Ice		SNI
Potassium carbonate	K_2CO_3	K_2CO_3
Magnesium chloride	$MgCl_2.6H_2O$	$MgCl_2$
Calcium chloride	$CaCl_2.2H_2O$	$CaCl_2$
Sodium formate	CHO_2Na	NaFo
Potassium acetate	CH3COOK	KAc
Potassium formate	CHO_2K	KFo

The results of NaCl with additives are depicted in figure 28.

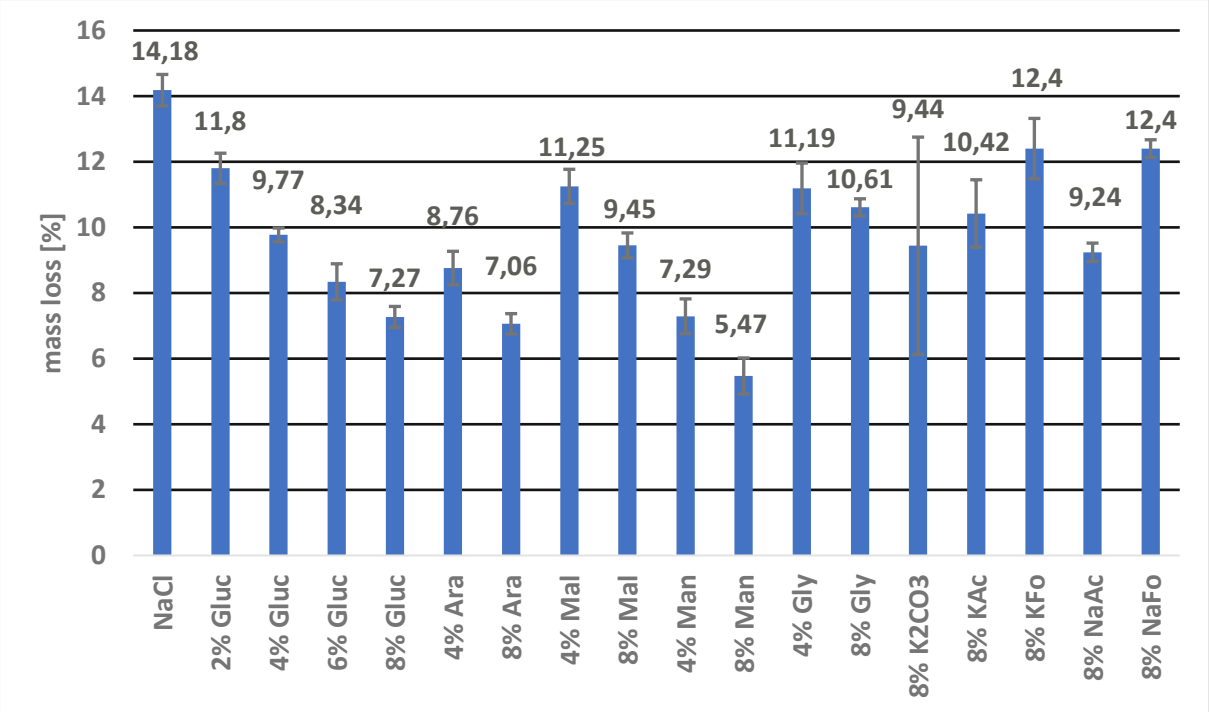

Figure 28: Results of the corrosion experiments or the iron samples. Samples were corroded with NaCl plus additives.

The corrosion behaviour measurements of sodium chloride with different additives include four sugars – Glucose, Arabinose, Mannose and Maltose – in different concentrations and, on demand of our clients at ÖBB and project partners, other salts which possess corrosion inhibiting capabilities. These substances are potassium carbonate (K_2CO_3), glycerine (Gly) potassium acetate (KAc), potassium formate (KFo), sodium acetate (NaAc) and potassium acetate (NaFo).

The results indicate that the non- sugar additives are not as efficient as the sugars in their inhibition ability. The non- sugar additive with the lowest mass loss is for a concentration of 8 % sodium acetate with a loss value of 9,24 %. Sugar additives with a concentration of 8 % have a mass loss of only 7,2 %, hence they are much more effective than the other tested components.

To gain information about the amount of sugar needed to be added to the de-icing agent, a concentration series was recorded. Corrosion experiments of NaCl with an additive of 2 %, 4 %, 6 % and 8 % glucose were performed. The results are depicted in figure 28. The results show a significant corrosion reduction from pure NaCl at a mass loss of 14,18 % to NaCl + 2 % glucose with a mass loss of 11,8 % and to NaCl + 4 % glucose with a mass loss of 9,77 %. At a concentration of 6 % and 8 % glucose the decrease in corrosion rate does not continue as steep anymore with loss values of 8,34 % and 7,27 %, respectively. These results show that adding continuously more sugar to the NaCl does not increase the corrosion inhibition linearly. Economically concentration values of 8 % sugar are obviously most efficient. From the sugars mannose is clearly the best inhibitor with a mass loss of 5,47 %. The worst of these four sugars is maltose with a mass loss of 9,45 %. Glucose and arabinose are somewhere in between 7,27 % and 7,06 % mass loss.

This corrosion setup then was used by our project partners to gather additional information and measure the corrosion effects of even more de-icing salts but also corrosion on different materials like galvanised steel or copper plates. Figures 29, 30 and 31 show the results of these measurements performed by our project partners in continuation of this winter maintenance project (Hoffmann et al., 2021).

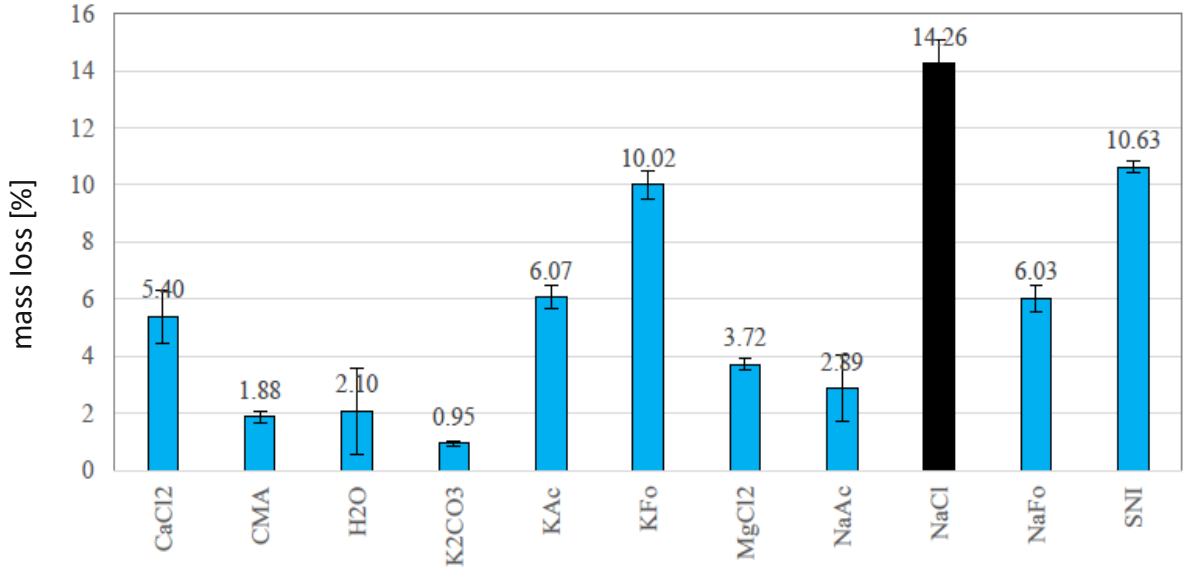

Figure 29: Corrosion of basic de-icing salts on iron plates. This is nearly the same as the results shown in figure 27, the only difference being that after the completion of this thesis, another basic de-icing salt was measured namely calcium magnesium acetate (CMA).

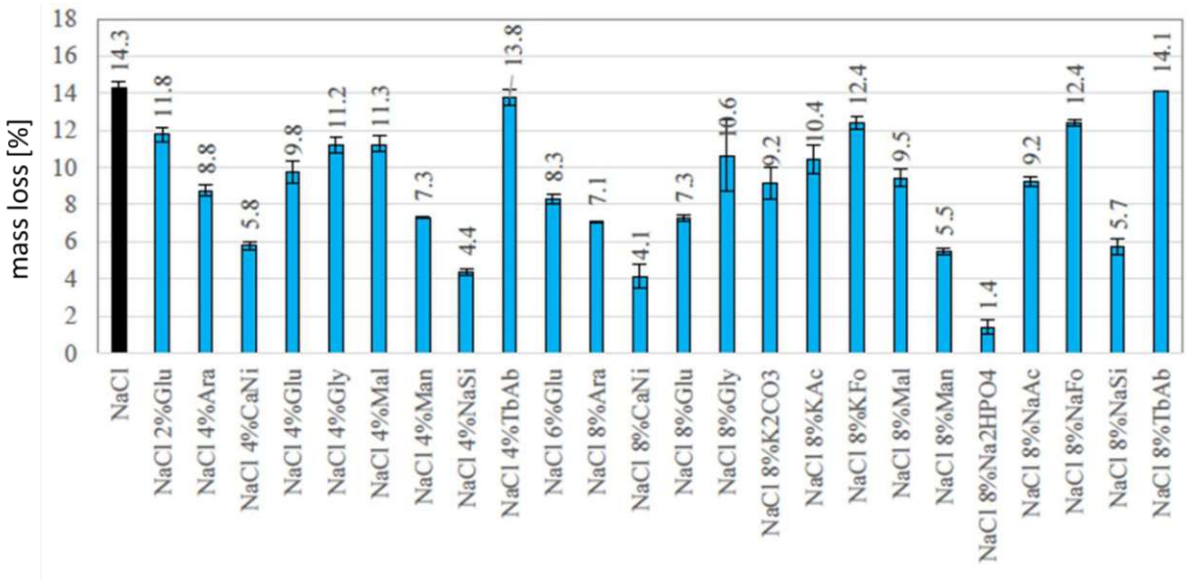

Figure 30: Here shown are the results of the corrosion behaviour of NaCl + additives on iron. These results are shown in figure 28, expanded with some additional measurements of different additives.

TbAb…tetrabuthylammonium bromide
CaNi… calcium nitrite
NaSi… sodium silicate
Na_2HPO_4… sodium dihydrogen phosphate

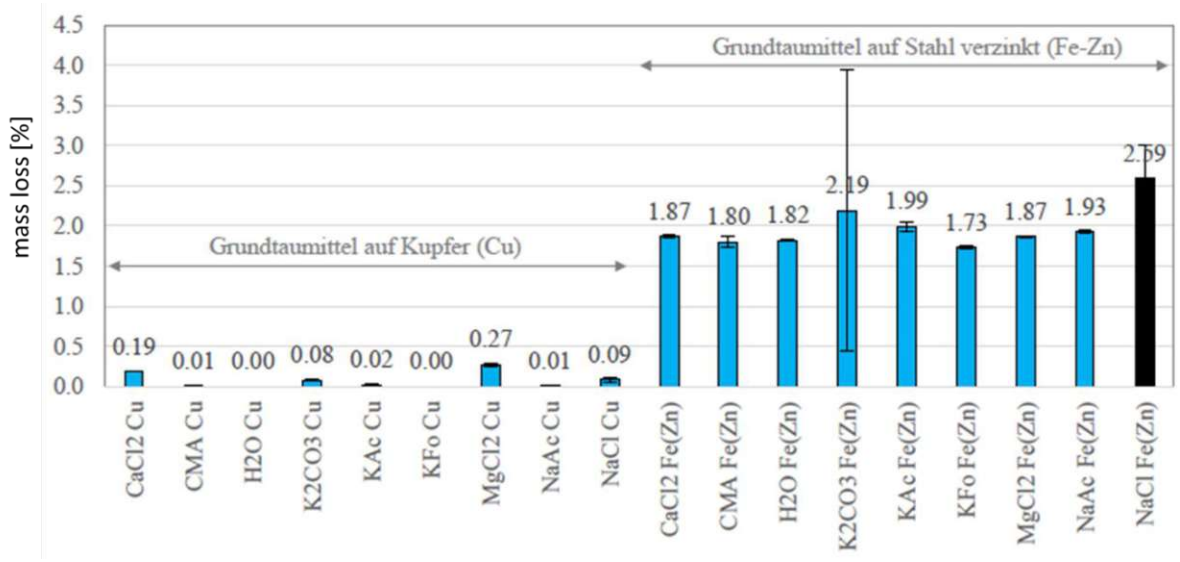

Figure 31: Results of mass loss from basic de-icing agents on copper (Cu) and galvanised steel (FeZn)

4.2 Surface analysis of corroded metal plates

4.2.1 Laser profilometry and atomic force microscopy

Due to the reasons described in chapter 3.3, most of the topographic examinations were recorded on the profilometer. 7 iron samples were analysed after the surface was cleaned from the corrosion products. Figures 31 to 37 depict the topographical maps, measured with a lateral resolution of 50 µm.

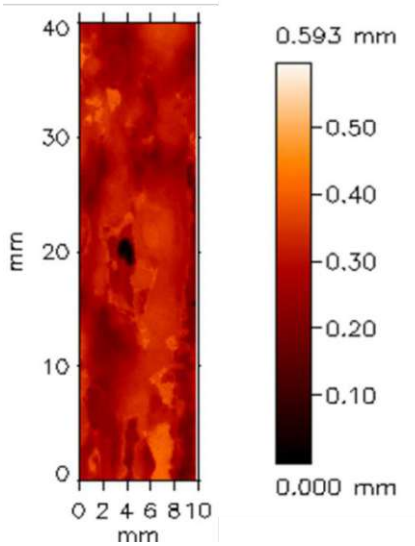

Figure 32: Fe- plate corroded with sodium chloride (NaCl)

Figure 31 shows the iron plate corroded by pure NaCl and is used as reference point. The map clearly shows some pitting corrosion, at 4 mm/20 mm, which is characteristic for corrosion in chloride containing environment.

As corrosion parameter the arithmetic average height R_a is used. As described in chapter 2.1., R_a is a mean value of height differences from a calculated median line. The software calculates an arithmetic average height R_a of 9 µm.

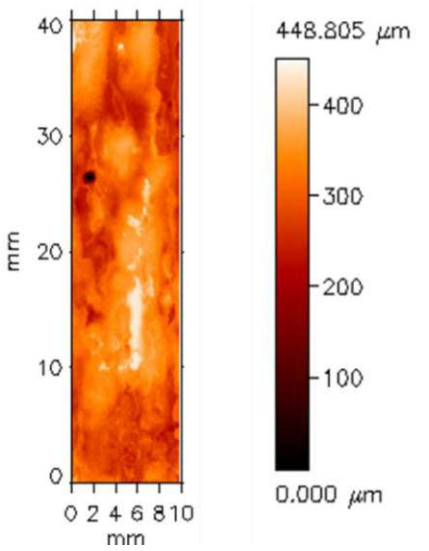

Figure 33: Fe- sample corroded with NaCl +8% Glocose

Figure 33 exhibits the impact of Glucose on NaCl. This sample also has pitting corrosion (2 mm/27 mm), but the overall height difference is lower than in the pure NaCl sample. This is also shown by the arithmetic average height R_a which for this sample is 7,8 µm.

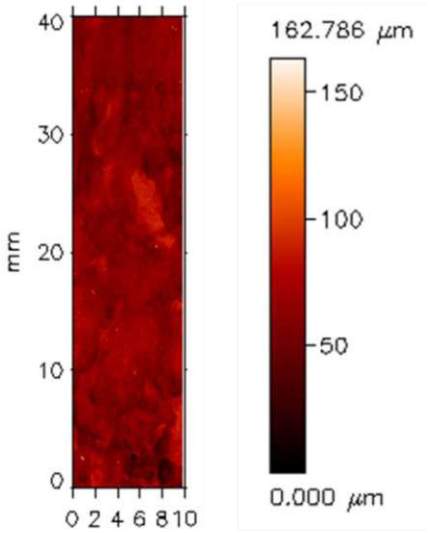

Figure 34: Fe- sample corroded with sodium acetate (NaAc)

Figure 34 shows the topographical analysis of iron weathered with sodium acetate. Obviously, less corrosion occurred than with NaCl.

Arithmetic average height R_a for this sample is 4,2 µm.

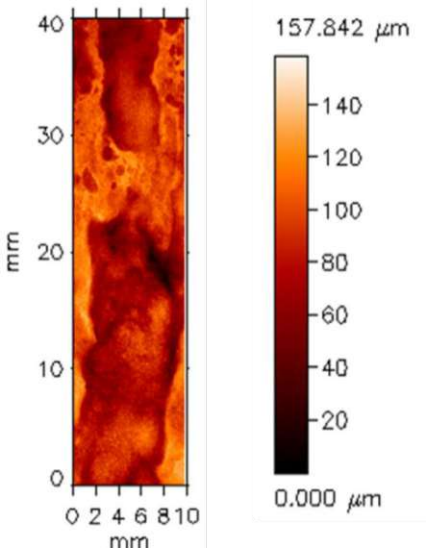

Figure 35: Fe- sample corroded with potassium acetate (KAc)

Potassium acetate shows a rougher surface than its sodium counterpart. The legend shows that the height difference is similar, but more pronounced peaks and valleys can be distinguished.

The average height R_a, it is 4,9 µm for this sample.

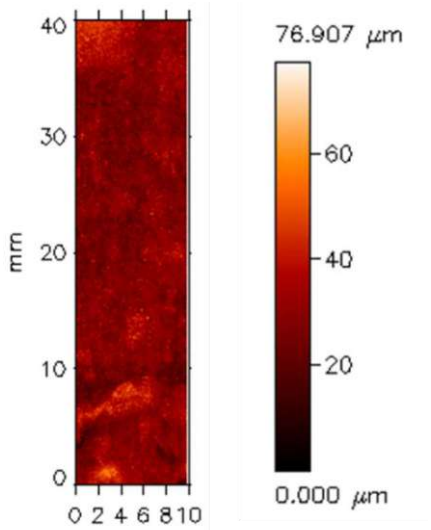

Figure 36: Fe- sample corroded with magnesium chloride ($MgCl_2$)

The magnesium chloride sample does not cause any pitting corrosion, despite the presence of chloride ions. In general corrosion is less visible in this map which concurs with the observation in chapter 4.2, that $CaCl_2$ and $MgCl_2$ show surprisingly little mass loss during the corrosion process.

R_a for this sample is 2,8 µm.

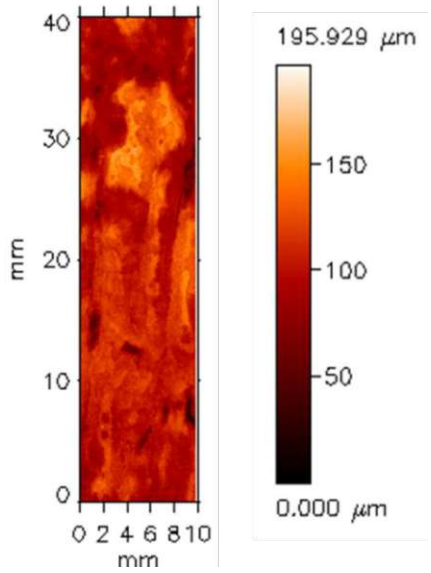

Figure 37: Fe- sample corroded with calcium chloride ($CaCl_2$)

The corrosion pattern on the calcium chloride sample is very pronounced. The start of pitting corrosion in some areas is also apparent.

The roughness value R_a for this sample is 4,7 µm.

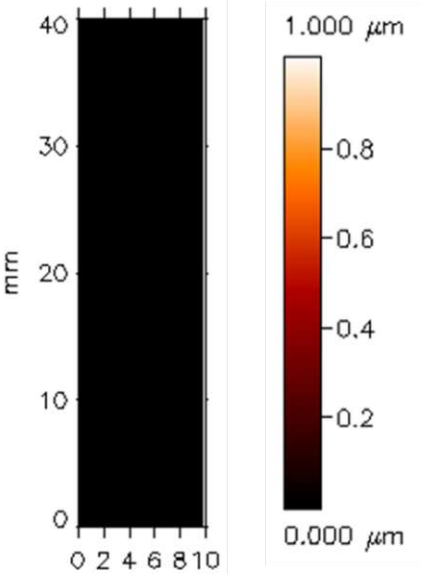

Figure 38: Fe- sample corroded with potassium carbonate (K_2CO_3)

The potassium carbonate sample shows no signs of corrosion in the laser profilometry analysis. The surface is completely smooth without any traces of peaks or valleys. The software shows this lack of height difference by giving a completely black map as a result. This concurs very well with the mass loss measurements of K_2CO_3.

R_a for this sample is 1,5 µm.

On first assessment it seems that the more corrosion occurs the more roughness we find on the sample surface. If there exists a direct correlation between the two parameters, they could be used to monitor the corrosion process. If we put the two values for every sample into one graph, we recieve figure 39.

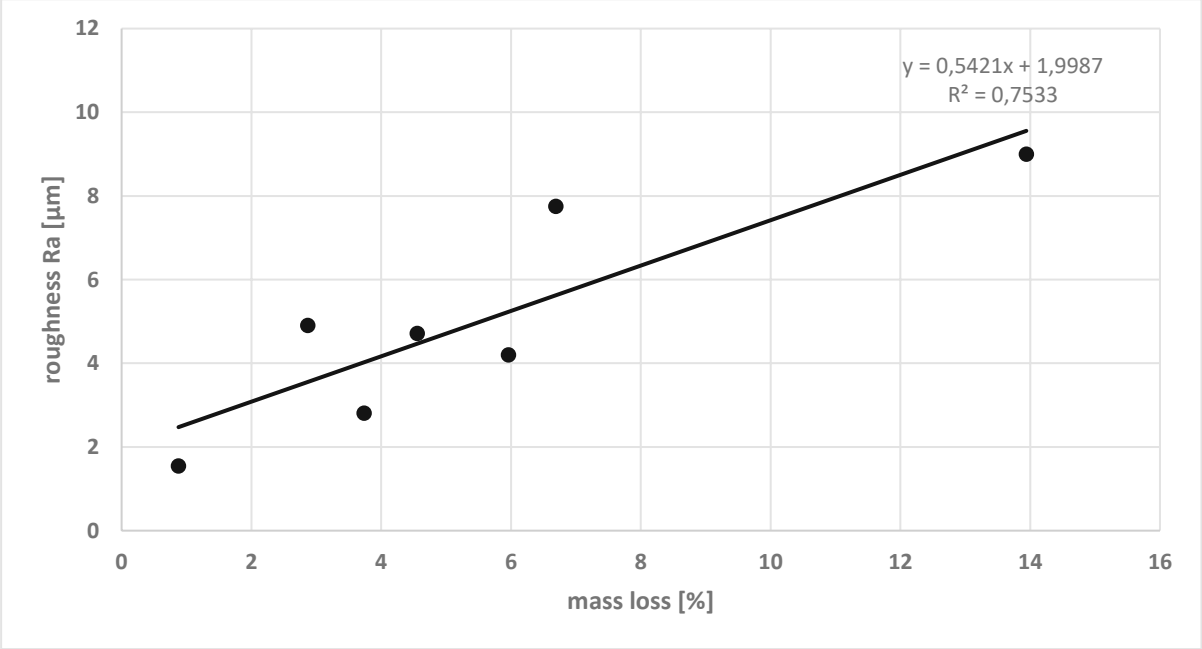

Figure 39: Correlation of roughness and mass loss.

Apparently, there is a trend, but the linear coefficient (0,7533) is insufficient to devise a solid mathematical correlation between roughness and mass loss. The values shown in figure 39 are depicted without error, because they were measured only one time, but we assume that the errors are in the range of 30 %. The reason for this is that the measured area was only 4 cm^2, which is much too little to be representative. Scanning larger areas of the sample plate would have given a more solid linear correlation between roughness and mass loss and might be a task for further projects.

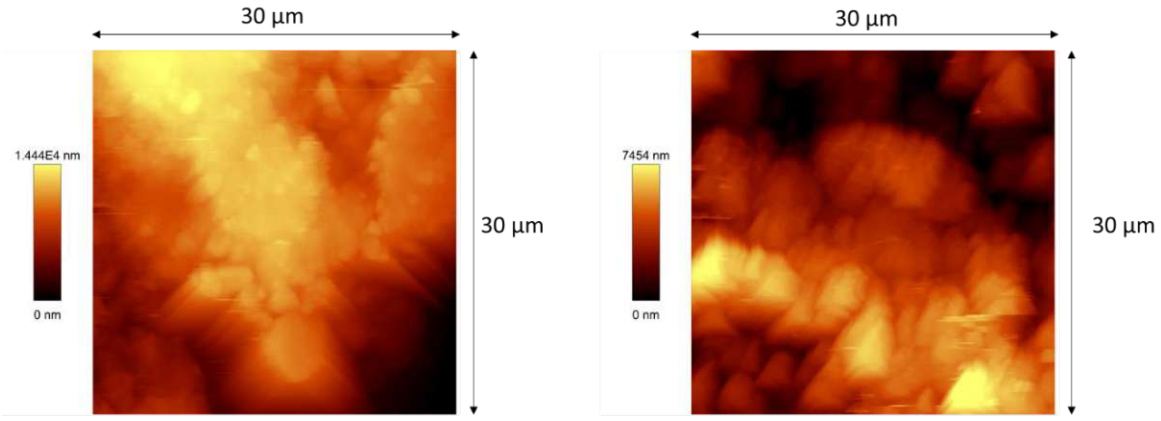

Figure 40: AFM scans of Fe samples corroded with NaCl

Figure 40 shows two pictures of AFM scans. These were two of the very few scans which could be recorded by AFM. The lateral resolution is way higher, than with the profilometer, but the very rough surfaces make AFM unrepresentable for the corrosion experiments.

4.2.2 X- Ray Photoelectron spectroscopy (XPS)

The analytical instrumentation center (AIC) of the TU Wien provided us with XPS-measurements of our corroded metal surfaces. There are survey spectra, which show a binding energy range from 0 eV to 1350 eV and detail spectra which show areas of particular interest in greater detail. The survey spectra can be found in the appendix, but the detail spectra, which in our case depict the metal-oxygen bond will be discussed in the following part.

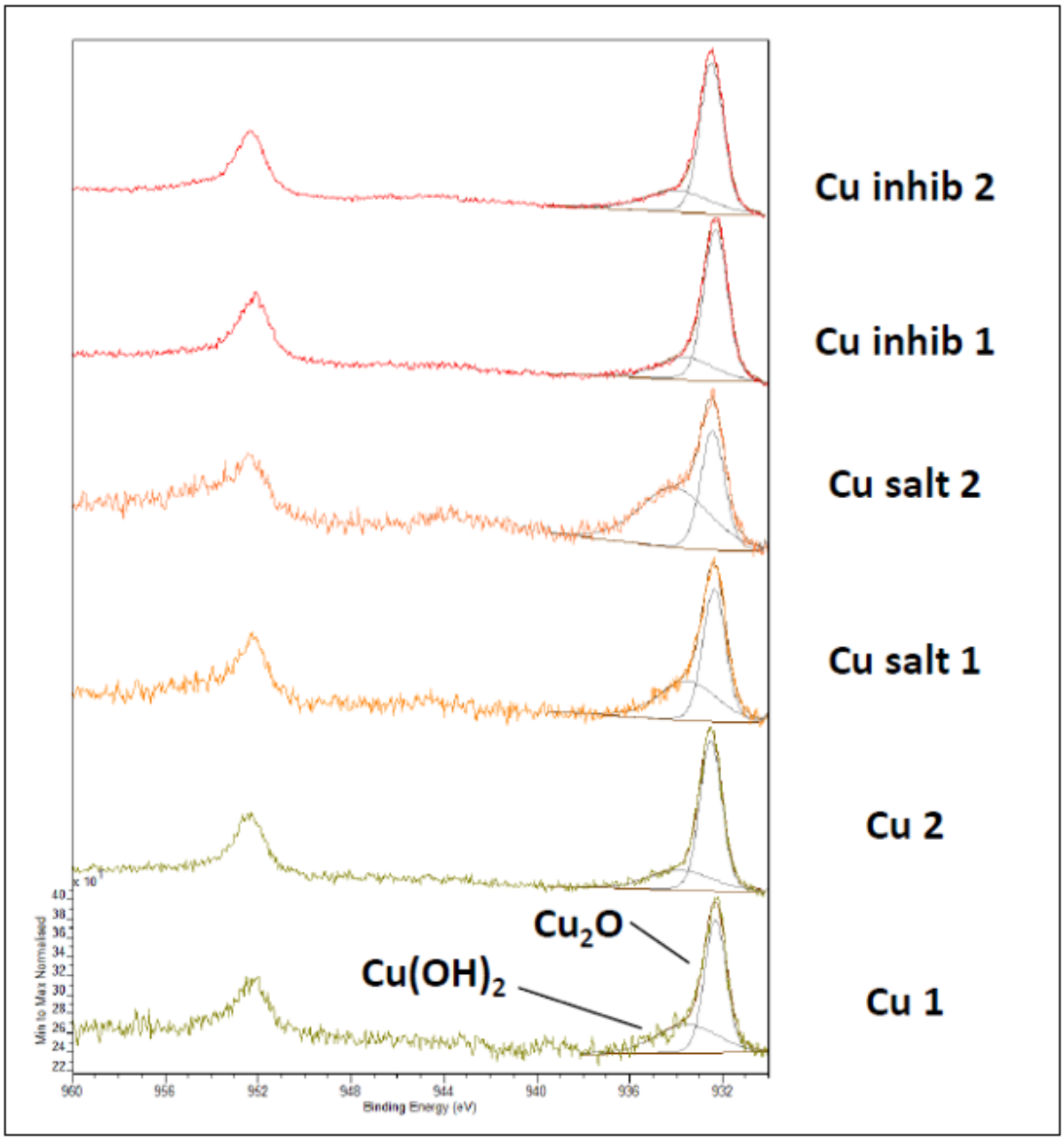

Figure 41: Detail spectrum of the Cu 2p peak. The X-Axis shows the binding energy in eV, the Y- Axis shows the normalized signal.

Figure 41 shows the detail spectrum of the Cu2p binding energy area: One copper sample which is not corroded (Cu), one weathered with NaCl (Cu salt) and one corroded with NaCl + 3% glucose (Cu inhib). At an energy level of 933 eV two peaks are observable which are intertwined. The software fits the signal in a way that they are distinguishable. One can recognize the peak of CuO_2, which is the natural oxide- layer which forms on pure copper. Figure 41 shows that the amount of $Cu(OH)_2$ formed in the weathering process with NaCl + Glucose (Cu inhib) is the same as in the uncorroded sample (Cu). This means that no additional corrosion products have formed during the corrosion process. The samples weathered with pure

NaCl (Cu salt) show higher amounts of $Cu(OH)_2$, which indicates a faster corrosion process. The corrosion inhibiting effects of glucose are clearly recognizable from this experiment.

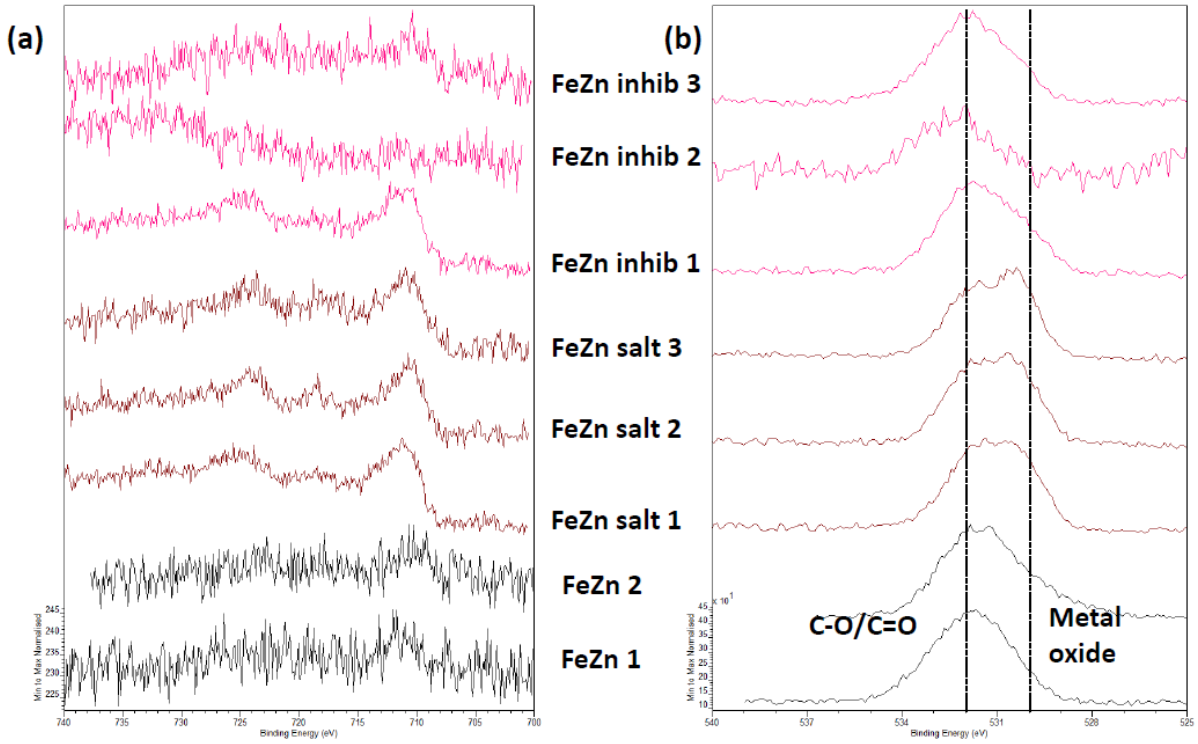

Figure 42: Fe 2p (a) and O 1s (b) detail spectra

Figure 42 shows the detailed spectra of galvanised steel. The amount of carbon on the samples, resulting from environmental influence, is so high that all other peaks are too small to be recognized, which means the signal to noise ratio is too low to gather any information from these spectra.

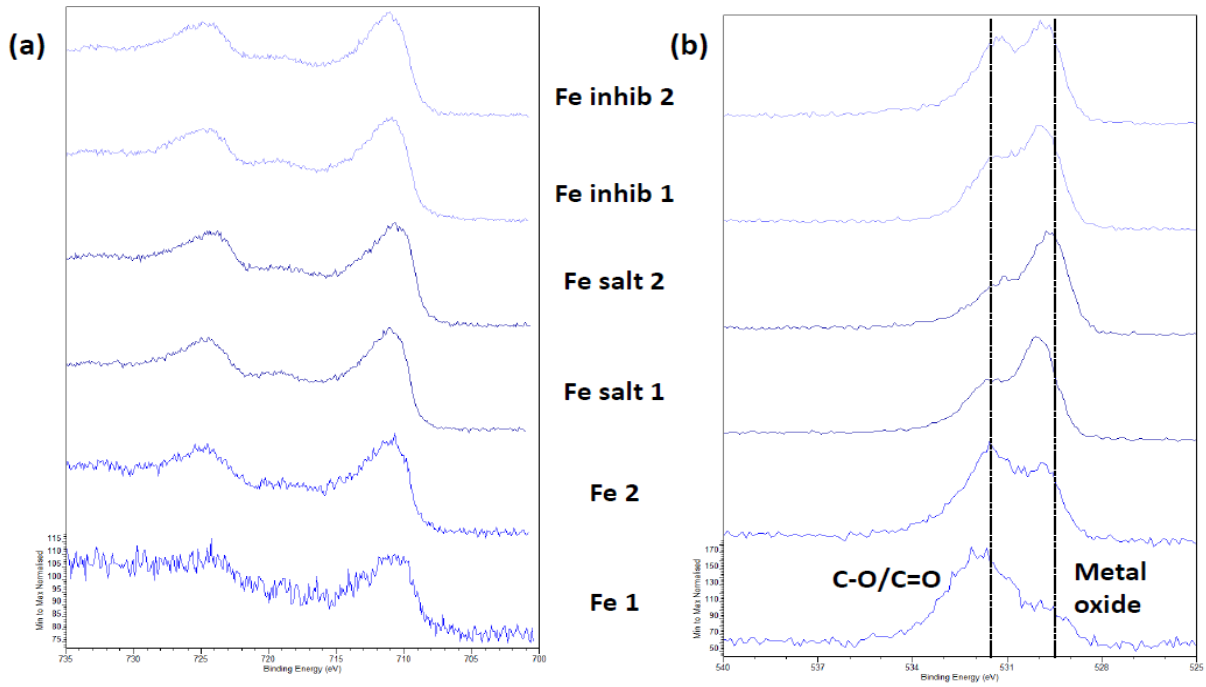

Figure 43: Detail spectra of Fe 2p (a) and O 1s (b) before heating.

Figure 43 again shows that the amount of carbon on the surface is too high to distinguish any other signal, so we requested another measurement, this time only from the iron samples, but the samples were heated to 415°C for 1 hour, inside the XPS- chamber. This heat treatment volatilised the organic molecules from the surface, causing a cleaner spectrum.

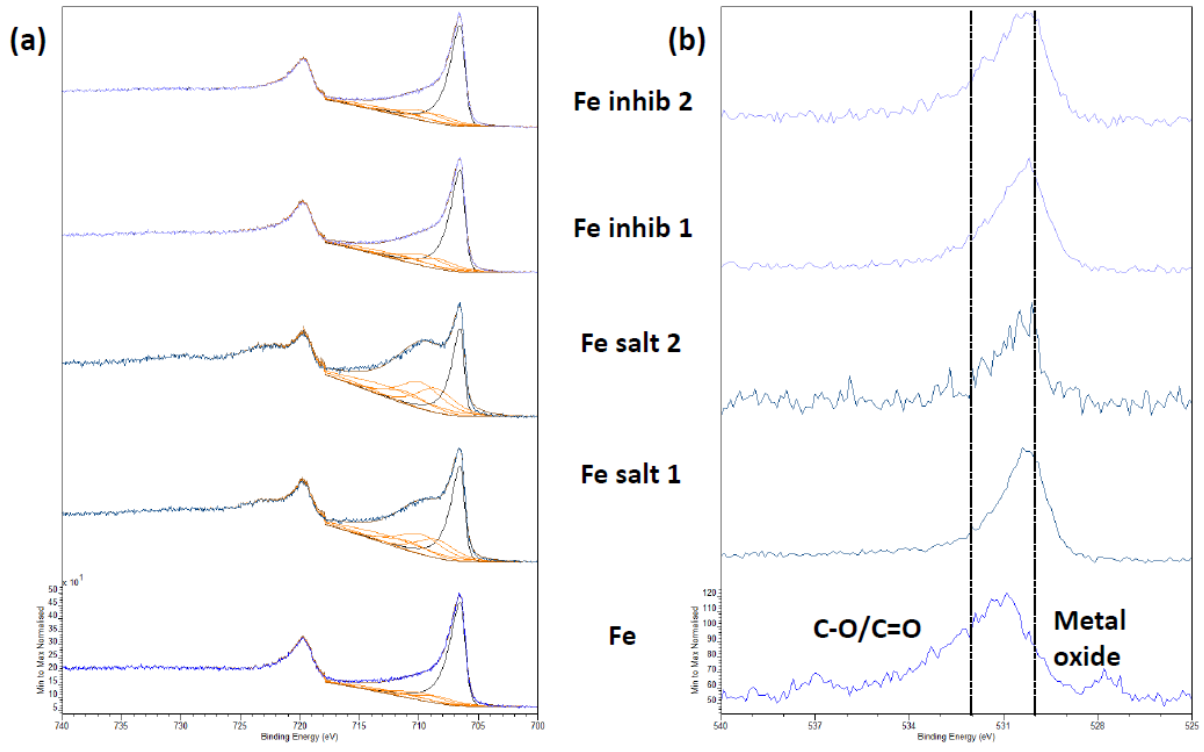

Figure 44: Detail spectra of Fe 2p (a) and O 1s (b) after heating to 415°C.

After the treatment the carbon – oxygen peak (figure 44b) is way smaller making it easier to fit the other peaks. The Fe2p area (figure 44 a) shows for the uncorroded sample (Fe) only one distinguished peak at a binding energy of 707 eV. The samples weathered with NaCl (Fe salt) show an overlap of 3 different peaks at an energy of 909 eV. We conclude that these peaks are caused by the formation of different iron oxides in the corrosion process. The samples weathered with NaCl and corrosion inhibitor (Fe inhib) also show these peaks, but to a significantly smaller extent. This clearly shows the corrosion inhibiting effect of glucose on steel substrates.

4.2.3 X- Ray Powder Diffraction (XRD)

The X- ray diffraction spectra (provided in the appendix) give us the phase composition of the measured rust samples. Figure 45 shows these composition values as a bar chart.

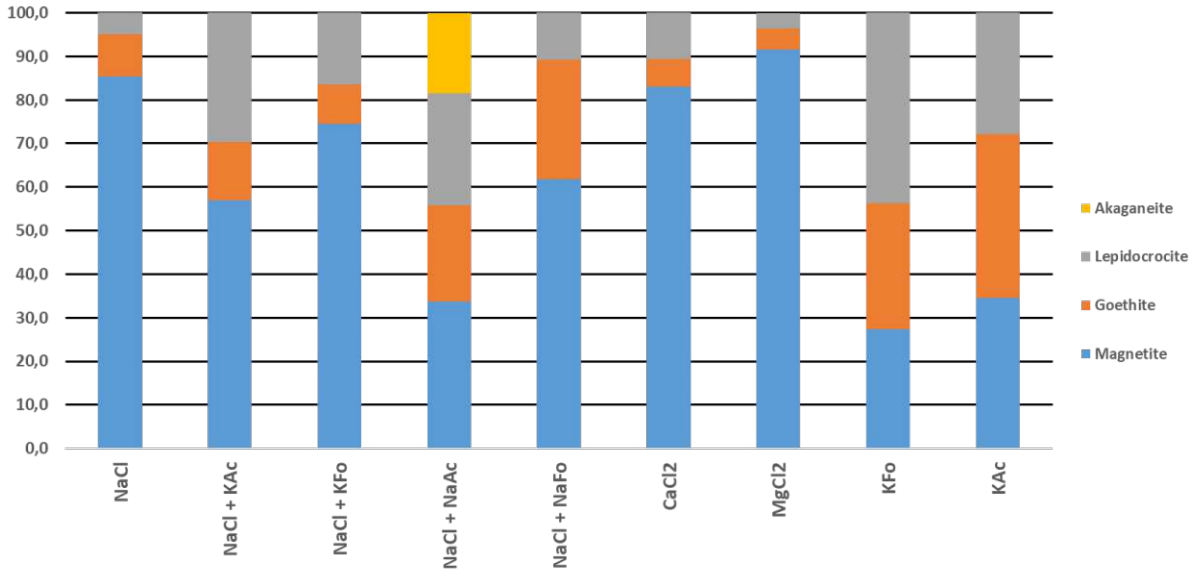

Figure 45: Chemical composition of rust samples after corroding with different de-icing salts.

As stated in chapter 1.3 the oxidation process of iron follows a distinct pattern. The first product that forms is $FeO(OH)_2$. It has two modifications which are called lepidocrocite (grey) and goethite (orange). subsequently the stable product Fe_2O_3 (magnetite, blue) is formed. This means that from the composition of the rust, we can determine how fast the corrosion progressed. This begs the question why the magnetite concentration in the calcium chloride and magnesium chloride samples is so high. We concluded that these two salts have a surprisingly low corrosion behaviour, but the chloride ion is accelerating the final step of the chemical conversion process. $MgCl_2$ and $CaCl_2$ catalyse the reaction from $FeO(OH)_2$ to Magnetite. Potassium formate and potassium acetate do not exhibit those high amounts of magnetite which

confers with our theory. When adding inhibitors to the sodium chloride corrosion was lowered and formation of magnetite was prohibited. However, to confirm this theory more experiments should be conducted. Akageneite is a similar mineral to lepidocrocite and goethite, it has a chloride ion instead of an oxygen built in. The chemical formula is: FeO(OH,Cl).

Powder Diffraction is an excellent way to analyse the bulk composition of our corrosion products. It is the only method to provide information of the progress of the corrosion process. Additionally, it confirms the effectiveness of the added corrosion inhibitors.

5. Conclusion

5.1 Conclusion Melting Rate and Corrosion Behaviour

This data together with the experiments on storage stability and of course the cost calculation, provided by our project partners, will allow the ÖBB to evaluate the de-icing agents and choose the one that best fits their needs. Based only on melting rate and corrosion behaviour we can make some assumptions which melting agent would be best for the ÖBB.

The first product discussed is potassium carbonate. It has a mediocre melting rate but by far the best corrosion behaviour of all basic de-icing salts. In some places, even in Vienna, it is used as effective substitute for NaCl in winter maintenance. It comes with its own set of problems though, mainly being able to interfere with the pH of the soil. NaCl is pH- neutral, while K_2CO_3 raises the pH. This can have some severe consequences for environment, flora and fauna. This means that in Austria, there are strict rules in place on where one can use potassium carbonate as de- icer and where not (Hartl & Erhart, 2002). If the station is eligible for K_2CO_3- use, this substance could very well be an alternative for the ÖBB.

Probably the most inexpensive solution to the winter maintenance problem, besides sodium chloride, are calcium chloride $CaCl_2$ or magnesium chloride $MgCl_2$. Both these salts are formed as waste product, in case of $CaCl_2$ it is produced by the Solvay process (Steinhauser, 2008), in case of $MgCl_2$, it is a side product in the industrial potassium chloride production. They both combine low melting rates, with a surprisingly low corrosion rates, which could be interesting for our clients. Problem with these two salts is their high hygroscopicity. If not adequately stored they absorb water vapour, forming different crystal water systems making it impossible to disperse them on the ground. If a solution to this problem can be found, these two chlorides might be an option for future winter maintenance.

Another interesting substance is sodium formate. It has the best melting rate to corrosion rate relation of all the tested basic de-icing salts, is not hygroscopic and easy storable. It has low impact on environment and in water it reacts basic, again some studies need to be inquired to test if the environmental impact is too high or not. If not, this could be a great alternative to sodium chloride. It even is used on airports as a non- corrosive de-icing agent (Trzaskos & Klein-Paste, 2020).

If the complete evaluation of the ÖBB concludes that there is no way around NaCl (probably related to the costs) our second field of studies could be the solution. We had great success with using sugar- based corrosion inhibitors mixed with sodium chloride. The corrosion rate dropped to half with glucose and even more with mannose. Sugars mean no risk to the environment, are readily available and have proven to have a very positive impact on the de-icing salt. If there can be found an economical way to mix these substances, this might be the best solution.

Some other substances, tested after the practical part of this thesis was concluded, have proven to have astonishingly good inhibition qualities. As can be seen in figure 30, disodium hydrogen phosphate (Na_2HPO_4), sodium silicate (NaSi) and calcium nitrite (CaNi) nearly blocked corrosion completely. Here the problems is the availability and the negative environmental impact of these substances.

5.2 Conclusion Chemical analysis

Our analysis of sample surface before and after corrosion, before and after cleaning and the analysis of corrosion products have given valuable information of the corrosion process on metal surfaces. Differences in corrosion behaviour of de-icing agents have been observed and explained due to the analytical methods.

We found a correlation between roughness and corrosion rate, but the reproducibility of our experiment is insufficient, since the sample area we measured with the profilometer was too small. It would have been interesting to conduct field studies directly on the train station, to see if there are differences between the real samples and samples gathered from the lab experiment.

The X- ray photoelectron spectroscopy confirmed the viability of sugars as corrosion inhibitors, as a cost-efficient possibility, which can be easily applied to winter maintenance worldwide.

With the X- ray powder diffraction technique we could monitor the corrosion process in its steps, making a thorough examination of corrosion products and corrosion process possible.

5.3 General conclusion and outlook

This project showed that there are huge improvements possible to the winter maintenance system in general. Mixing of different de- icing agents and additives can prove beneficial to winter maintenance providers around the world from an economical, as well as from an ecological standpoint.

We found a way to measure melting rate of de- icing agents more accurately and efficiently than ever before, making it possible to test a huge variety of different de- icing agents, compare them and provide a comprehensive list of efficient de-icing salts.

In addition to the melting rate, we were able to provide qualitative and quantitative data about the corrosion rate of de-icing agents. With several chemical analysis methods, we could display the steps of the corrosion process of iron under influence of different de-icing agents, making it possible to find ideal combinations of good melting rate and corrosion behaviour of de-icers.

We have proven that saccharides are a great additive to de- icing salts regarding their corrosion behaviour, lowering the corrosion rate to a half of that of the pure agent.

This project provides the groundwork for many more projects in the future. Many different substances could be tested and analysed with the methods described in this thesis, to find a de-icer with the ideal combination of good melting rate and corrosion behaviour. Other additives can be tried for their corrosion inhibiting effect, possibly lowering the corrosion rate of NaCl even more.

More surface sensitive or electrochemical methods could be used to gather even more information about the corrosion process and how to stop it.

To conclude it can be said that winter maintenance is a very vital part of the lives of many people around the world and that scientific insight is very important, to make sure streets, train stations, rails and other paths where people commute are as safe as possible.

Appendix

Melting rate curves with 95 % confidence interval and 95 % prognose bands:

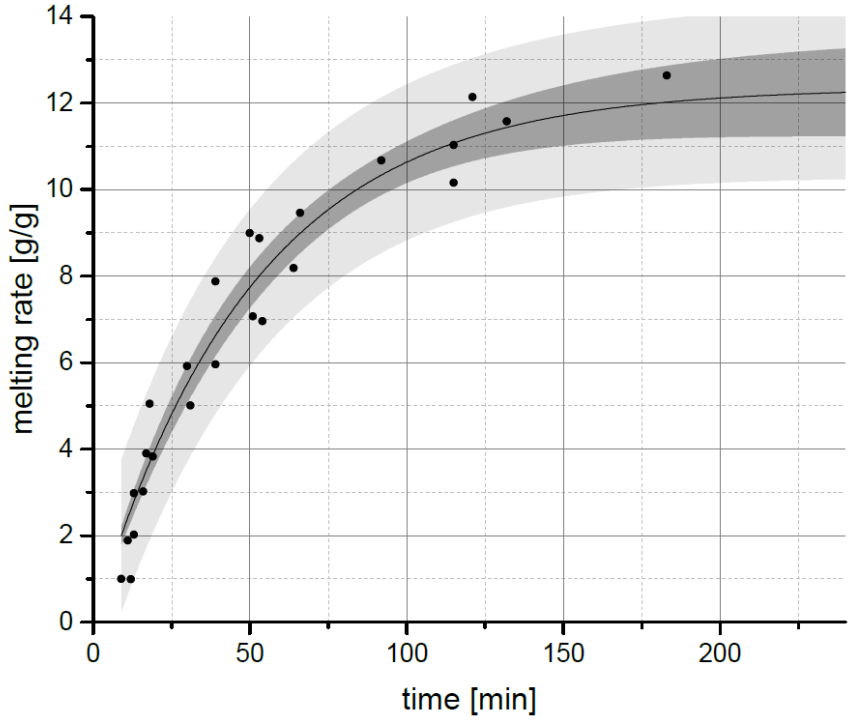

Appendix 1: sodium chloride (NaCl)

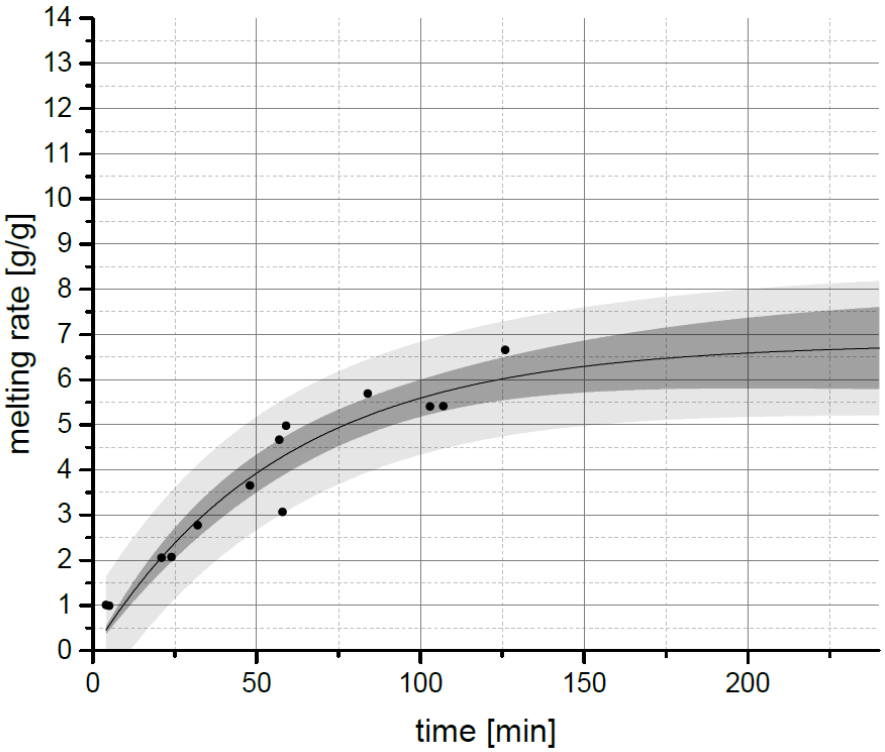

Appendix 2: Magnesium chloride ($MgCl_2$)

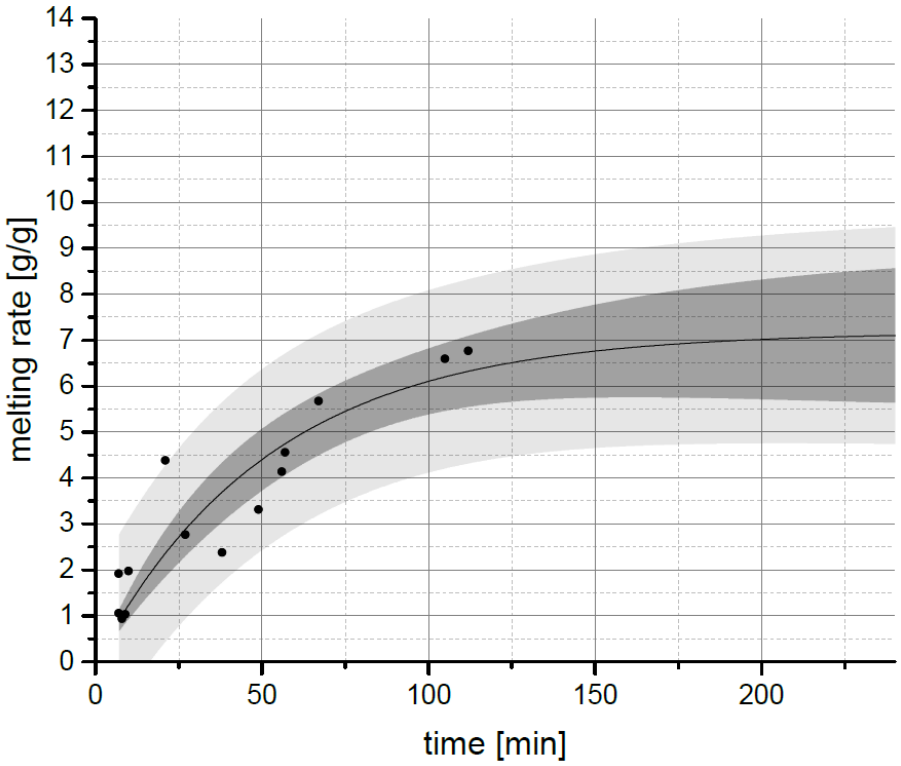

Appendix 3: Calcium chloride $CaCl_2$

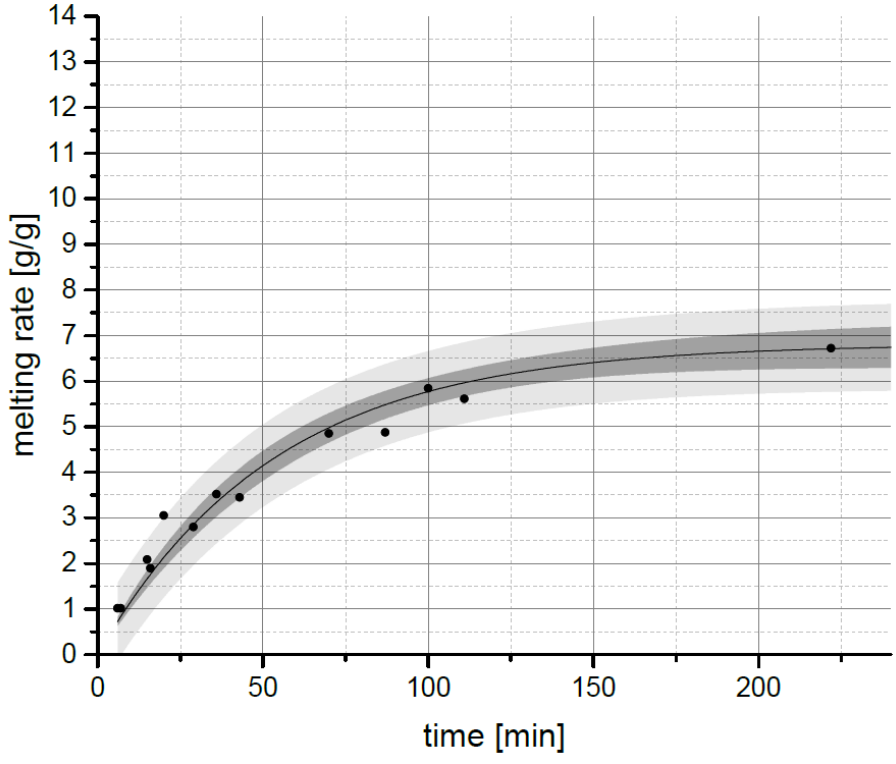

Appendix 4: potassium carbonate (K_2CO_3)

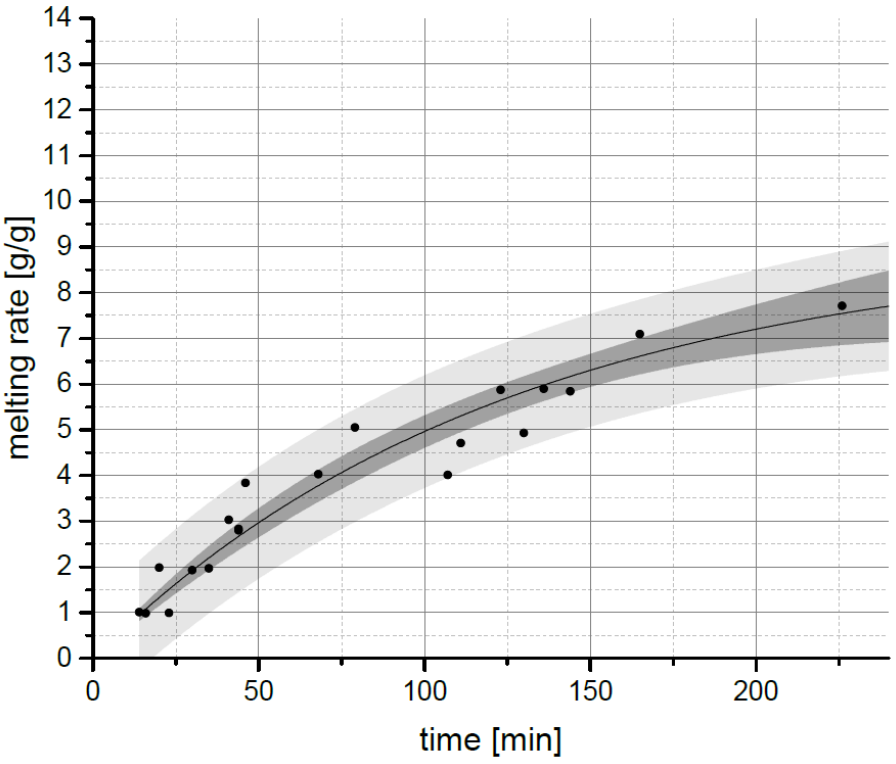

Appendix 5: Sodium acetate (NaAc)

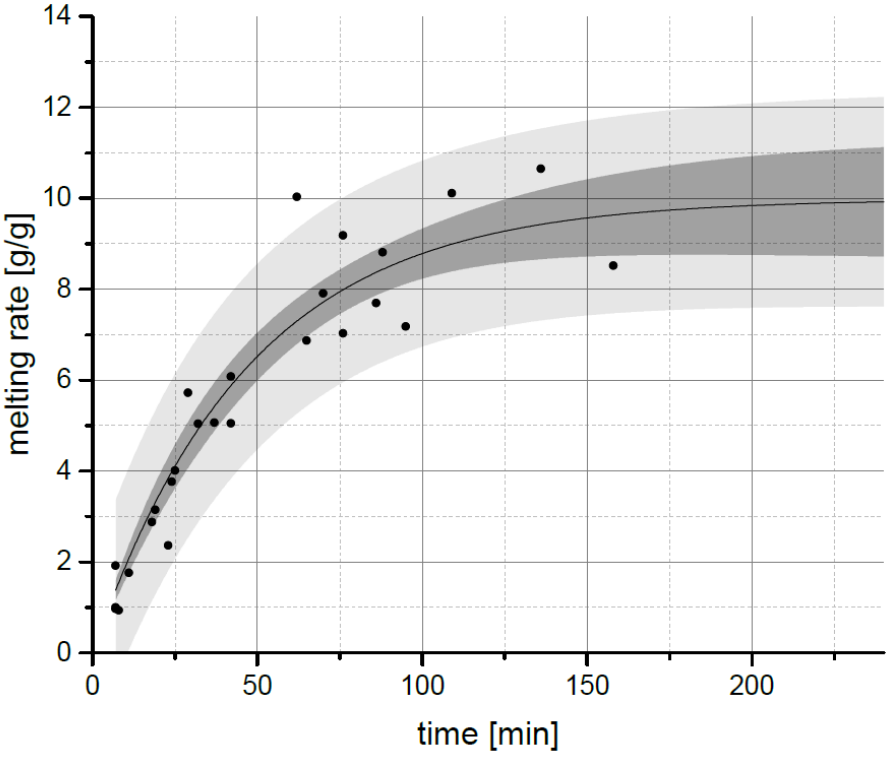

Appendix 6: Potassium acetate (KAc)

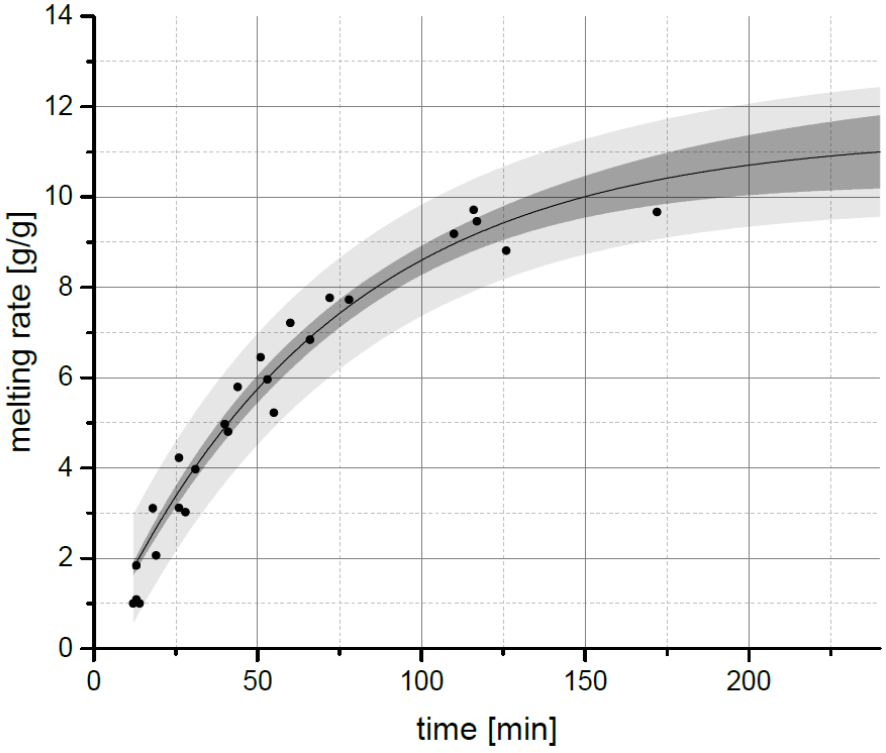

Appendix 7: Sno- N- Ice (SNI)

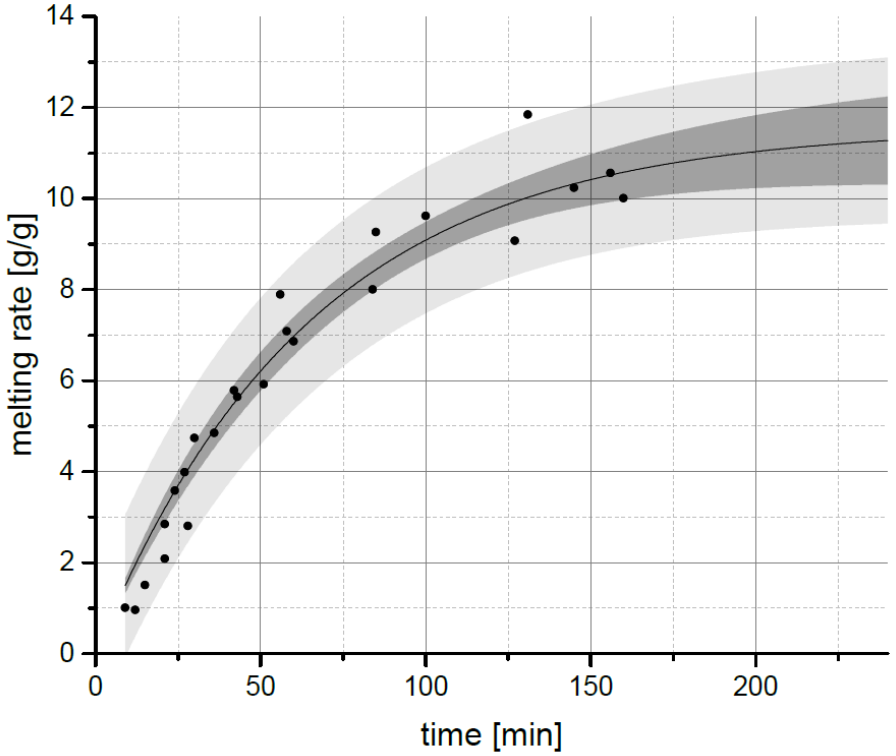

Appendix 8: sodium formate (NaFo)

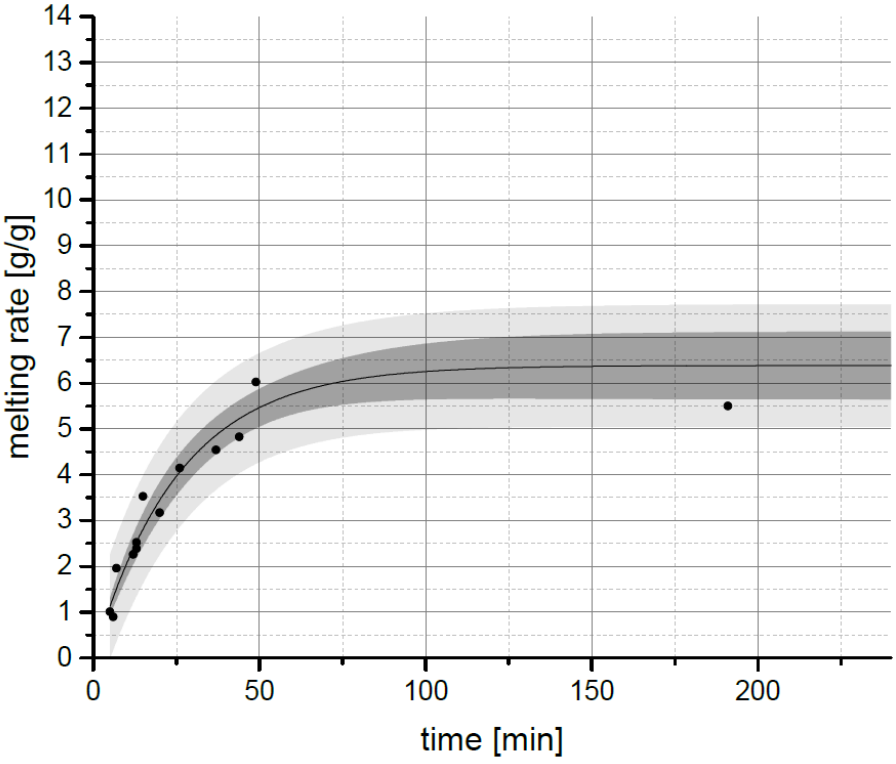

Appendix 9: potassium formate (KFo)

XPS spectra:

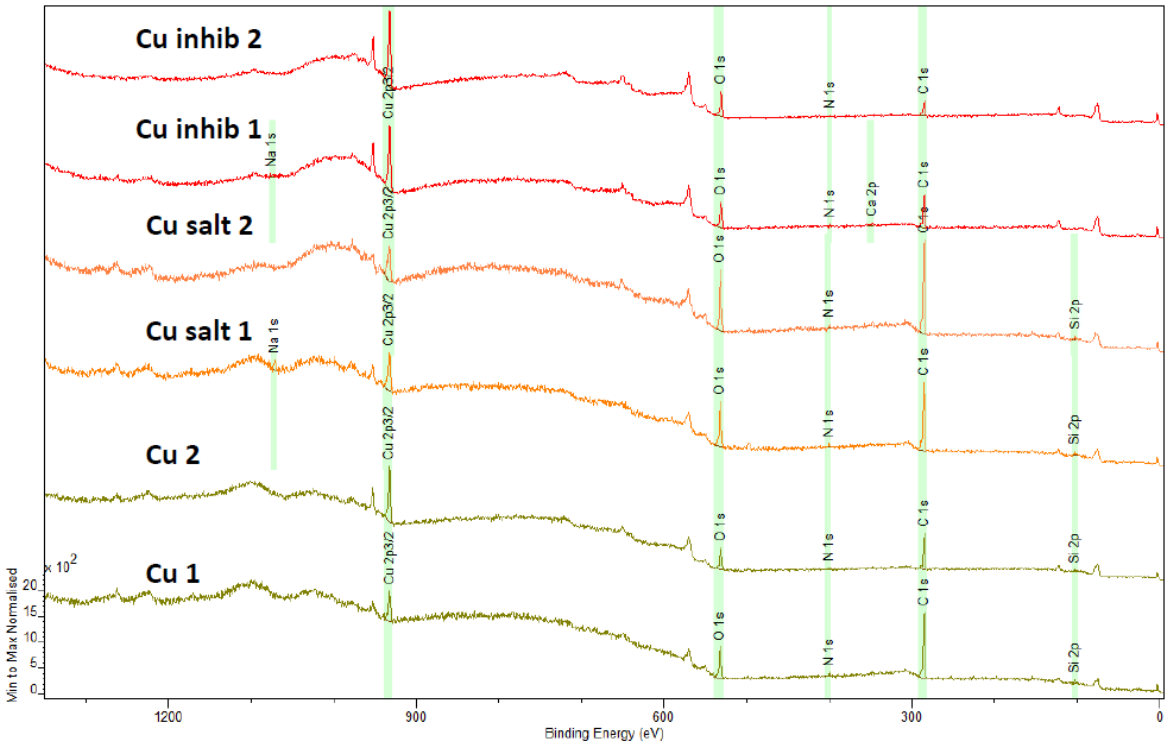

Appendix 10: XPS- survey spectrum of copper samples

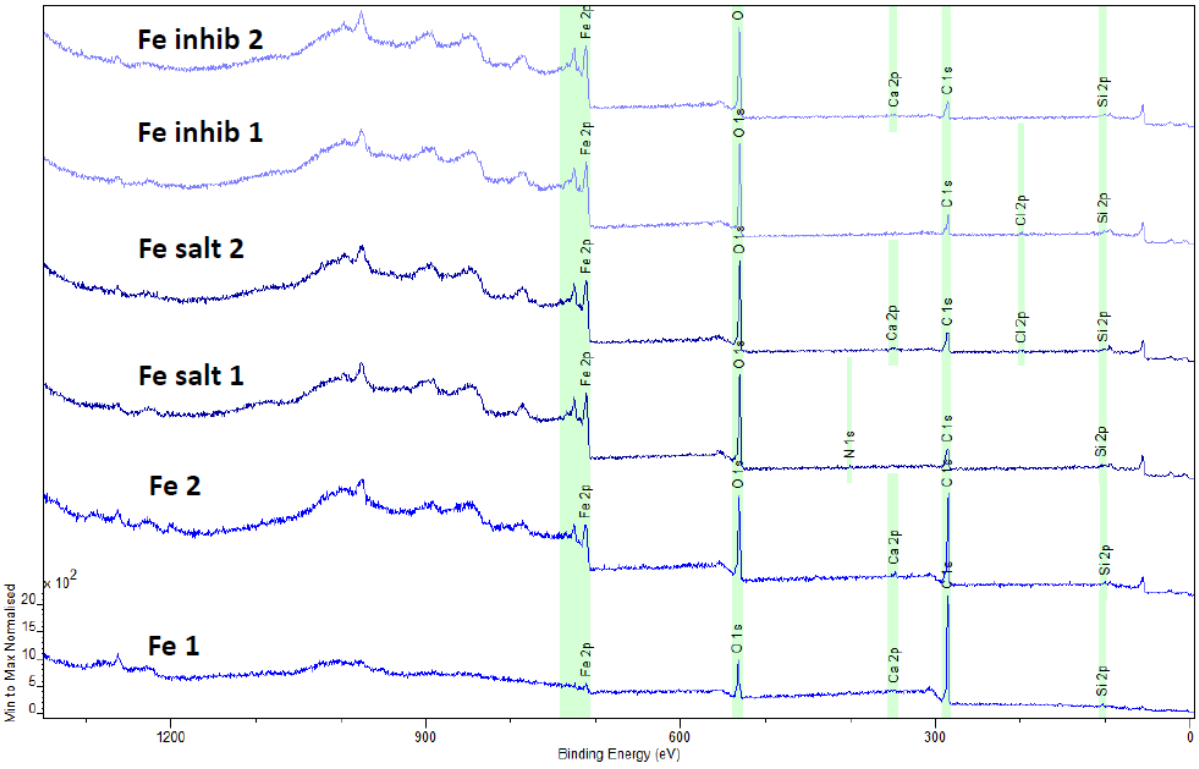

Appendix 11: XPS survey spectrum of iron samples before heating

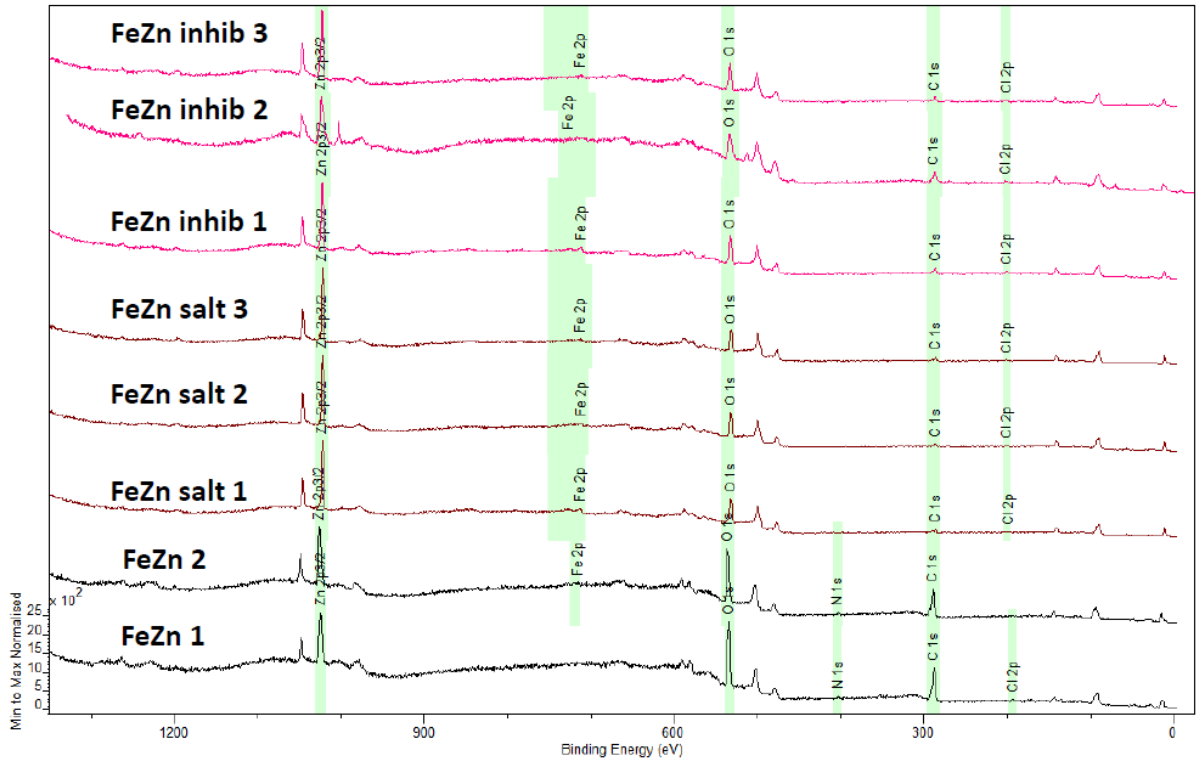

Appendix 12: XPS survey spectrum of galvanised steel.

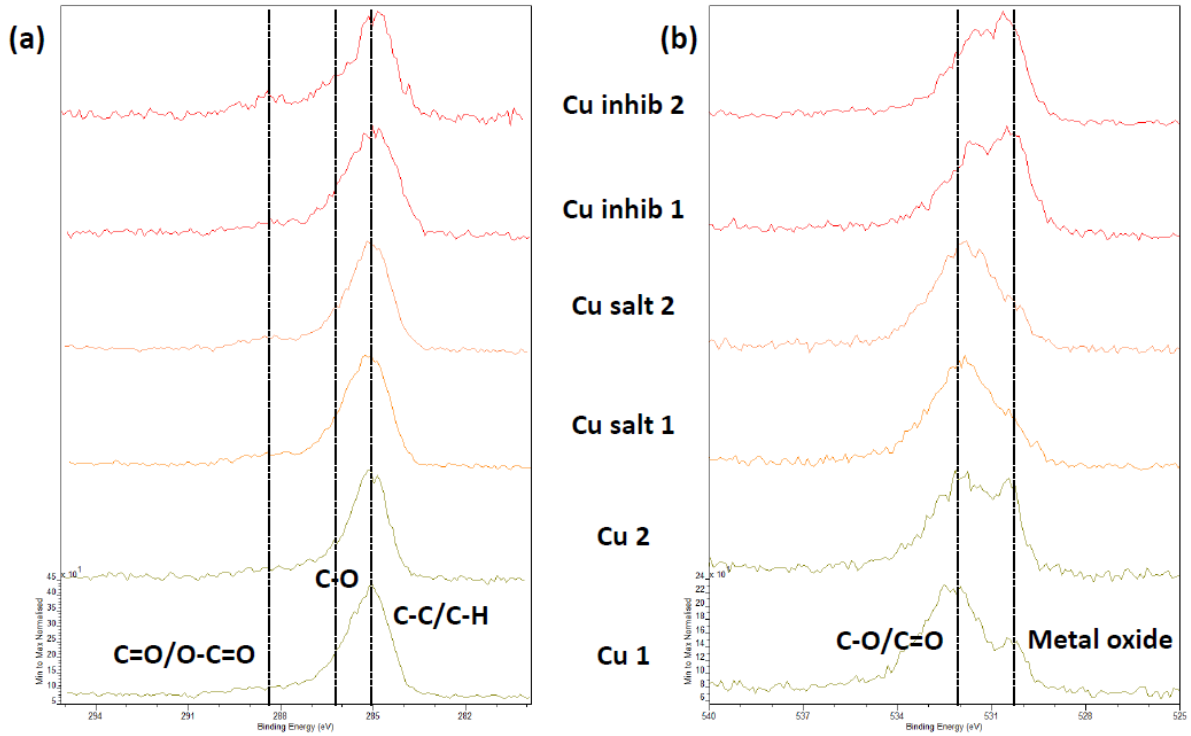

Appendix 13: XPS detail spectrum of C 1s (a) and O 1s (b) on copper samples.

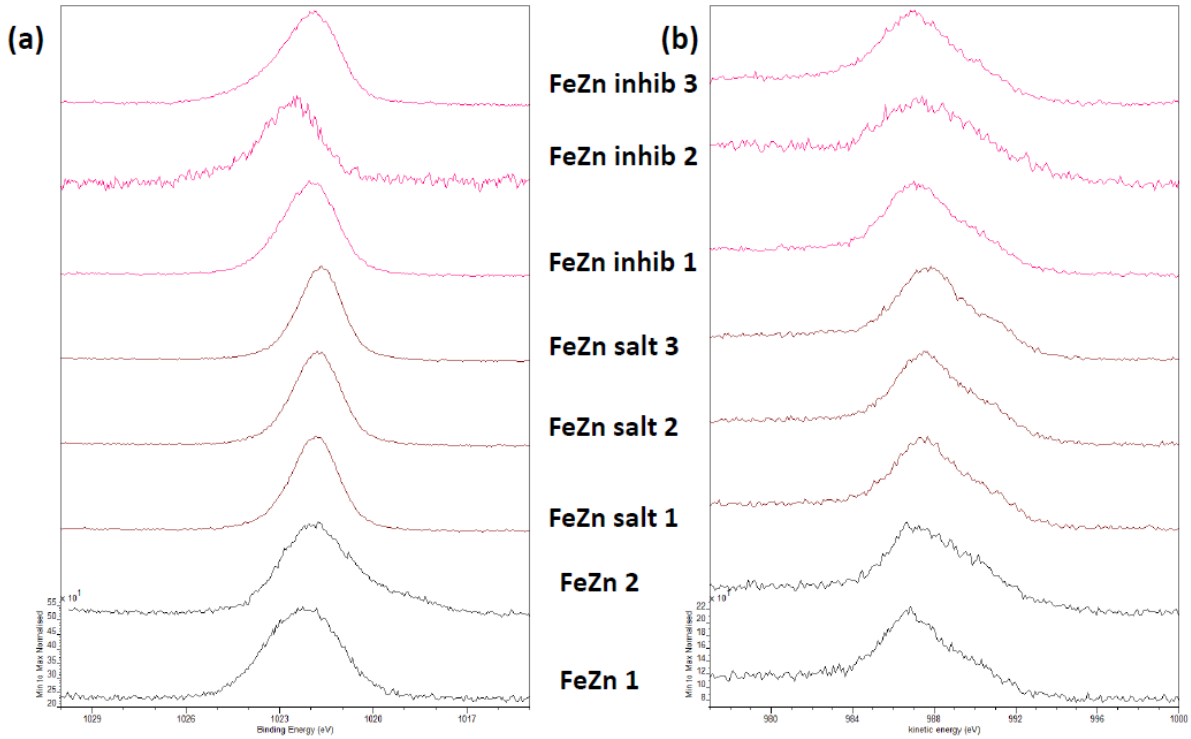

Appendix 14: XPS detail spectra of Zn 2p (a) and Zn LMM (b) of galvanised steel samples.

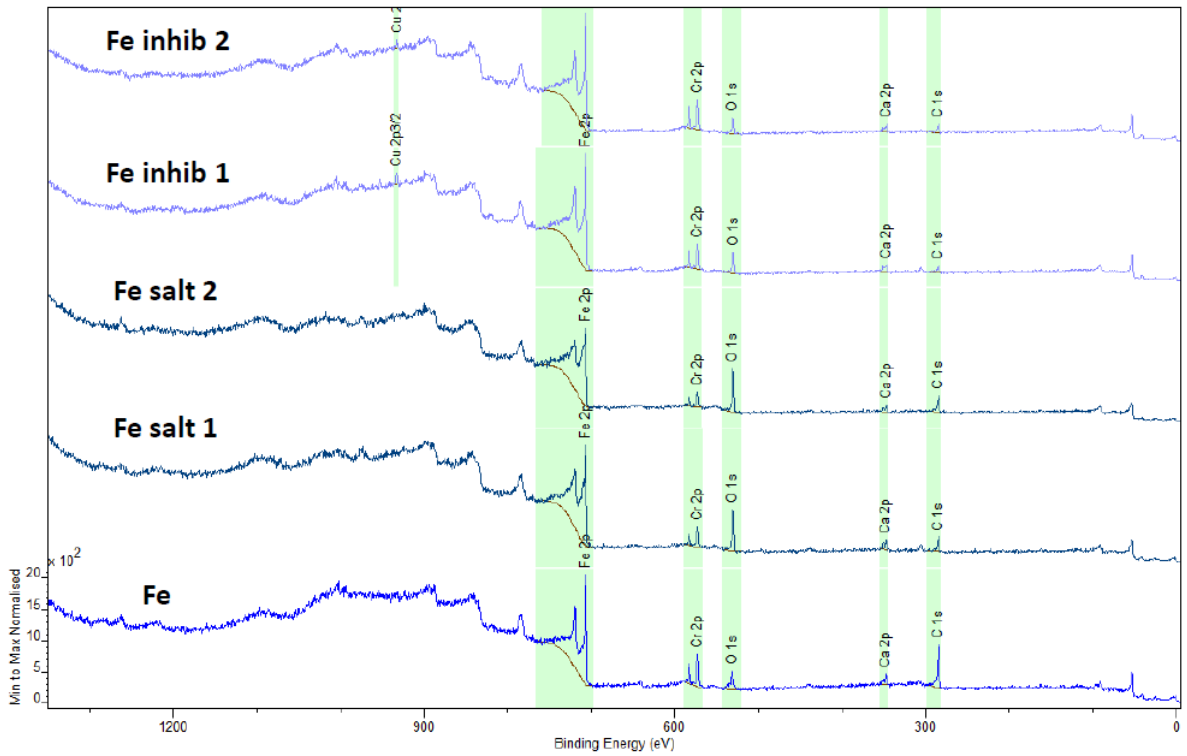

Appendix 15: XPS survey spectrum of iron samples after heating.

XRD spectra:

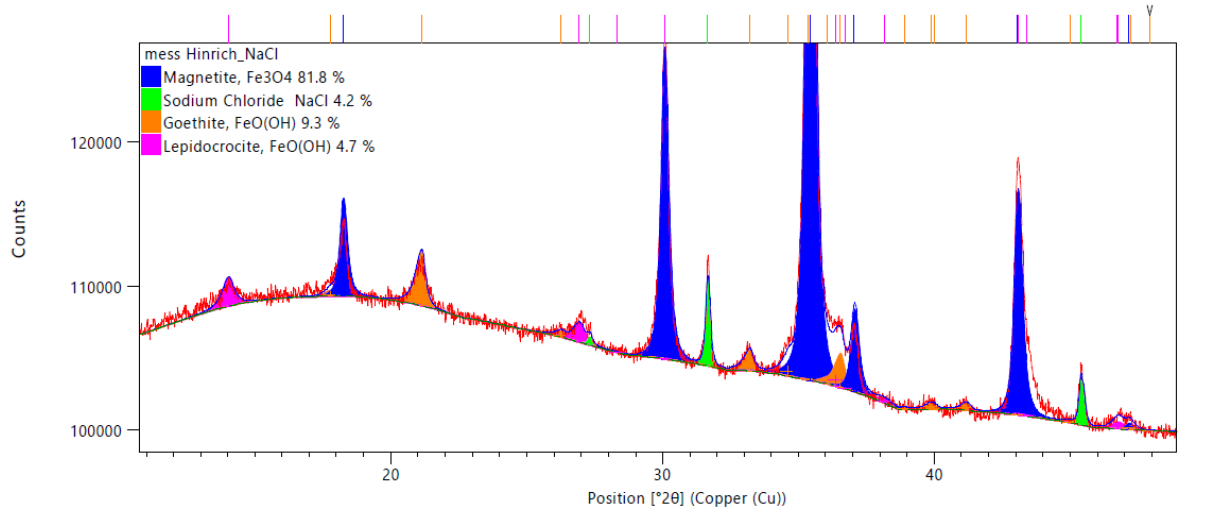

Appendix 16: Xrd spectrum of rust sample corroded with pure NaCl

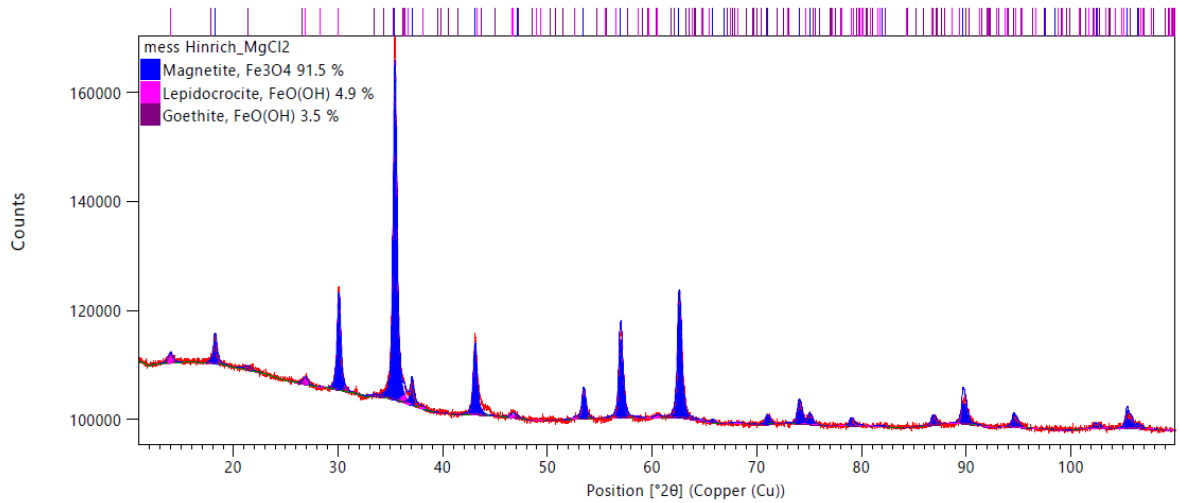

Appendix 17: XRD spectrum of rust corroded with magnesium chloride ($MgCl_2$)

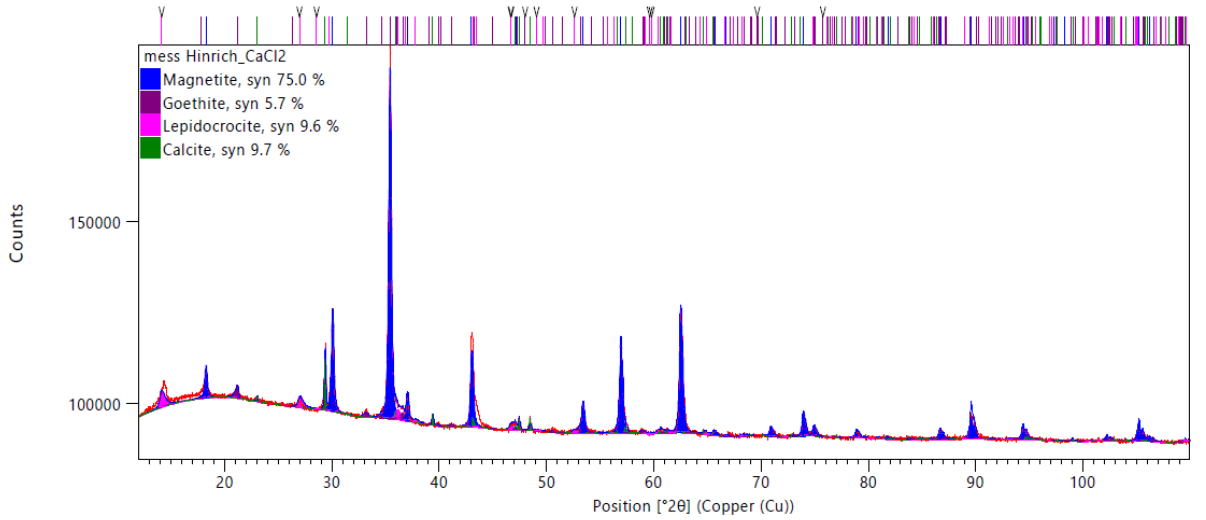

Appendix 18: XRD spectrum of rust corroded with calcium chloride ($CaCl_2$)

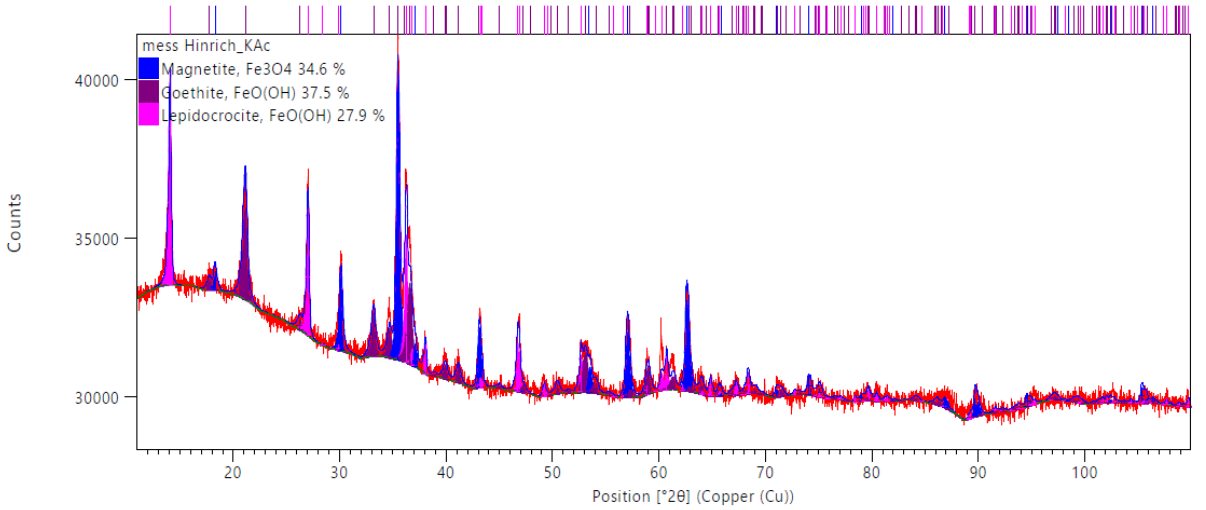

Appendix 19: XRD spectrum of rust corroded with potassium acetate (KAc)

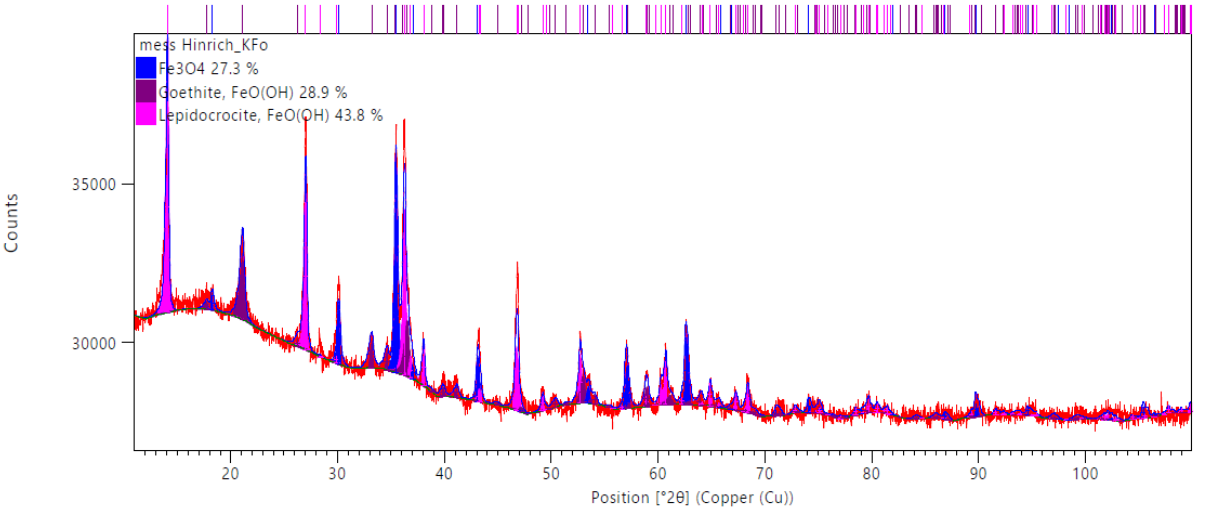

Appendix 20: XRD spectrum of rust corroded with potassium formate (KFo)

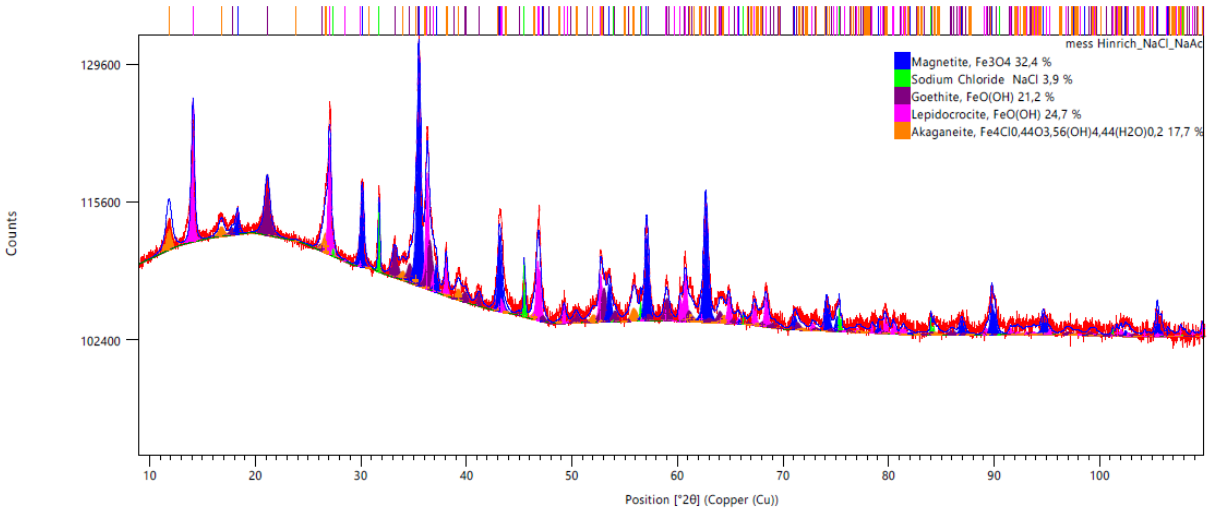

Appendix 21: XRD spectrum of rust corroded with NaCl + 8% sodium acetate

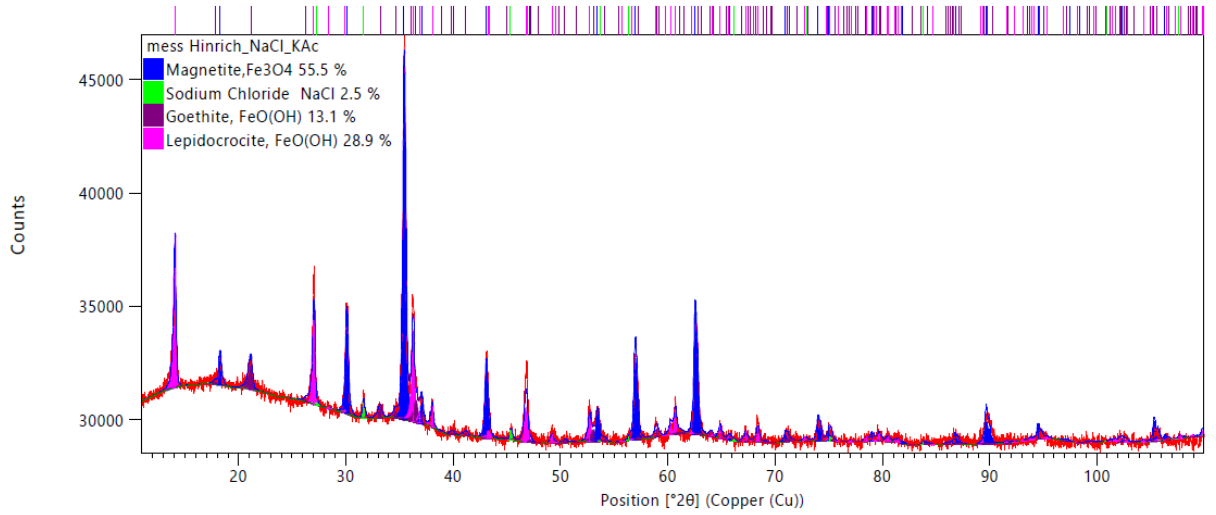

Appendix 22: XRD spectrum of rust corroded with NaCl + 8% potassium acetate

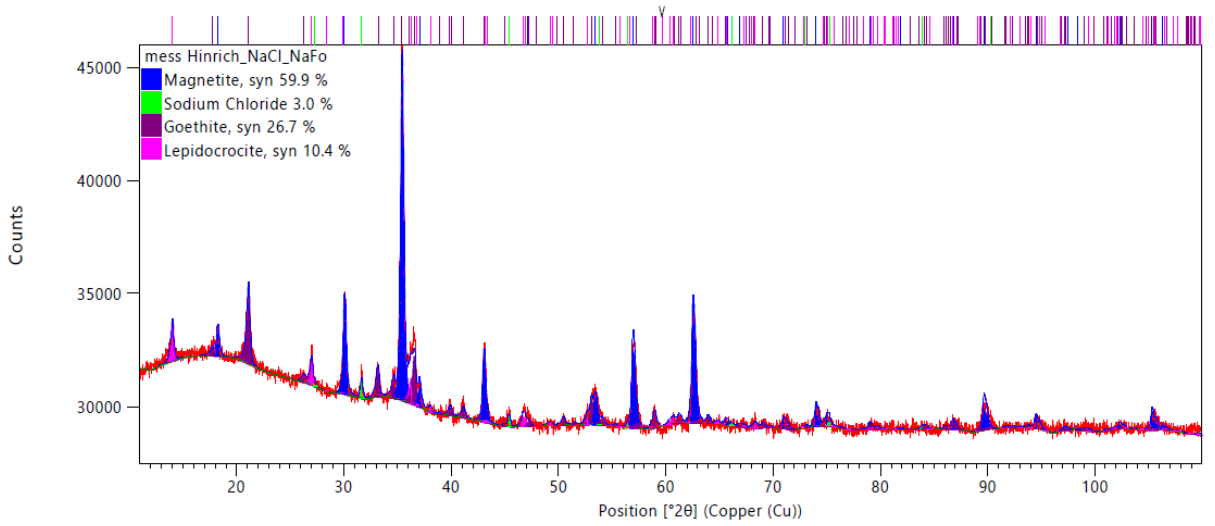

Appendix 23: XRD spectrum of rust corroded with NaCl + 8% sodium formate

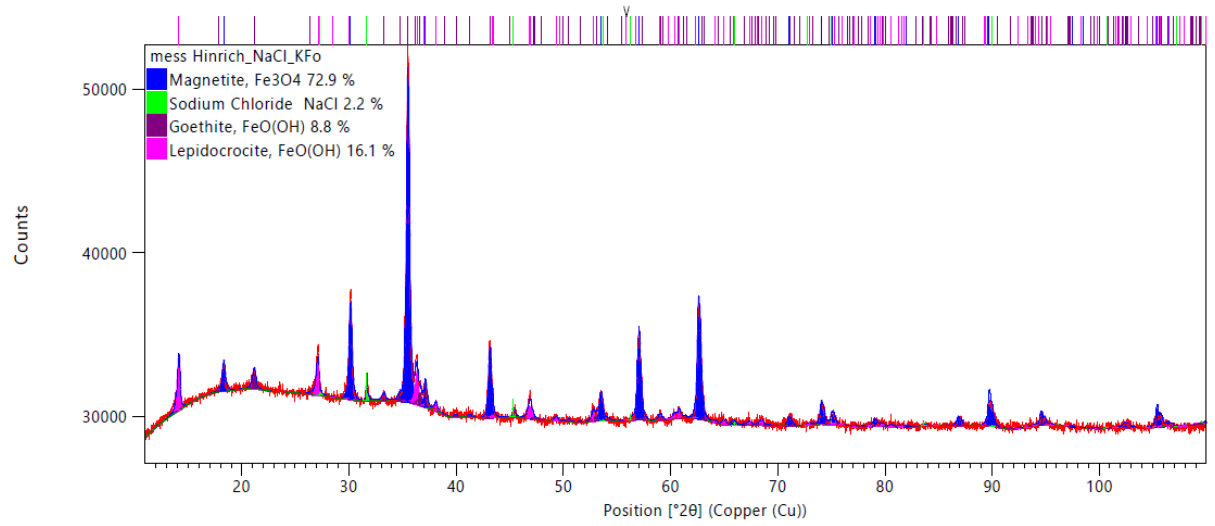

Appendix 24 XRD spectrum of rust corroded with NaCl + 8% potassium formate

Bibliography

Aziz, M., & Ismail, A. F. (2017). X-Ray Photoelectron Spectroscopy (XPS). In *Membrane Characterization*. Elsevier B.V. https://doi.org/10.1016/B978-0-444-63776-5.00005-X

Binnig, G., Gerber, C., Stoll, E., Albrecht, T. R., & Quate, C. F. (1987). Atomic resolution with atomic force microscope. *Epl*, *3*(12), 1281–1286. https://doi.org/10.1209/0295-5075/3/12/006

Chauhan, A. (2014). Powder XRD Technique and its Applications in Science and Technology. *Journal of Analytical & Bioanalytical Techniques*, *5*(6). https://doi.org/10.4172/2155-9872.1000212

Chauhan, L. R., & Gunasekaran, G. (2007). Corrosion inhibition of mild steel by plant extract in dilute HCl medium. *Corrosion Science*, *49*(3), 1143–1161. https://doi.org/10.1016/j.corsci.2006.08.012

Chiaradonna, S., Di Giandomenico, F., & Masetti, G. (2020). Trading dependability and energy consumption in critical infrastructures: Focus on the rail switch heating system. *Proceedings of IEEE Pacific Rim International Symposium on Dependable Computing, PRDC*, *2020-Decem*, 150–159. https://doi.org/10.1109/PRDC50213.2020.00026

Christodoulou, P. I., Kermanidis, A. T., & Haidemenopoulos, G. N. (2016). Fatigue and fracture behavior of pearlitic Grade 900A steel used in railway applications. *Theoretical and Applied Fracture Mechanics*, *83*, 51–59. https://doi.org/10.1016/j.tafmec.2015.12.017

Cornell, J. S., Pillard, D. A., & Hernandez, M. T. (2000). Comparative measures of the toxicity of component chemicals in aircraft deicing fluid. *Environmental Toxicology and Chemistry*, *19*(6), 1465–1472. https://doi.org/10.1002/etc.5620190601

Crowther, R. A., & Hynes, H. B. N. (1977). The effect of road deicing salt on the drift of stream benthos. *Environmental Pollution (1970)*, *14*(2), 113–126. https://doi.org/10.1016/0013-9327(77)90103-3

Friedbacher, G., Bubert, H. (2011). *Surface and Thin Films Analysis*.

Gadelmawla, E. S., Koura, M. M., Maksoud, T. M. A., Elewa, I. M., & Soliman, H. H. (2002). Roughness parameters. *Journal of Materials Processing Technology*, *123*(1), 133–145. https://doi.org/10.1016/S0924-0136(02)00060-2

Giesko, T., Zbrowski, A., & Czajka, P. (2007). Laser profilometers for surface inspection and profile measurment. *Problemy Eksploatacji*, *nr 1*, 97–108.

Hartl, W., & Erhart, E. (2002). Effects of potassium carbonate as an alternative road de-icer to sodium chloride on soil chemical properties. *Annals of Applied Biology*, *140*(3), 271–277. https://doi.org/10.1111/j.1744-7348.2002.tb00181.x

Hellstén, P. P., Salminen, J. M., Jørgensen, K. S., & Nystén, T. H. (2005). Use of potassium formate in road winter deicing can reduce groundwater deterioration. *Environmental Science and Technology*, *39*(13), 5095–5100. https://doi.org/10.1021/es0482738

Hoffmann, M., Gruber, M., Leuboldt, J., Grothe, H., Koyun, A., Seifireid, T., Stinglmayr, D., & Hofko, B. (2021). *Winterlife- Winterdienst mit effektiven, nachhaltigen und nicht aggressiven Taumitteln, sowie optimalen Life Cycle Costs der Bahn; Endbericht VIF 2018 -Verkehrsinfrastrukturforschung*.

Hong, M. I., & Woo, C. K. (2013). Development of a constant power AC/DC converter for point heater equipment. *Proceedings of the 2013 International Conference on Advanced Information Engineering and Education Science, ICAIEES 2013*, *Icaiees*, 234–237.

Jovancicevic, V., Bockris, J. O., Carbajal, J. L., Zelenay, P., & Mizuno, T. (1986). Adsorption and Absorption of Chloride Ions on Passive Iron Systems. *Journal of The Electrochemical Society*, *133*(11), 2219–2226. https://doi.org/10.1149/1.2108377

Karraker, N. E., Gibbs, J. P., & Vonesh, J. R. (2008). Impacts of road deicing salt on the demography of vernal

pool-breeding amphibians. *Ecological Applications*, *18*(3), 724–734. https://doi.org/10.1890/07-1644.1

Kelly, M. A. (1999). A new electron energy analyzer for electron spectroscopy. *Journal of Electron Spectroscopy and Related Phenomena*, *98–99*(March 1998), 55–66. https://doi.org/10.1016/s0368-2048(98)00275-8

Koch, G., Varney, J., Thompson, N., Moghissi, O., Gould, M., & Payer, J. (2016). *NACE IMPACT report*.

Křivý, V., Kubzová, M., Konečný, P., & Kreislová, K. (2019). Corrosion processes on weathering steel bridges influenced by deposition of de-icing salts. *Materials*, *12*(7). https://doi.org/10.3390/ma12071089

Kunert, A. T., Lamneck, M., Helleis, F., Pöhlker, M. L., Pöschl, U., & Fröhlich-Nowoisky, J. (2018). Twin-plate ice nucleation assay (TINA) with infrared detection for high-throughput droplet freezing experiments with biological ice nuclei in laboratory and field samples. *Atmospheric Measurement Techniques Discussions*, 1–25. https://doi.org/10.5194/amt-2018-230

Magistrat der Stadt Wien. (2003). *L 670-000 - Winterdienst- Verordnung*.

McCafferty, E. (2009). Introduction of corroion science. In *Springer* (Vol. 1).

Montemor, M. F., Simões, A. M. P., & Ferreira, M. G. S. (2003). Chloride-induced corrosion on reinforcing steel: From the fundamentals to the monitoring techniques. *Cement and Concrete Composites*, *25*(4-5 SPEC), 491–502. https://doi.org/10.1016/S0958-9465(02)00089-6

Muralidharan, S., Phani, K. L. N., Pitchumani, S., Ravichandran, S., & Iyer, S. V. K. (1995). Polyamino-Benzoquinone Polymers: A New Class of Corrosion Inhibitors for Mild Steel. *Journal of The Electrochemical Society*, *142*(5), 1478–1483. https://doi.org/10.1149/1.2048599

Muševič, I. (2000). Atomic force microscopy. In *Informacije MIDEM* (Vol. 30, Issue 4). https://doi.org/10.1093/oso/9780198856559.003.0016

Nilssen, K., Klein-Paste, A., & Wåhlin, J. (2016). Accuracy of ice melting capacity tests: Review of melting data for sodium chloride. *Transportation Research Record*, *2551*, 1–9. https://doi.org/10.3141/2551-01

Novotny, E. V., Murphy, D., & Stefan, H. G. (2008). Increase of urban lake salinity by road deicing salt. *Science of the Total Environment*, *406*(1–2), 131–144. https://doi.org/10.1016/j.scitotenv.2008.07.037

Oh, H. S., Park, C. B., Lee, S. H., Lee, J. B., Kim, T. H., & Lee, H. W. (2019). A study on de-icing for railway turnouts using 250kHz-200W-class induction heating system. *AIP Advances*, *9*(12). https://doi.org/10.1063/1.5129857

Robert, R. B., De Noyelles, F. G., & Locke, C. E. (1992). *Handbook of Test Methods for Evaluating C h emical Deicers* (pp. 31–42).

Rojan, M. A., Azmi, M. S. M., Majid, M. S. A., Daud, R., & Basaruddin, K. S. (2019). Fracture toughness of railway for higher speed rail corridors in Malaysia. *IOP Conference Series: Materials Science and Engineering*, *670*(1). https://doi.org/10.1088/1757-899X/670/1/012065

Steinhauser, G. (2008). Cleaner production in the Solvay Process: general strategies and recent developments. *Journal of Cleaner Production*, *16*(7), 833–841. https://doi.org/10.1016/j.jclepro.2007.04.005

Tamura, H. (2008). The role of rusts in corrosion and corrosion protection of iron and steel. *Corrosion Science*, *50*(7), 1872–1883. https://doi.org/10.1016/j.corsci.2008.03.008

Trzaskos, M. P., & Klein-Paste, A. (2020). Effect of Temperature and Prewetting for Ice Penetration with Sodium Formate. *Transportation Research Record*, *2674*(6), 140–150. https://doi.org/10.1177/0361198120917974

Waseda, Y., Matsubara, E., & Shinoda, K. (2011). *X- Ray Diffraction Crystallography*. https://doi.org/10.1007/978-3-642-16638-8

Wedler, G., & Freund, H. J. (2012). *Lehrbuch der physikalischen Chemie* (Vol. 6).